TECHNICAL UNIVERSITY
OF CLUJ-NAPOCA
ROMANIA

HABILITATION THESIS

Buckling analysis of thin-walled members and vibration analysis of civil engineering structures

Assoc. Prof. Mihai NEDELCU, PhD

Civil Engineering Faculty

The Technical University of Cluj-Napoca

15.10.2013

Table of Contents

HABILITATION THESIS

"Buckling analysis of thin-walled members and vibration analysis of civil engineering structures"

a) ABSTRACT

Present thesis summarises the scientific activity of the candidate after defending the PhD Thesis at The Technical University of Cluj-Napoca, confirmed by The Ministry of Education and Research, on the basis of Order no. 6026, dated 27.11.2009. The scientific activity and achievements presented here are developed in two thematic directions.

The first one entitled "*Buckling analysis of thin-walled members*" represents the dominant part of the candidate's research activity, it started with the scientific work developed during the candidate's PhD programme entitled "Stability aspects for metallic structures", supervisor: prof. Cornel BIA, and since then it has significantly evolved by new theoretical formulations in the field of thin-walled structures. In this area, the candidate's work is related to the Generalised Beam Theory (GBT), a specialised theory for the analysis of thin-walled members, which is thoroughly presented in this thesis. The candidate extended GBT for special cases of thin-walled members and analysis types, and his personal contributions of theoretical nature, published in ISI and conference papers, can be summarised as follows:

a. *GBT formulation to analyse the behaviour of thin-walled members with variable cross-section.* This formulation added new equations to GBT in order to handle tapered thin-walled members with small tapering slopes.
b. *GBT formulation to analyse the buckling behaviour of isotropic conical shells.* GBT was already developed for cylindrical shells and tubes and through the candidate's work, that formulation was extended for conical shells, yielding very promising results even for large values of the tapering slope.
c. *Buckling mode decomposition from Finite Element Analysis (FEA) of thin-walled members.* The candidate proposed a method capable to quantify the modal participation of the pure deformation modes (of Global, Distortional and Local nature) in a general buckling mode. Even if similar methods were very recently reported by other researches, the method developed by the candidate is, at present time, the fastest and the most stable, due to a special algorithm based on the orthogonality features of the pure deformation modes.

The second scientific direction entitled "*Vibration analysis of civil engineering structures*" contains theoretical and also experimental work. The theoretical work started under the topic "Vibration mode decomposition from FEA of thin-walled members" and is mainly concentrated on the applicability of the modal decomposition method (briefly described above, at point *c.*) to the modal shapes derived from FEA, associated with the natural frequencies of thin-walled members. The topics of the experimental work are (i) *Experimental modal analysis,* and (ii) *Tension estimation of cables based on vibration analysis*. The candidate was recently (2011) nominated as coordinator of the laboratory „Actions in Buildings and Structures", Department of Structural Mechanics, Faculty of Civil Engineering, Technical University of Cluj-Napoca. The laboratory contains Bruel&Kjaer and PCB Piezotronics equipment and dedicated software suited to perform experimental vibration analyses. At present time, under the candidate supervision, successful experimental modal analyses were performed on real-world structures (beam and suspension bridges, metallic structures, tall concrete buildings, hollow-core slabs etc.) and also on small elements inside laboratory. The candidate conducted many vibrations measurements and analyses in

time/frequency domain for bridges and other civil engineering structures (acceleration, velocity, displacement, level of vibrations) with the purpose of: optimisation of structure's dynamic characteristics (mass, stiffness, damping), risk assessment of having the resonance phenomenon, prediction of dynamic behaviour, evaluating the damping for inclusion in FE models, correlation of FE models with real structures, damage detection and assessment, long term building monitoring, experimental assessment of traffic or other human activities induced vibrations.
The tension estimation of cables by means of vibration response is another recent scientific area in which the candidate obtained very promising results. The vibration method uses the experimental modal analysis to extract the natural frequencies of the cable and next, the tension force is determined by using appropriate analytical closed-form or numerical algorithm-form relationship between natural frequencies and the cable tension. The cable response is mainly affected by its flexural stiffness, sag-extensibility and the rotational stiffness of the end-supports. Until present time, the candidate considered hinged supports for his experiments, and the "sag" effect was neglected, but all the influencing terms were analysed in numerical studies.
The main achievements and results are presented in detail in Chapter (b-i): *Scientific, professional and academic achievements*.

In what concerns the future research and development plans of the candidate, related to the fields of research presented above, the following research topics will continue or will be developed:
Analysis of thin-walled members
- buckling/vibration analysis of tapered thin-walled members with arbitrary cross-sectional variation
- buckling/vibration analysis of conical shells based on GBT
- improving the modal decomposition method
- buckling/vibration mode decomposition for tapered thin-walled members, cylindrical and conical shells
- buckling/vibration mode decomposition for thin-walled members with arbitrary holes
- the effect of imperfections in non-linear analysis of thin-walled members

Experimental vibration analyses:
- perform new experimental modal analyses on real complex structures such as civil and industrial constructions and also on small structures and scale models inside laboratory
- tension estimation of cables by means of vibration response taking into consideration the "sag" effect and the real rotational stiffness of the end-supports

A short description of each topic has been done in Chapter (b-ii): *Scientific, professional and academic future development plans*.
Finally, it have to be underlined that the active role of the candidate will continuously increase by participation with new research topics to international conferences and papers published in specialised journals.

b) ACHIEVEMENTS AND DEVELOPMENT PLANS

(b-i) Scientific, professional and academic achievements

1. Introduction

Present thesis summarises the research activity of the candidate after defending the PhD Thesis at The Technical University of Cluj-Napoca, confirmed by The Ministry of Education and Research, on the basis of Order no. 6026, dated 27.11.2009. The research activity and achievements presented here are developed in two thematic directions.
The first one entitled "*Buckling analysis of thin-walled members*" represents the dominant part of the candidate's research activity, it started with the scientific work developed during the candidate's PhD programme entitled "Stability aspects for metallic structures", supervisor: prof. Cornel BIA, and since then it has significantly evolved by new theoretical formulations in the field of thin-walled structures. In this area, the candidate's work is related to the Generalised Beam Theory (GBT), a specialised theory for the analysis of thin-walled members, which is thoroughly presented in this thesis. The candidate extended GBT for special cases of thin-walled members and analysis types, and his personal contributions of theoretical nature, published in ISI and conference papers, can be summarised as follows:

a. *GBT formulation to analyse the behaviour of thin-walled members with variable cross-section.* This formulation added new equations to GBT in order to handle tapered thin-walled members with small tapering slopes.
b. *GBT formulation to analyse the buckling behaviour of isotropic conical shells.* GBT was already developed for cylindrical shells and tubes and through the candidate's work, that formulation was extended for conical shells, yielding very promising results even for large values of the tapering slope.
c. *Buckling mode decomposition from Finite Element Analysis (FEA) of thin-walled members.* The candidate proposed a method capable to quantify the modal participation of the pure deformation modes (of Global, Distortional and Local nature) in a general buckling mode. Even if similar methods were very recently reported by other researches, at present time, the method developed by the candidate is the fastest and the most stable, due to a special algorithm based on the orthogonality features of the pure deformation modes.

The second research direction entitled "*Vibration analysis of civil engineering structures*" contains theoretical and experimental scientific work. The theoretical work started under the topic "Vibration mode decomposition from FEA of thin-walled members" and is mainly concentrated on the applicability of the modal decomposition method (briefly described above, at point *c.*) to the modal shapes derived from FEA, associated with the natural frequencies of thin-walled members. The topics of the experimental work are (i) *Experimental modal analysis,* and (ii) *Tension estimation of cables based on vibration analysis*. The candidate was recently (2011) nominated as coordinator of the laboratory „Actions in Buildings and Structures", Department of Structural Mechanics, Faculty of Civil Engineering, Technical University of Cluj-Napoca. The laboratory contains Bruel&Kjaer and PCB Piezotronics equipment and dedicated software suited to perform experimental vibration analyses. At present time, under the candidate supervision, successful experimental modal analyses were performed on real-world structures (beam and suspension bridges, metallic structures, tall concrete buildings, hollow-core slabs etc.) and also on small elements inside laboratory. The candidate conducted many vibrations measurements and analyses in

time/frequency domain for bridges and other civil engineering structures (acceleration, velocity, displacement, level of vibrations) with the purpose of: optimisation of structure's dynamic characteristics (mass, stiffness, damping), risk assessment of having the resonance phenomenon, prediction of dynamic behaviour, evaluating the damping for inclusion in FE models, correlation of FE models with real structures, damage detection and assessment, long term building monitoring, experimental assessment of traffic or other human activities induced vibrations.

The tension estimation of cables by means of vibration response is another recent research area in which the candidate obtained very promising results. The vibration method uses the experimental modal analysis to extract the natural frequencies of the cable and next, the tension force is determined by using appropriate analytical closed-form or numerical algorithm-form relationship between natural frequencies and the cable tension. The cable response is mainly affected by its flexural stiffness, sag-extensibility and the rotational stiffness of the end-supports. Until present time, the candidate considered hinged supports for his experiments, and the "sag" effect was neglected, but all the influencing terms were analysed in numerical studies.

2. Articles constituting the habilitation thesis

1. **Nedelcu M** (2010) „GBT formulation to analyse the behaviour of thin-walled members with variable cross-section", Thin-Walled Structures, 48(8), pp. 629-638, (DOI:10.1016/j.tws.2010.03.001) (5 ISI citations).
2. **Nedelcu M** (2011) „GBT formulation to analyse the buckling behaviour of isotropic conical shells". Thin-Walled Structures, 49(7), pp. 812-818, (DOI:10.1016/j.tws.2011.02.006) (4 ISI citations).
3. **Nedelcu M** (2012) „GBT-based buckling mode decomposition from Finite Element Analysis of thin-walled members". Thin-Walled Structures, 54, pp. 156-163, (DOI:10.1016/j.tws.2012.02.009).
4. **Nedelcu M,** Cucu HL (2013) „Buckling modes identification from FEA of thin-walled members using only GBT cross-sectional deformation modes". Thin-Walled Structures, Article in Press, (DOI: 10.1016/j.tws.2013.06.007).
5. **Nedelcu M** (2011) „GBT-based Analysis of Tapered Thin-Walled Members: Recent Developments", Acta Tech. Napocensis: Civil Eng. & Arch., 54(1), ISSN 1221-5848 (B+ journal).
6. **Nedelcu M**, Chiorean CG (2011) „GBT formulation to analyse the stability of isotropic conical shells", Proceedings of the 6th International Conference on Thin Walled Structures 05 – 07 September 2011, Timisoara, Romania, Vol. 1, ISBN: 978-92-9147-102-7, pp. 953-961.
7. **Nedelcu M**, Groza P, Cucu HL (2012) „The estimation of dynamic properties of a fixed beam using experimental modal testing", Acta Tech. Napocensis: Applied Mathematics and Mechanics, 55(3), ISSN 121-5872 (B+ journal).
8. **Nedelcu M**, Frățilă E, Iliescu M (2012) „Experimental modal testing of a concrete bridge". Acta Tech. Napocensis: Applied Mathematics and Mechanics, 55(3), UTCN, Cluj-Napoca , ISSN 121-5872 (B+ journal).
9. **Nedelcu M**, Chira N, Cucu HL (2013) „Vibration mode decomposition from finite element analysis of axially compressed thin-walled members", Proceedings of International Conference on Metal Structures**:** Design Fabrication and Economy of Metal Structures, Miskolc, Hungary, 24-26 April 2013, ISBN: 978-3-642-36690-1. pp. 139-144.
10. **Nedelcu M**, Sauca A, Chira N (2013) "Tension estimation of cables by means of vibration analysis", C60 International Conference "Tradition and Innovation – 60 Years of Constructions in Transylvania", 7-9 November 2013, Cluj-Napoca, Romania.

Scientific, professional and academic experience of the candidate

Reviewer of ISI journals:

- Thin-Walled Structures (www.elsevier.com)
- Mechanics & Industry (http://journals.cambridge.org)
- Journal of Mechanical Engineering Science (SAGE Publications Journal - http://pic.sagepub.com/)

Research Projects

- Project manajer of Td CNCSIS Grant 2003-2005: „ Buildings earthquake protection using seismic isolators", Contract: no.33532/2003_ Td7, CNCSIS code: 50, financed by: National University Research Council (CNCSIS), Romania, total amount 17000 euro.
- Team member of the research project PN-II-ID-PCE ID_193/2008 „Design And Seismic Performance Evaluation Of 3d Frame Structures Using Advanced Nonlinear Static Analysis Method", project manager prof. dr. eng. Cosmin Chiorean (http://users.utcluj.ro/~ccosmin/RESEARCHPROJECT.htm), 2009-2011.
- Team member of the SERIES research project, Framework Programme 7 „Seismic behavior of structural systems composed of cast in situ concrete walls", under direction of prof. dr. eng. Cristina M. Câmpian (http://www.series.upatras.gr/SESYCOWA), 2010-2012.

Organizational Experience

- Since 2011: Coordinator of Laboratory „Actions in Buildings and Structures", Department of Structural Mechanics, Technical University of Cluj-Napoca, http://constructii.utcluj.ro/cercetare_laboratoare.php

Awards

- The first three articles of section 2 were awarded by UEFISCDI (http://uefiscdi.gov.ro/articole/1722/Articole.html), total amount: 450euro/article

Member of AICPS – Romanian Association of Structural Engineers

Structural Design:

a. personal works: approx. 50,000m^2 cast-in-place/precast concrete and steel civil and industrial buildings
b. design team partner: approx. 220,000m^2

Teaching Activity:

Current courses: Theory of Elasticity, Strength of Materials, Experimental Methods in Structural Engineering (Master)

Past courses: Computer Programming and Design Applications (I, II, III), Statics, Advanced Structural Analysis (Master), Advanced Structural Mechanics (Master)

Supervisor of 4 Master's Theses defended in 2013, Faculty of Civil Engineering, UTCN, and currently (2013-2015), supervisor of 16 Master's Theses.

More information on personal web-page: http://users.utcluj.ro/~mnedelcu/index_en.htm

3. Buckling analysis of thin-walled members

Starting with the Ph.D. Thesis, the candidate's main research field is the study of thin-walled members. Regarding the buckling of thin-walled members, the most complete design codes were developed for metallic members: ENV 1993-1-3 Eurocode 3 (Europe) [1], NAS 2001 (North America) [2], [3], AS/NZS 1996 (Australia and New Zeeland) [4]. The design methods are generally very similar, the buckling evaluation consists of (i) computation of the elastic critical load, (ii) consideration of the degradation caused by the various kinds of imperfections as well as the possible favourable effect of post-buckling reserve. The buckling phenomena may be classified as Global, Distortional and Local buckling (see Figure 1), and even if widely accepted definitions for these fundamental (pure) types do not exist, they are usually defined on the basis of in-plane cross-sectional deformations.

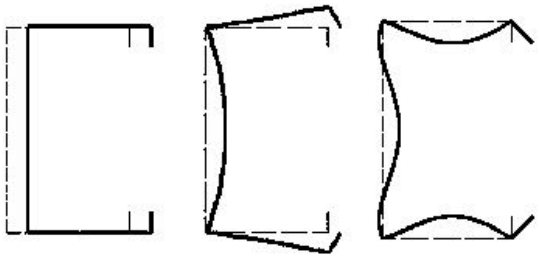

Figure 1. The fundamental buckling types of thin-walled members

A very popular solving strategy (The Effective Width Method) uses a reduced "effective" cross-section, avoiding in this manner the critical load computation for distorsional and local buckling, more difficult to obtain. The computation of the effective cross-section is a tedious iterative process for the structural design engineer. To overcome this problem, Schafer developed the "Direct Strength Method" introduced in 2004 in NAS - Appendix 1 [5]. The method does not use the principle of effective cross-section, nor require iterations for determining effective properties; instead the method uses member elastic buckling solutions based on gross properties to determine the member strength in global, distortional and local buckling. For the evaluation of these elastic critical loads, Schafer et al. created CUFSM [6], free-license analysis software based on the Constrained Finite Strip Method (cFSM) and the hypotheses of the Generalised Beam Theory (GBT).

The behaviour of thin-walled members can be analysed by using various methods, among which the GBT proved to be, in the last decades, as one of the most elegant and powerful. Originally developed by R. Schardt ([7], [8]), GBT provides a general solution for the linear/nonlinear analysis of prismatic thin-walled structures, using bar elements capable to describe the cross-section rigid-body motions and distortions. Due to its unique modal decomposition features, GBT provides a general and unified approach to obtain accurate, elegant and clarifying solutions for several problems. By decomposing the member deformed configuration into a linear combination of cross-sectional deformation modes, which account for both rigid-body motions and in-plane deformations, and being able to assess the contribution of each of them, GBT offers possibilities which are not available, even through the use of very potent numerical techniques, such as the Finite Element or Finite Strip methods − indeed, this modal decomposition cannot be done in Finite Element Analysis (FEA) or Finite Strip Analysis (FSA), since all degrees of freedom are of nodal (not modal) nature (i.e., the GBT-based analyses reveal all the "structural ingredients" of a member deformed configuration or buckling/vibration mode, while retaining a numerical accuracy fully matching that of the FEA or FSA). Therefore, GBT may be viewed as either (i) a bar

theory that incorporates cross-section in-plane deformation or (ii) a folded-plate theory that includes plate rigid-body motions.
The candidate made important contributions in extending this theory, contributions that are next presented.

3.1 GBT formulation to analyse the behaviour of thin-walled members with variable cross-section

Introduction

Nowadays GBT is fully developed for thin-walled members having a large variety of constant cross-sections. Article 1 provided the extension of GBT for the special case of tapered thin-walled members with open cross-section. The paper offered a new analysis method for structures as: box shaped bridges, beams, pylons of variable cross-section, conical shell towers, hyperbolic towers etc. (see article 5). The results were also disseminated by oral presentation and publication of the following articles in the proceedings of two important conferences:

- **Nedelcu M.**, Popa AG (2011) "New GBT Approach for Tapered Thin-walled Members with Closed Cross-sections", Proceedings of International Symposium IABSE-IASS, Taller, Longer, Lighter, London, UK, 20-23 September 2011, ISBN: 578-0-7079-7122-3.
- **Nedelcu M**, Chira N (2011) "GBT buckling analysis of tapered thin-walled members subjected to non-uniform bending", Proceedings of the International Conference Eurosteel 2011, August 31 - September 2, 2011, Budapest, Hungary, ISBN: 978-92-9147-103-4.

The analysis of thin-walled members with variable cross-section is a problem often encountered in the engineering practice. Starting with the 1st order analysis (linear analysis) difficulties arise when both torsion rigidities (Saint-Venant and warping), variable along the member length, are taken into account. Eisenberger [9] and Sapountzakis, Mokos [10] gave different solutions to this problem, developing an analytical method and a boundary element method, respectively. However, *superior* deformation modes involving cross-section distortion are difficult to describe using a *bar theory*, especially for the nonlinear analysis.
GBT is based on Vlasov's classical thin-walled hypotheses and it is a bar theory capable to describe superior deformation modes. In fact any member deformation can be described as a linear combination of pre-determined *pure* deformation modes. Working with one-dimensional elements (bar elements), GBT is extremely computationally efficient. It is also capable to provide the contribution of each pure deformation mode to the final configuration and so it helps to a better understanding of the analysed structural behaviour.
Recently GBT was developed for a large variety of cross-sections, in chronological order: open un-branched, one cell closed, circular, open arbitrarily branched and finally, complete arbitrary cross-sections [11]. Nowadays GBT can also handle: orthotropic materials [12], [13], vibration [14], post-buckling behaviour [15], arbitrary loading/boundary conditions and imperfections [16]. The first and, at this hour, the single publicly available computer program fully based on this theory is GBTUL [17] . The GBT hypotheses were also implemented by Adany and Shafer in the conventional Finite Strip Method, in order to decompose the member deformation into pure deformation modes [18], thus the Constrained Finite Strip Method was developed and implemented into CUFSM software [6].
The candidate extended the general GBT formulation for the analysis of elastic linear and buckling behaviour (referred here as 1st and 2nd order analysis) of isotropic thin-walled tapered members displaying continuously variable open cross-section. The extension of GBT was derived using the approximation that the warping displacements are still perpendicular to the cross-sectional plane. This approximation gives good results for tapered members with small tapering slope, which is a structural characteristic largely used in practice.

Taking into account the variable member rigidities, new terms are added to the system of equilibrium differential equations. Of course this new extended formulation will also accept members with constant cross-section. Next, the derivation methods of the variable stiffness matrices are analysed. For a special case of cross-section uniform variability, the member stiffness components can be easily and efficiently computed. For the rest, a more approximate way is suggested. Finally, for the validation of this new GBT formulation two illustrative examples are given, one in which the GBT results obtained by the candidate are compared with values already presented in scientific literature and obtained by means of different analysis methods, and the other in which the GBT results are compared with those obtained from a shell FEA. The second example also illustrates the limits of applicability of the GBT extension for tapered members taking into account the magnitude of the tapering slope.

3.1.1 GBT for constant cross-sections

For the arbitrary open-section thin-walled member shown in Figure 2, one defines the local coordinate system *x-s-z* and the corresponding displacement field *u-v-w*.

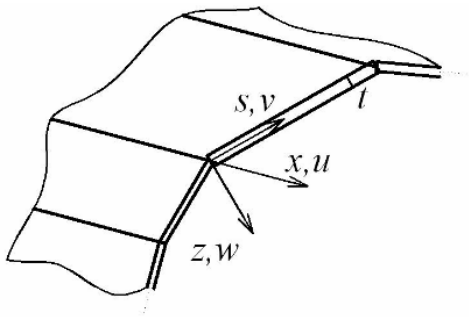

Figure 2. Local coordinate system and displacement components

The stress and strain field is expressed by taking into consideration the membrane and bending behaviour of the thin-walls: $\sigma_x = \sigma_x^M + \sigma_x^B$, $\varepsilon_x = \varepsilon_x^M + \varepsilon_x^B$ etc. Each strain component includes linear and non-linear terms: $\varepsilon_x^M = \varepsilon_x^{M,L} + \varepsilon_x^{M,NL}$.

The simplifying classical Kirchhoff-Love hypotheses are adopted for each wall and also Vlasov's hypotheses: $\varepsilon_s^{M,L} = 0$ and $\gamma_{xs}^{M,L} = 0$. Neglecting the non-relevant strain components, the geometrical relations are written

$$\begin{aligned} &\varepsilon_x^M = \varepsilon_x^{M,L} + \varepsilon_x^{M,NL} = u' + (v'^2 + w'^2)/2 \qquad && \varepsilon_x^B = -zw'' \\ &\varepsilon_s^B = -z\ddot{w} && \gamma_{xs}^B = \gamma_{sx}^B = -2z\dot{w}' \end{aligned} \tag{1}$$

where $()' = \partial()/\partial x$, $\dot{()} = \partial()/\partial s$.

In this study the effect of the membrane shear strain non-linear term $\gamma_{xs}^{M,NL} = \dot{w}w'$ is neglected. The constitutive relations related to the relevant stress components are written:

$$\sigma_x^M = E\varepsilon_x^M \qquad \begin{Bmatrix} \sigma_x^B \\ \sigma_s^B \\ \tau_{xs}^B \end{Bmatrix} = \frac{E}{1-\mu^2} \begin{bmatrix} 1 & \mu & 0 \\ \mu & 1 & 0 \\ 0 & 0 & \dfrac{1-\mu}{2} \end{bmatrix} \begin{Bmatrix} \varepsilon_x^B \\ \varepsilon_s^B \\ \gamma_{xs}^B \end{Bmatrix}. \tag{2}$$

The displacements $u(s,x)$, $v(s,x)$ and $w(s,x)$ are written as a product of two functions

$$u(s,x)=u(s)\mathrm{f}'(x) \qquad v(s,x)=v(s)\mathrm{f}(x) \qquad w(s,x)=w(s)\mathrm{f}(x) \tag{3}$$

Any general cross-section displacement is considered as a linear combination of *n* orthogonal deformation modes. The number *n* depends on the cross-section type, the number of the fold-lines and the considered intermediate nodes. Thus, the displacement field is expressed as

$$u(s,x)=\sum_{k=1}^{n}u_k(s)\mathrm{f}_k'(x) \quad v(s,x)=\sum_{k=1}^{n}v_k(s)\mathrm{f}_k(x) \quad w(s,x)=\sum_{k=1}^{n}w_k(s)\mathrm{f}_k(x) \tag{4}$$

where $u_k(s)$, $v_k(s)$, $w_k(s)$ are *the cross-section deformation mode components* and $\mathrm{f}_k(x)$ are the amplitude functions describing their longitudinal variation. Based on Vlasov's simplifying hypotheses, the cross-section displacements $v_k(s)$ and $w_k(s)$ can be computed based on the warping displacements $u_k(s)$ which are considered linear over the cross-section. At the beginning of the process, the functions $\overline{u}_k(s)$, $\overline{v}_k(s)$, $\overline{w}_k(s)$ (named *elementary* or *initial functions*) are chosen in the following manner: unit warping displacements ($\overline{u}_{k,r}=1$) at each independent natural node *r* and unit flexural displacements ($\overline{w}_{k,r}=1$) at each intermediate node and independent end node (dependent nodes appear only for branched cross-sections [19]).

Next the member equilibrium equations are written based on the principle of virtual work applied in its variational form

$$\mathrm{d}V=\mathrm{d}W_{\mathrm{int}}+\mathrm{d}W_{ext}+\mathrm{d}\Pi_{\mathrm{s}}=0 \tag{5}$$

where V is the member total potential energy, W_{int} is the member strain energy, W_{ext} is the virtual work of the external loads and Π_{s} is the virtual work of the pre-buckling longitudinal normal stresses.

Taking into account the Vlasov's hypothesis, the variation of the strain energy reads

$$\mathrm{d}W_{\mathrm{int}}=\int_0^l\int_A(\mathrm{s}_x^M\mathrm{d}\varepsilon_x^M+\mathrm{s}_x^B\mathrm{d}\varepsilon_x^B+\mathrm{s}_s^B\mathrm{d}\varepsilon_s^B+\mathrm{t}_{xs}^B\mathrm{d}\gamma_{xs}^B)dAdx \tag{6}$$

where l and A are the member length and cross-section area. The variations of the strain components involved in the above expressions result from Eqs. (1) and (4)

$$\begin{aligned}
&\mathrm{d}\varepsilon_x^{M,L}=\sum_{k=1}^{n}u_k\mathrm{d}\mathrm{f}_k'' \qquad \mathrm{d}\varepsilon_x^{M,NL}=\sum_{j=1}^{n}\sum_{k=1}^{n}\left(v_jv_k+w_jw_k\right)\mathrm{f}_j'\mathrm{d}\mathrm{f}_k' \\
&\mathrm{d}\varepsilon_x^B=-\sum_{k=1}^{n}zw_k\mathrm{d}\mathrm{f}_k'' \qquad \mathrm{d}\varepsilon_s^B=-\sum_{k=1}^{n}z\ddot{w}_k\mathrm{d}\mathrm{f}_k \qquad \mathrm{d}\gamma_{xs}^B=-\sum_{k=1}^{n}2z\dot{w}_k\mathrm{d}\mathrm{f}_k'
\end{aligned} \tag{7}$$

Each term of the Eq. (6) is now expressed by introducing the initial functions $\overline{u}_k(s)$, $\overline{v}_k(s)$, $\overline{w}_k(s)$ and $\overline{\mathrm{f}}_k(x)$. The first term reads

$$\mathrm{d}W_{\mathrm{s}_x^M}=\int_0^l\int_A\mathrm{s}_x^M\mathrm{d}\varepsilon_x^M dAdx=\int_0^l\int_A Eu'\mathrm{d}u'dAdx \tag{8}$$

and taking into account Eqs. (4) and (7)

$$\mathrm{d}W_{\mathrm{s}_x^M}=\sum_{i=1}^{n}\sum_{k=1}^{n}\int_0^l\int_A E\overline{u}_i\overline{u}_k\overline{\mathrm{f}}_i''\mathrm{d}\overline{\mathrm{f}}_k''dAdx=\sum_{i=1}^{n}\sum_{k=1}^{n}\int_0^l\overline{C}_{ik}^M\overline{\mathrm{f}}_i''\mathrm{d}\overline{\mathrm{f}}_k''dx \tag{9}$$

where $\bar{C}_{ik}^{M} = E\int_A \bar{u}_i \bar{u}_k dA$ and it is important to underline that this expression is *constant* as long as the member cross-section is constant along its length.

By double integration the above equation becomes

$$\delta W_{s_x^M} = \sum_{i=1}^{n}\sum_{k=1}^{n}\left(\bar{C}_{ik}^{M}\bar{f}_i''\delta\bar{f}_k'\Big|_0^l - \bar{C}_{ik}^{M}\bar{f}_i'''\delta\bar{f}_k\Big|_0^l + \int_0^l \bar{C}_{ik}^{M}\bar{f}_i^{IV}\delta\bar{f}_k dx\right) \tag{10}$$

In the same manner one determines the other terms of Eq. (6) which becomes

$$\begin{aligned}\delta W_{\text{int}} = &\sum_{i=1}^{n}\sum_{k=1}^{n}\left(\int_0^l\left(\bar{C}_{ik}\bar{f}_i^{IV} - \bar{D}_{ik}\bar{f}_i'' + \bar{B}_{ik}\bar{f}_i\right)\delta\bar{f}_k dx + \right.\\ &\left.+\left(\bar{C}_{ik}\bar{f}_i'' + \mu\bar{D}_{2,ik}\bar{f}_i\right)\delta\bar{f}_k'\Big|_0^l + \left(-\bar{C}_{ik}\bar{f}_i''' + \left(\bar{D}_{1,ik} - \mu\bar{D}_{2,ik}\right)\bar{f}_i'\right)\delta\bar{f}_k\Big|_0^l\right)\end{aligned} \tag{11}$$

The stiffness matrices are

$$\begin{aligned}&\bar{C}_{ik} = \bar{C}_{ik}^{M} + \bar{C}_{ik}^{B} = E\int_s t\bar{u}_i\bar{u}_k ds + \int_s K\bar{w}_i\bar{w}_k ds\\ &\bar{D}_{1,ik} = \frac{G}{3}\int_s t^3\dot{\bar{w}}_i\dot{\bar{w}}_k ds \qquad \bar{D}_{2,ik} = \int_s K\ddot{\bar{w}}_i\bar{w}_k ds \qquad \bar{D}_{ik} = \bar{D}_{1,ik} - \mu\left(\bar{D}_{2,ik} + \bar{D}_{2,ki}\right)\\ &\bar{B}_{ik} = \int_s K\ddot{\bar{w}}_i\ddot{\bar{w}}_k ds\end{aligned} \tag{12}$$

where $K = \dfrac{Et^3}{12(1-\mu^2)}$ is the wall bending stiffness. All the matrices described above have constant components along the member length as long as the cross-section is constant.

If for the time being we are concerned only with linear analysis ($\delta\Pi_s = 0$) and the variation of virtual work of the external loads is considered zero ($\delta W_{ext} = 0$), Eq. (5) becomes $\delta W_{\text{int}} = 0$. Based on the independent nature of the initial functions ${}^k\bar{u}(s)$, ${}^k\bar{v}(s)$ and ${}^k\bar{w}(s)$, one obtains from Eq. (11) a coupled system of *n* differential equations of 4th order which written in matrix formulation has the expression

$$\bar{C}\bar{f}^{IV} - \bar{D}\bar{f}'' + \bar{B}\bar{f} = 0 \tag{13}$$

and $2n$ boundary conditions for $x=0$ and $x=l$.

In order to uncouple the differential equations system, a process of simultaneous diagonalisation of the stiffness matrices $\bar{C}$ and $\bar{B}$ is performed. The resulting system has the form

$$Cf^{IV} - Df'' + Bf = 0 \tag{14}$$

The system is still coupled by the elements of *D* matrix, but now the stiffness matrices have more clear structural meaning and the functions $u_k(s), v_k(s)$, $w_k(s)$ and $f_k(x)$ describe orthogonal deformation modes. Introducing the vector of normal stress resultants $W = -Cf''$ the boundary conditions have the form

$$\left(W_k - \mu\sum_{j=1}^{n} D_{2,jk}\varphi_j\right)\delta\varphi_k'\Big|_0^l = 0$$
$$\left(W_k' + \sum_{j=1}^{n}\left(D_{1,jk} - \mu D_{2,jk}\right)\varphi_j'\right)\delta\varphi_k\Big|_0^l = 0 \quad for\ k = 1\ldots n \tag{15a,b}$$

Next the virtual work of the external loads is taken into account. The external loads are applied in the cross-sectional nodes, both principal (the folding lines) and intermediate. Their total number is noted with *p*. The loads are also projected into transversal loads acting along the *s* coordinate and axial loads. Eq.(14) now becomes

$$C\varphi^{IV} - D\varphi'' + B\varphi = q + q_x' \tag{16}$$

where $q_k(x) = \sum_{r=1}^{p} q_{s,r}(x)v_{k,r}$ is the virtual work of the 0transversal loading and $q_{x,k}(x) = -\sum_{r=1}^{p} q_{x,r}(x)u_{k,r}$ is the virtual work of the axial loading. One extra term $q_{x,k}\delta\varphi_k\Big|_0^l$ is added to Eq. (15b).

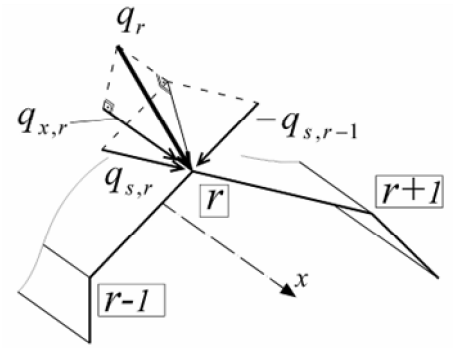

Figure 3. Transversal and axial components of an arbitrary node load

The third term of Eq. (5) *i.e.*, the variation of virtual work done by the critical buckling longitudinal normal stresses (σ_x^{cr}) has the expression

$$\delta\Pi_\sigma = \int_0^l\int_A \sigma_x^{cr}\delta\varepsilon_x^{M,NL}dAdx \tag{17}$$

The longitudinal normal stress is further expressed by *m* normal stress resultants and the warping functions u_j.

$$\sigma_x = -\sum_{j=1}^{m}\frac{W_j(x)u_j(s)}{C_{jj}} \tag{18}$$

One assumption is imposed, saying that all the critical stress resultants depend linearly on the same load parameter λ ($W_{j,cr} = \lambda W_{j,0}$). Using the geometrical relations from Eq. (1), Eq. (17) becomes

$$\delta\Pi_\sigma = \lambda\sum_{j=1}^{m}\sum_{i=2}^{n}\sum_{k=2}^{n}\int_0^l W_{j,0}X_{jik}\varphi_i'\delta\varphi_k'dx \tag{19}$$

X is called the stiffness degradation matrix due to acting membrane longitudinal stresses and it is defined as

$$X_{jik} = \frac{1}{C_{jj}} \int_s u_j (v_i v_k + w_i w_k) t ds \tag{20}$$

where j indicates the stress distribution, i indicates the elastic deformation and k indicates the equilibrium condition in which the variation of virtual work is computed. Notice that the elements of this matrix are also constant along the member length.

Now Eq. (5) gives the member equilibrium for the non-linear analysis.

$$C\mathrm{f}^{IV} - D\mathrm{f}'' + B\mathrm{f} + \mathrm{l} \sum_{j=1}^{m} X_{jik} \left(W_{i,0} \mathrm{f}' \right)' = 0 \tag{21}$$

The vector W^0 ($j = 1..m$) contains the resultants of the applied pre-buckling stresses, namely: (i) axial force $W_1^0 = N$, (ii) major and minor axis bending moments $W_2^0 = M_y$, $W_3^0 = M_z$, and (iii) bimoment $W_4^0 = B$, (so $m = 4$). The boundary conditions are:

$$\left(W_k - \mathrm{m} \sum_{i=2}^{n} D_{2,ik} \mathrm{f}_i \right) \mathrm{d}\mathrm{f}'_k \Big|_0^l = 0$$

$$\left(W'_k + \sum_{i=2}^{n} \left(D_{1,ik} - \mathrm{m} D_{2,ik} \right) \mathrm{f}'_i - \mathrm{l} \sum_{j=1}^{m} \sum_{i=2}^{n} X_{jik} W_j \mathrm{f}'_i \right) \mathrm{d}\mathrm{f}_k \Big|_0^l = 0 \quad for\ k = 2 \ldots n \tag{22a,b}$$

3.1.2 GBT for variable cross-sections

This chapter represents the original contribution of the candidate to the extension of GBT for variable cross-sections.

The study focused on thin-walled bars which have continuous cross-sectional variation according to the element axis. To determine the equilibrium equations, the same path explained in the previous chapter was followed, using the principle of virtual work. Eq. (9) becomes:

$$\mathrm{d}W_{\mathrm{s}_x^M} = \sum_{i=1}^{n} \sum_{k=1}^{n} \int_0^l \bar{C}_{ik}^M (x) \bar{\mathrm{f}}_i'' \mathrm{d}\bar{\mathrm{f}}_k'' dx \tag{23}$$

where $\bar{C}_{ik}^M (x) = \int_{A(x)} \bar{u}_i \bar{u}_k dA$ is no longer constant along the member's length even if the initial functions are chosen in the classical manner. By double integration the above equation becomes

$$\mathrm{d}W_{\mathrm{s}_x^M} = \sum_{i=1}^{n} \sum_{k=1}^{n} \left(\bar{C}_{ik}^M \bar{\mathrm{f}}_i'' \mathrm{d}\bar{\mathrm{f}}'_k \Big|_0^l - \bar{C}_{ik}^{M\prime} \bar{\mathrm{f}}_i'' \mathrm{d}\bar{\mathrm{f}}_k \Big|_0^l - \bar{C}_{ik}^M \bar{\mathrm{f}}_i''' \mathrm{d}\bar{\mathrm{f}}_k \Big|_0^l + \int_0^l \left(\bar{C}_{ik}^M \bar{\mathrm{f}}_i^{IV} + 2\bar{C}_{ik}^{M\prime} \bar{\mathrm{f}}_i''' + \bar{C}_{ik}^{M\prime\prime} \bar{\mathrm{f}}_i'' \right) \mathrm{d}\bar{\mathrm{f}}_k dx \right) \tag{24}$$

All the terms of Eq. (5) are determined in a similar way, as well as the diagonalisation process. The matrix D_2 is a stiffness matrix resulting from the evaluation of $\mathrm{d}W_{\mathrm{s}_x^B} = \int_0^l \int_A \mathrm{s}_x^B \mathrm{d}\mathrm{e}_x^B dA dx$ and usually its elements are extremely small comparing with the

other stiffness elements. For this reason the stiffness elements $D_{2,ik}'$ and $D_{2,ik}''$ are neglected in the following expressions.

In the case of linear analysis, the state of equilibrium is expressed by the following differential equations system:

$$\left(C\varphi''\right)'' - \left(D\varphi'\right)' + B\varphi = q + q_x' \tag{25}$$

with the boundary conditions:

$$\begin{aligned} &\left(W_k - \mu\sum_{i=1}^{n} D_{2,ik}\varphi_i\right)\delta\varphi_k'\Big|_0^l = 0 \\ &\left(W_k' - C_{kk}'\varphi_k'' + \sum_{i=1}^{n}\left(D_{1,ik} - \mu D_{2,ik}\right)\varphi_i'\right)\delta\varphi_k\Big|_0^l = 0 \quad for\ k = 1\ldots n \end{aligned} \tag{26a,b}$$

In the case of non-linear analysis, the differential equations system becomes

$$\left(C\varphi''\right)'' - \left(D\varphi'\right)' + B\varphi + \lambda\sum_{j=1}^{m}\left(X_{jik}W_{0,j}\varphi'\right)' = 0 \tag{27}$$

and the boundary conditions are

$$\begin{aligned} &\left(W_k - \mu\sum_{i=2}^{n} D_{2,ik}\varphi_i\right)\delta\varphi_k'\Big|_0^l = 0 \\ &\left(W_k' - C_{kk}'\varphi_k'' + \sum_{i=2}^{n}\left(D_{1,ik} - \mu D_{2,ik}\right)\varphi_i' - \lambda\sum_{j=1}^{m}\sum_{i=2}^{n} X_{jik}W_j\varphi_i'\right)\delta\varphi_k\Big|_0^l = 0 \quad for\ k = 2\ldots n \end{aligned} \tag{28a,b}$$

Derivation of the variable stiffness matrices C, D, B, X

(i) Analytical approach

An analytical approach was developed by the candidate for the special bar type for which all the section walls have constant thickness and the same variation law in width. This kind of tapering will be further referred as “uniform tapering”. Examples are given in Figure 4.

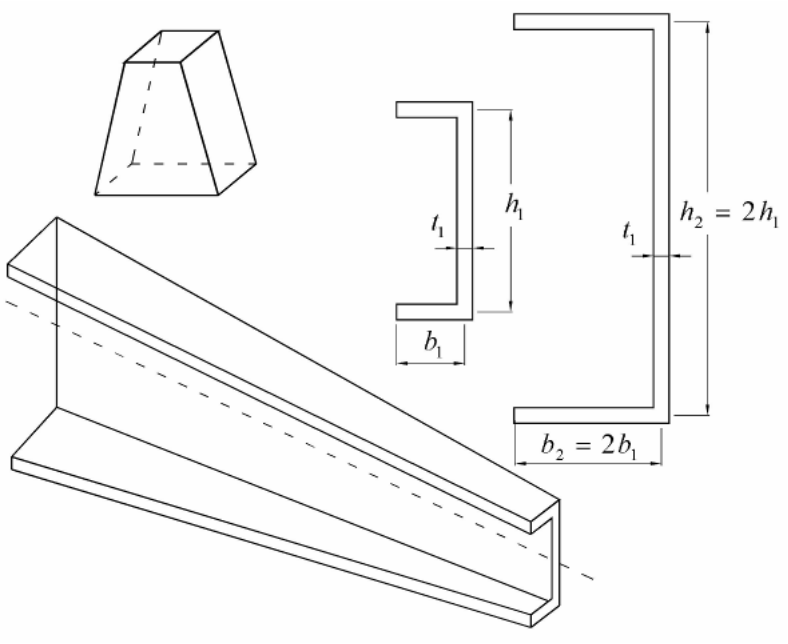

Figure 4. Examples of bars with uniform tapering

One considers that all the wall widths $b_r, r = 1..p$ have the same variation law described below

$$b_r(x) = b_{r0} g(x) \tag{29}$$

where $b_{r0}, r = 1..p$ are the wall widths in one arbitrary section x_0 and $g(x)$ defines the variation law. One example is given for the bar described in Figure 5.

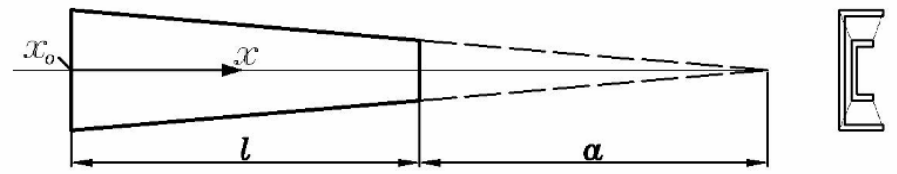

Figure 5. Description of the bar geometry

For this element the wall widths have linear variation and their expression is

$$b_r(x) = b_{r0} - \frac{b_{r0}}{l+a} x = b_{r0} \left(\frac{l+a-x}{l+a} \right) \tag{30}$$

Introducing the notation $g(x) = \left(\frac{l+a-x}{l+a} \right)$ one obtains Eq.(29).

One starts with the computation of the stiffness matrices in the initial state.

$$\bar{C}_{ik}^{M}(x) = E \int_{A(x)} \bar{u}_i \bar{u}_k dA = E \sum_{r=1}^{p} t_r \int_0^{b_r(x)} \bar{u}_i \bar{u}_k ds \tag{31}$$

The initial displacement functions are chosen in the classical manner described in the previous chapter and as a consequence, the initial warping displacements are functions independent of variable x. Introducing the notation $\mathsf{h} = s/b_r$ the warping function has the expression (see Figure 6a)

$$\bar{u}_r(s)=\bar{u}_{r,1}+\frac{\bar{u}_{r,2}-\bar{u}_{r,1}}{b_r}s=\bar{u}_{r,1}+\left(\bar{u}_{r,2}-\bar{u}_{r,1}\right)\eta \tag{32}$$

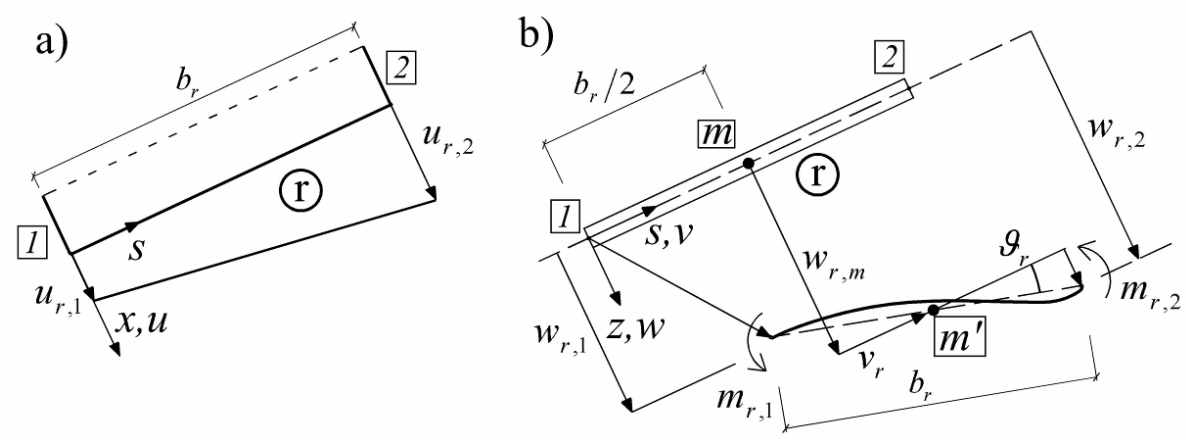

Figure 6. Unit deformation values of a cross-section wall r: a) warping function; b) displacements in the s-z plane

The elements of the primary warping stiffness matrix become

$$\begin{aligned}&\bar{C}^M_{ik}(x)=E\sum_{r=1}^{p}t_r b_r(x)\int_0^1\bar{u}_i\bar{u}_k d\eta=\\&=g(x)E\sum_{r=1}^{p}t_r b_{r0}\left(\frac{\bar{u}_{i,r1}\bar{u}_{k,r1}+\bar{u}_{i,r2}\bar{u}_{k,r2}}{3}+\frac{\bar{u}_{i,r1}\bar{u}_{k,r2}+\bar{u}_{i,r2}\bar{u}_{k,r1}}{6}\right)=g(x)\bar{C}^M_{0,ik}\end{aligned} \tag{33}$$

where $\bar{C}^M_{0,ik}$ are the elements of the primary warping stiffness matrix in section x_0.

This was the simplest situation because the initial warping displacements are independent of variable *x*. For the other stiffness matrices, the variation of the initial displacements of plane *s*-*z* along the member length must be evaluated (see Figure 6b). From the Vlasov's hypothesis $\gamma^{M,L}_{xs}=v'+\dot{u}=0$ and (3) we have for initial/unit transversal membrane displacements, the expression:

$$v_r=-\dot{u}_r(s)=-\frac{u_{r,2}-u_{r,1}}{b_r(x)}=-\frac{u_{r,2}-u_{r,1}}{b_{r0}g(x)}=g(x)^{-1}v_{r0} \tag{34}$$

The end-nodes flexural displacements *w* are given in [7] depending on the relative inclination ($\Delta\alpha_r$) between two adjacent walls and their transversal membrane displacements

$$w_{r-1,2}=\frac{v_r}{\sin\Delta\alpha_r}-\frac{v_{r-1}}{\tan\Delta\alpha_r},\quad w_{r,1}=\frac{v_r}{\tan\Delta\alpha_r}-\frac{v_{r-1}}{\sin\Delta\alpha_r} \tag{35}$$

Since the relative inclination is constant along *x* the variation law according to *x* results:

$$w_{r,1}=g(x)^{-1}w_{r0,1},\ w_{r,2}=g(x)^{-1}w_{r0,2} \tag{36}$$

One defines the middle flexural displacement as $w_{r,m}(x)=\frac{w_{r,1}+w_{r,2}}{2}$, the wall rotation in the cross-sectional plane as $\vartheta_r(x)=\frac{w_{r,2}-w_{r,1}}{b_r(x)}=g(x)^{-2}\vartheta_{r0}$ and the relative rotation between

adjacent walls as $\Delta \mathsf{J}_r(x) = \mathsf{J}_r(x) - \mathsf{J}_{r-1}(x) = g(x)^{-2} \Delta \mathsf{J}_{r0}$. Using the force method or the displacement method one obtains the values of the end-nodes moments for each wall:

$$m_{r,1} = g(x)^{-3} m_{r0,1}, \quad m_{r,2} = g(x)^{-3} m_{r0,2} \tag{37}$$

To write the flexural displacements w(s,x) by using the discrete values given in Figure 6 we use the expression given in [7], chapter 7:

$$w(\mathsf{h}, x) = w_{r,m} + \mathsf{J}_r(2\mathsf{h} - 1)\frac{b_r}{2} + \frac{m_{r,1} + m_{r,2}}{2}(\mathsf{h} - \mathsf{h}^2)\frac{b_r^2}{2K_r} - \frac{m_{r,2} - m_{r,1}}{2}(\mathsf{h} - 3\mathsf{h}^2 + 2\mathsf{h}^3)\frac{b_r^2}{6K_r}. \tag{38}$$

where K_r is the wall *r* bending stiffness. We see that:

$$w(s, x) = g(x)^{-1} w_{r0}(s) \tag{39}$$

From (12) and the integration aids given in [7], chapter 7, a general expression was determined by the candidate:

$$\overline{SM}(x) = g(x)^{\bar{\mathsf{z}}}\, \overline{SM}_0 \tag{40}$$

where $\overline{SM}$ stands for "stiffness matrix" in the initial state. The power of $g(x)$ is given in Table 1.

Table 1. The power of $g(x)$ for the initial stiffness matrices

$\overline{SM}$	$\bar{\mathsf{z}}$	$\overline{SM}$	$\bar{\mathsf{z}}$
${}^{ik}\bar{C}^M$	1	${}^{ik}\bar{D}_2$	-3
${}^{ik}\bar{C}^B$	-1	${}^{ik}\bar{B}$	-5
${}^{ik}\bar{D}_1$	-3	${}^{ijk}\bar{X}$	-2

During the diagonalisation process, using the Jacobi method in three stages, the eigenvalue vectors (the warping vectors $\tilde{u}$) are normalized in order to have a clear structural meaning. And so the elements of a final stiffness matrix receive different powers of $g(x)$. The introduction of the supplementary degrees of freedom corresponding to the intermediate node and independent end nodes (flexural displacements w_{in}) will further complicate the computations. It is easier to give the general expression of the unit displacement vectors (specified by "*udv*") in relation with the unit displacement vectors of section x_0 ("udv_0").

$$udv(x) = g(x)^{\mathsf{z}}\, udv_0 \tag{41}$$

where the power of $g(x)$ is given in Table 2.

Table 2. The power of $g(x)$ for the unit displacement vectors

udv	z	*udv*	z
${}^1u$	0	${}^4u$	2
${}^2u$	1	${}^ku, (k > 4)$	0
${}^3u$	1	w_{in}	2

The final stiffness matrices can be computed from Eq. (12) using the unit displacement functions instead of the initial ones or by the use of the modal matrix U which contains the unit displacement vectors in its columns. The final stiffness matrices are computed from the following relation

$$SM = U^T \cdot \overline{SM} \cdot U \tag{42}$$

(ii) Numerical approach

For arbitrary variable cross-section the author of this paper used a simple numerical approach. A mesh is defined along the bar length and in each mesh point the stiffness matrices are computed as described for members with constant cross-section. Knowing that the stiffness matrices are continuous functions of *x*, the intermediate values are computed by interpolation.

Illustrative Examples

The systems described by Eqs.(25) and (27) are coupled systems of ordinary differential equations of fourth order with boundary conditions described by (26a,b) and (28a,b), respectively. They were solved using a Runge-Kutta numerical method, namely the collocation method Lobatto IIIA of fourth order. This method uses a finite-dimensional space of candidate solutions for $\mathsf{f}_k(x)$ (usually, polynomials up to a certain degree) and a mesh of points ($0 < x_1 < x_2 <\ldots< L$) in the domain (the collocation points), and then selects the solution which satisfies the given differential equation at the collocation points. The solving method for boundary value problems is implemented in the Matlab programming language [20] through the function bvp4c.

(i) 1st order analysis of an element with open variable cross-section ("uniform tapering")

Eisenberg developed an analytical method to study this case of nonuniform torsion [9] and Sapountzakis, Mokos developed a boundary element method [10]. Both papers analyzed the metallic cantilever described in Figure 7, 40cm long and twisted at the free end by an end torque $M_t = 300 daNcm$. Material properties were taken as $E = 2.1\times10^6 daN/cm^2$ and $G = 8.05\times10^5 daN/cm^2$. No intermediate nodes were introduced. The stiffness matrices were evaluated by the analytical approach previously described and they are compared in Table 3 with the values obtained by Sapountzakis, Mokos. In this case we have the function $g(x) = 1 - \frac{x}{2l}$ taking values from 1 to 0.5. The unit displacement vectors u_4 can be calculated from (41) as: $u_4 = g(x)^2 \cdot u_{0,4}$, where the subscript "0" referrers to the fixed end of the cantilever. From (42) the final warping stiffness matrix is: $C(4,4) = u_4^T \cdot \overline{C(4,4)} \cdot u_4$. Since from (40), $\overline{C(4,4)} = g(x)\overline{C(4,4)_0}$, we can write the expression of the variable warping stiffness in its final form: $C(4,4) = g(x)^5 C(4,4)_0$ relation which can be easily checked from the last column of Table 3. Following the same algorithm the expression of the variable torsional stiffness is obtained: $D(4,4) = g(x)D(4,4)_0$.

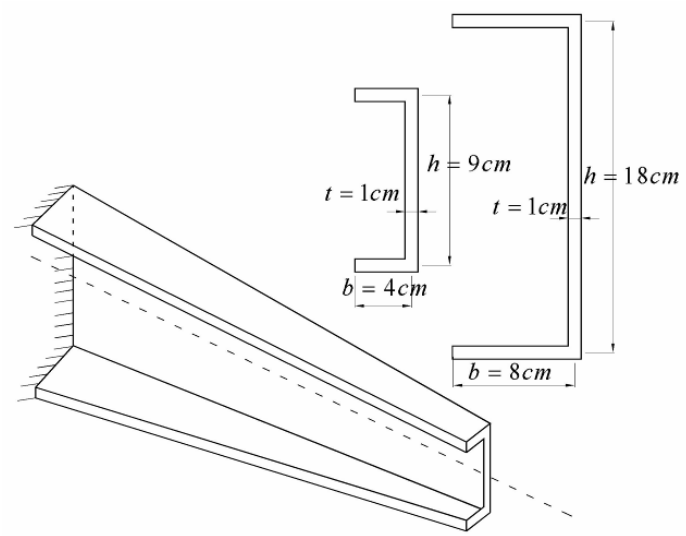

Figure 7. C section dimensions

Table 3. Torsional and warping stiffness - Sapountzakis, Mokos (GI_t , EC_M) vs. GBT ($D(4,4)$, $C(4,4)$)

Section no.	Distance (cm)	Sapountzakis, Mokos		GBT	
		GI_t [$daNcm^2$]	EC_M [$daNcm^4$]	$D(4,4)$ [$daNcm^2$]	$C(4,4)$ [$daNcm^4$]
1	0.0	9.1214E+06	2.6839E+10	9.1573E+06	2.6648E+10
2	3.158	8.7562E+06	2.1973E+10	8.7958E+06	2.1787E+10
3	7.368	8.2699E+06	1.6611E+10	8.3139E+06	1.6438E+10
4	11.579	7.7841E+06	1.2352E+10	7.8319E+06	1.2194E+10
5	15.789	7.2989E+06	0.9016E+10	7.3500E+06	0.8877E+10
6	20.000	6.8143E+06	0.6445E+10	6.868E+06	0.6324E+10
7	24.211	6.3301E+06	0.4498E+10	6.3860E+06	0.4395E+10
8	28.421	5.8464E+06	0.3054E+10	5.9041E+06	0.2969E+10
9	32.632	5.3631E+06	0.2008E+10	5.4221E+06	0.1939E+10
10	36.842	4.8802E+06	0.1271E+10	4.9402E+06	0.12181E+10
11	40.000	4.5183E+06	0.0876E+10	4.5787E+06	0.0833E+10

The twist angle at the free end:

- Eisenberg – $42.9340\times10^{-5}\,rad$
- Sapountzakis, Mokos - $42.19134\times10^{-5}\,rad$
- GBT for the variable cross-section - $42.5757\times10^{-5}\,rad$.

A comparison Eisenberg vs. GBT is given in Figure 8 regarding the twist angle and torsion moments (warping and St.Venant). A 3D deformation is shown in Figure 9 (the element mesh is used only for output values and graphical representation).

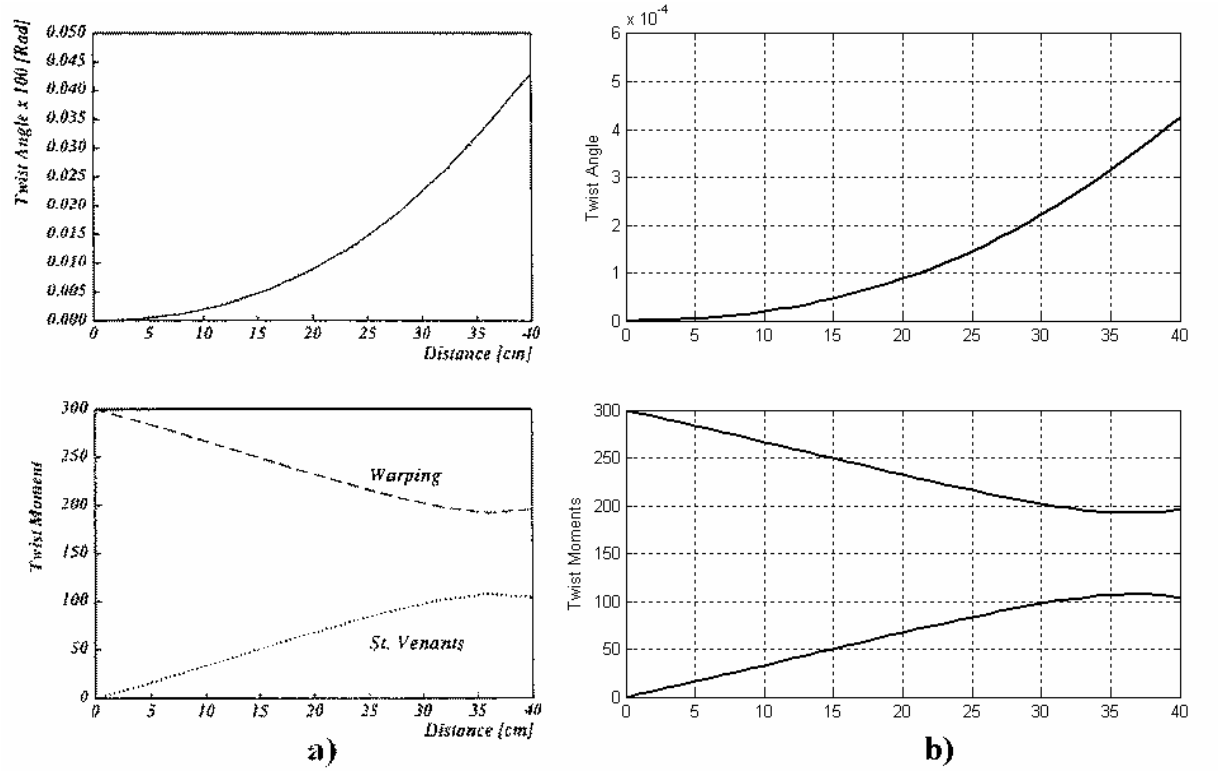

Figure 8. Eisenberg (a) vs. GBT (b) curves regarding the twist angle and torsion moments

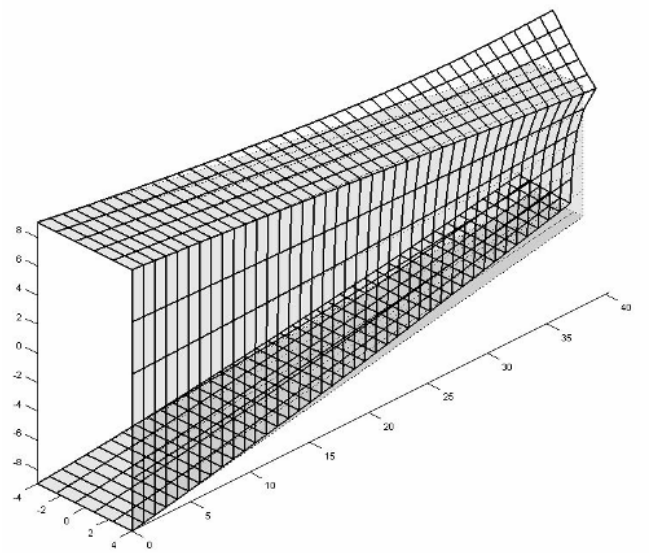

Figure 9. Example 1 – 3D deformation

(ii) 1st order analysis of an element with closed variable cross-section

Concerning single-cell closed cross-sections, the shear deformations of the cross-section mid-line induced by torsion cannot be considered using the Vlasov hypothesis of null membrane shear strain. An additional deformation mode is introduced by using the uniform shear flow hypothesis and following the Bredt formula, the term $G\int_s tv^2 ds$ obtained from the virtual work of the shear strains, is added to the components of stiffness matrix *D*.

Sapountzakis and Panagos developed in [21] using the analog equation method (AEM), a BEM-based method, an one-dimensional model capable to describe the behaviour of a Timoshenko beam with variable cross section undergoing large deflections under general

boundary conditions. The shear deformation effect was evaluated for linear and nonlinear analysis (regarding large deflections without stability loss). For the cantilever shown in Figure 10, loaded both axially by a distributed and a concentrated load and transversely by a distributed load, the GBT results are compared to the BEM (see Table 4) in terms of transverse deflection w and axial displacement u at the cantilever free end. In order to be consistent with the GBT hypotheses, the BEM values were taken from the linear analysis, neglecting the shear deformation effect.

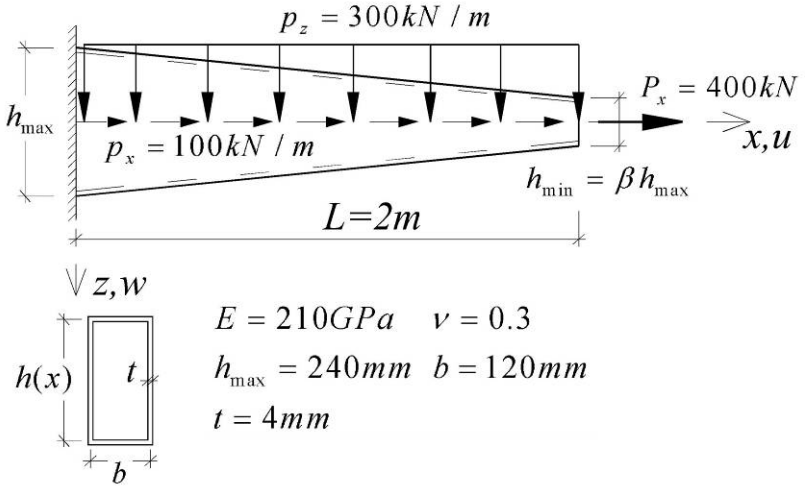

Figure 10. Cantilever beam with a hollow variable cross-section

Table 4. Displacements w and u at cantilever free-end and relative differences

b	w^{BEM} [cm]	w^{GBT} [cm]	Δ [%]	u^{BEM} [mm]	u^{GBT} [mm]	Δ [%]
0.67	15.554	15.106	2.97	1.902	1.854	2.59
0.5	17.232	16.863	2.19	2.039	1.984	2.77

(iii) buckling analysis of a column with open variable cross-section ("non-uniform tapering")

Ronagh et al. developed in [22] a theory regarding the nonlinear analysis of thin-walled beam/columns with tapered cross-sections. In [23] they used a finite element approach to investigate among others, the classical stability of the tapered column with a varying flange width shown in Figure 11. β is introduced as the "tapering ratio" and $\tan(\alpha/2)$ as the "tapering slope".

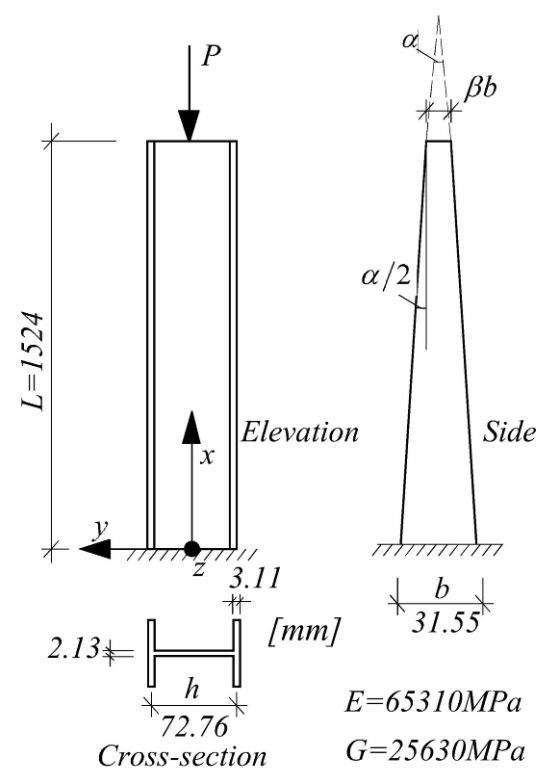

Figure 11. Tapered I-section cantilever column

At this slenderness there is no modal coupling, the global buckling occurs as bending over the minor axis. The critical load (Ronagh vs. GBT) is given in Figure12. The stiffness matrices were evaluated by the numerical approach previously described. No intermediary nodes were introduced and a longitudinal mesh of 5 points was enough to obtain accurate results.

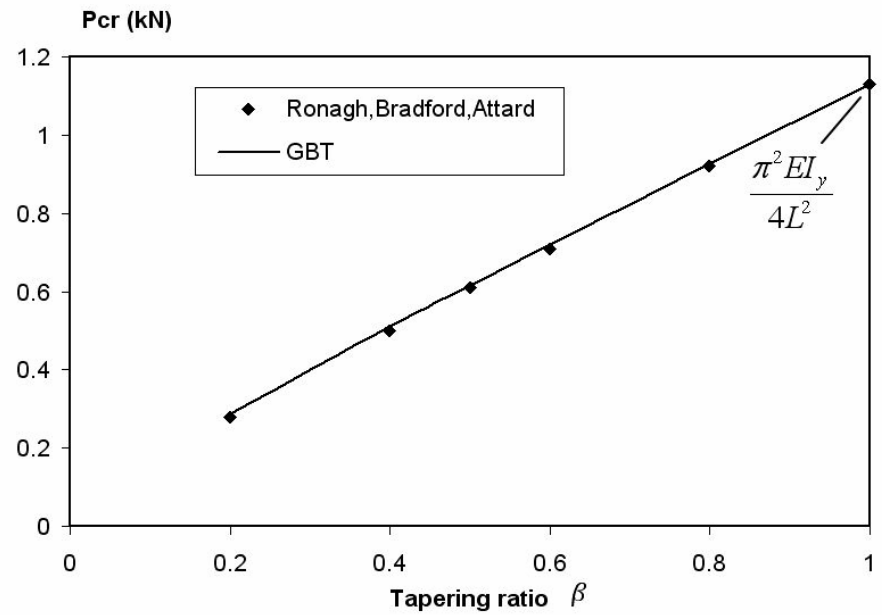

Figure12. Buckling load of tapered column

Next, the author investigated the structural response of the same element but with different lengths. A longitudinal mesh of 20 points was used. 7 intermediary nodes were introduced at equal intervals along the element web and this configuration gave 14 pure deformation modes. For this particular element, the first buckling mode occurs from a combination of odd pure modes which are presented in Figure 13.

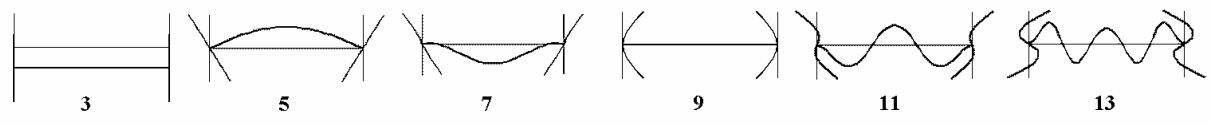

Figure 13. Cross-sectional plane deformations for the relevant pure deformation modes

Because of the greater contribution of pure modes 3, 5 and 7 to the general buckling, the corresponding elements from the main diagonal of the stiffness matrices are given in Table 5. The units used are *[kN, cm]*. The relative position 0.0 points to the fixed-end of the cantilever where all the stiffness elements are equal with the ones from the constant cross-section element. For the unit mode 3, the *D* and *B* stiffness elements are equal with 0 and the *X* stiffness elements are equal with -1.

Table 5. Stiffness matrices main diagonal elements 3, 5, 7

		C			*D*		*B*		*X*	
β	position	Modes: 3	5	7	5	7	5	7	5	7
1.0		10636.78	42.92	24.69	47.01	29.57	0.76	7.41	-0.34	-0.21
0.8	0.2	9415.31	39.97	25.67	44.79	34.02	0.751	8.173	-0.332	-0.215
	0.4	8291.51	37.30	26.76	42.62	39.48	0.745	9.100	-0.325	-0.224
	0.6	7261.30	34.90	27.96	40.51	46.19	0.739	10.228	-0.320	-0.234
	0.8	6320.61	32.75	29.27	38.46	54.41	0.733	11.604	-0.315	-0.245
	1.0	5465.38	30.84	30.67	36.47	64.45	0.729	13.285	-0.312	-0.257
0.6	0.2	8291.51	37.30	26.76	42.62	39.48	0.745	9.100	-0.325	-0.224
	0.4	6320.61	32.75	29.27	38.46	54.41	0.733	11.604	-0.315	-0.245
	0.6	4691.54	29.16	32.12	34.55	76.62	0.724	15.336	-0.309	-0.270
	0.8	3371.73	26.38	34.92	30.96	108.23	0.718	20.828	-0.308	-0.299
	1.0	2328.63	24.32	31.39	27.69	127.11	0.716	24.309	-0.311	-0.281
0.5	0.2	7764.96	36.07	27.35	41.56	42.66	0.742	9.636	-0.322	-0.229
	0.4	5465.38	30.84	30.67	36.47	64.45	0.729	13.285	-0.312	-0.257
	0.6	3674.47	27.01	34.26	31.83	99.38	0.719	19.261	-0.308	-0.292
	0.8	2328.63	24.32	31.39	27.69	127.11	0.716	24.309	-0.311	-0.281
	1.0	1364.29	22.56	28.06	24.09	156.36	0.722	31.571	-0.320	-0.281
0.4	0.2	7261.30	34.90	27.96	40.51	46.19	0.739	10.228	-0.320	-0.234
	0.4	4691.54	29.16	32.12	34.55	76.62	0.724	15.336	-0.309	-0.270
	0.6	2817.62	25.27	33.60	29.28	119.04	0.717	22.730	-0.309	-0.293
	0.8	1529.69	22.85	28.43	24.76	149.15	0.720	29.594	-0.318	-0.276
	1.0	717.87	21.61	29.86	21.11	210.53	0.743	49.533	-0.335	-0.366
0.2	0.2	6320.61	32.75	29.27	38.46	54.41	0.733	11.604	-0.315	-0.245
	0.4	3371.73	26.38	34.92	30.96	108.23	0.718	20.828	-0.308	-0.299
	0.6	1529.69	22.85	28.43	24.76	149.15	0.720	29.594	-0.318	-0.276
	0.8	534.07	21.46	27.09	20.14	199.37	0.761	51.708	-0.342	-0.368
	1.0	124.43	23.29	20.58	20.12	132.98	1.081	56.762	-0.369	-0.385

The proposed element was also modelled using the ABAQUS S4 [24] finite shell element and a comparison of the obtained buckling loads depending of the different tapering ratios is given in Figure 14. The modal participation diagram is given in Figure 15. It can be seen that the mode coupling is increasing for small lengths where the local buckling occurs (see Figure 16).

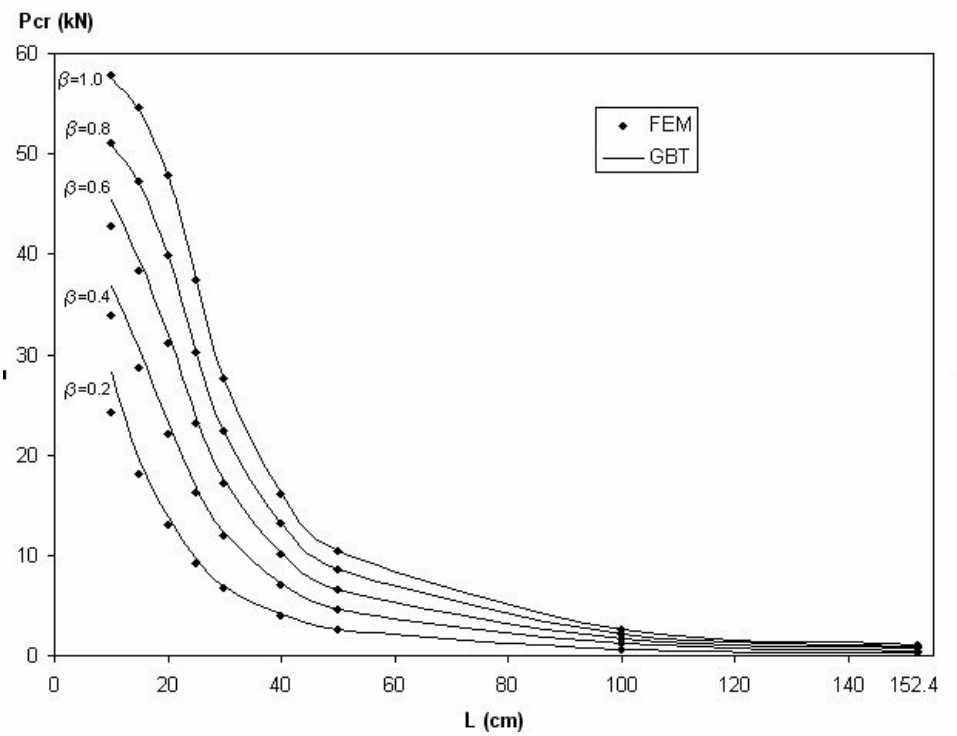

Figure 14. Critical buckling load vs. L.

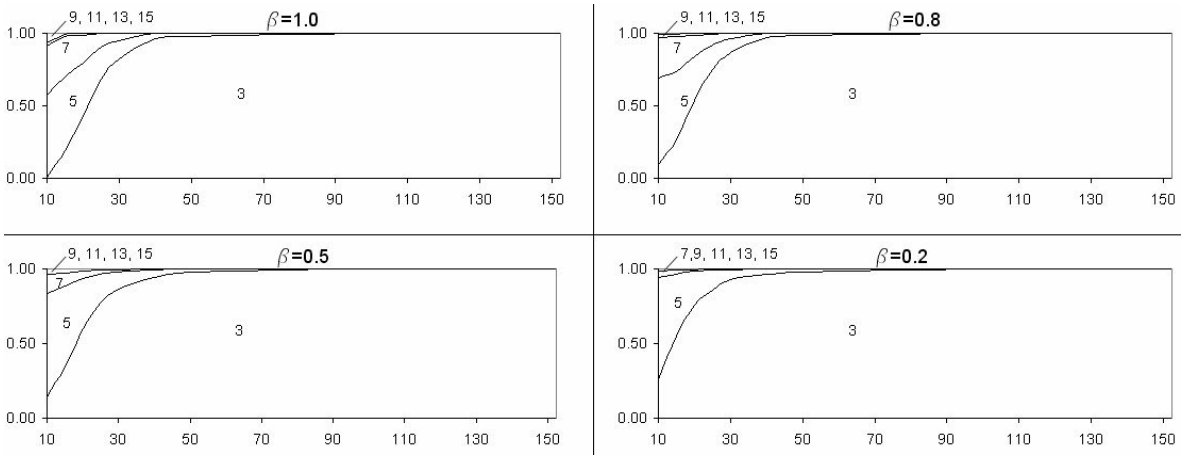

Figure 15. Modal participation diagram vs. L

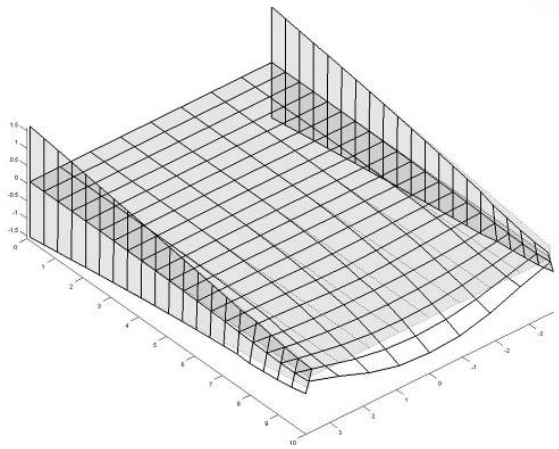

Figure 16. Buckling deformation for L=10cm

It can be seen how the difference between the GBT and FEM results (the "error") is increasing as the element becomes shorter and with smaller tapering ratios. This is normal because above certain values of the tapering slope, the approximation that the warping displacements are still perpendicular to the cross-sectional plane is no longer acceptable. In Figure 17 the error of the GBT values compared with the FEM results is given vs. the tapering slope. It can be concluded that the errors are acceptable as long as the tapering slope is not greater that 5%.

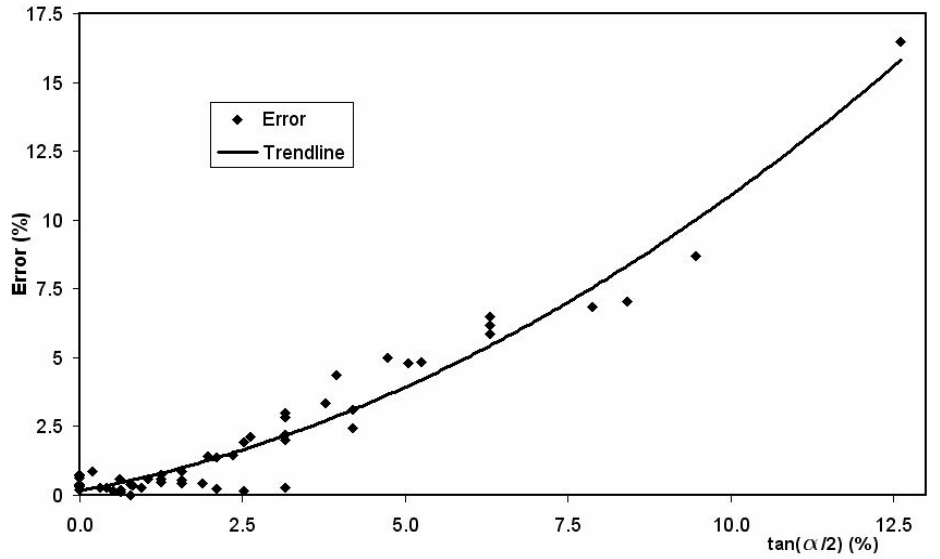

Figure 17. Error (%) vs. tapering slope (%)

(iv) buckling analysis of a beam with open variable cross-section

In this study the effect of the pre-buckling shear stresses was taken into consideration, following the formulation introduced by Bebiano et al. [25] that handles members subjected to variable bending moments. Eq. (5) describing the member equilibrium based on the principle of virtual work applied in its variational form, becomes

$$\mathrm{d}V = \mathrm{d}W_{\mathrm{int}} + \mathrm{d}\Pi_{\mathrm{s}} + \mathrm{d}\Pi_{\mathrm{t}} = 0 \tag{43}$$

where V is the member total potential energy, W is the member strain energy, Π_{s} and Π_{t} are the virtual works of the pre-buckling longitudinal normal and shear stresses. The last two terms of Eq. (43) are given as follows:

$$\mathrm{d}\Pi_{\mathrm{s}} = \int_0^l \int_A \mathrm{s}_{xx}^{0} \mathrm{d}e_{xx}^{M,NL} dA dx \qquad \mathrm{d}\Pi_{\mathrm{t}} = \int_0^l \int_A \mathrm{t}_{xs}^{0} \mathrm{d}g_{xs}^{M,NL} dA dx \tag{44}$$

The resulting system of equilibrium equations is expressed in modal form as follows ([25]):

$$EC_{ik}\mathrm{f}_k^{IV} - GD_{ik}\mathrm{f}_k'' + B_{ik}\mathrm{f}_k - \mathrm{l}\left[X_{jik}\left(W_j^{0}\mathrm{f}_k'\right)' - X_{jki}^{\mathrm{t}}\left(W_j^{0\prime}\mathrm{f}_k\right)' + X_{jik}^{\mathrm{t}}W_j^{0\prime}\mathrm{f}_k'\right] = 0 \tag{45}$$

where X and X^{t} are the cross-section geometrical stiffness matrices and it is important to underline that for prismatic elements they all have constant expressions according to x. All other terms in the above equation, were already explained. For tapered elements, taking into account that the components of the cross-section linear and geometrical stiffness matrices (C, D, B, X and X^{t}) are no longer constant according to x, new terms are added to the system

of equilibrium differential equations. In the case of non-linear analysis, the differential equations system becomes:

$$E\left(C_{ik}\mathsf{f}_k''\right)'' - G\left(D_{ik}\mathsf{f}_k'\right)' + B_{ik}\mathsf{f}_k - \mathsf{l}\left[\left(X_{jik}W_j^0\mathsf{f}_k'\right)' - \left(X_{jki}^{\mathrm{t}}W_j^{0\prime}\mathsf{f}_k\right)' + X_{jik}^{\mathrm{t}}W_j^{0\prime}\mathsf{f}_k'\right] = 0 \qquad (46)$$

For the validation of the present formulation, the numerical results given by Andrade et al. [26] were taken as reference. They developed a one-dimensional (1D) model capable to describe the lateral-torsional buckling behaviour of singly symmetric tapered thin-walled I-beams. They studied the critical loads for different types of I-cross-sections (equal and unequal flanges), tapering ratios and loading positions (top flange, centroid and bottom flange). The GBT formulation allows for the time being only centroidal loading but it is not restricted to a certain type of cross-section. The formulation described in this section is also capable to give the contribution of each pure deformation mode. For the following examples, the bending deformation mode after the major axis has the largest contribution (95-99%), followed by the torsional deformation mode (1-4%) and the other superior deformation modes (implying cross-sectional distortions) with less then 1%.

In the example shown in Figure 18 the tapering ratio $\mathsf{a} = 0.2$ was first applied to the member web and the results obtained by using the extended GBT formulation are compared with the values given in [26]. Next the same tapering ratio is applied to both web and flanges and the results are compared with values obtained from a FEA using ABAQUS S4R finite shell elements.

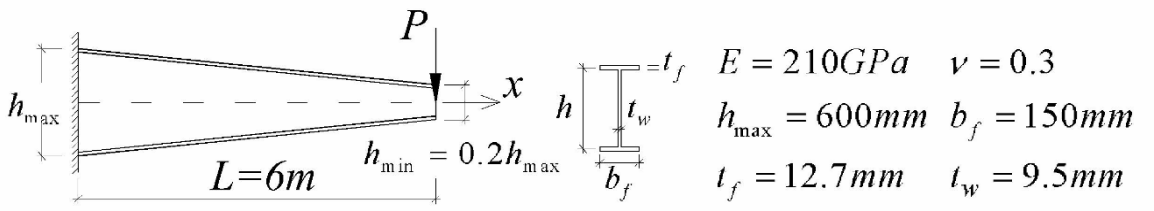

Figure 18. I-section cantilever: geometry, loading and material data

Table 6. Cantilever beams: linear critical loads (kN) and relative errors

Web-tapered cantilever (α=0.2)	P_{cr}^{GBT}	P_{cr}^{1D}	$\Delta(\%)$
	43,3	44,4	2,54
Web and flange-tapered cantilever (α=0.2)	P_{cr}^{GBT}	P_{cr}^{FEM}	$\Delta(\%)$
	12,1	11,9	1,51

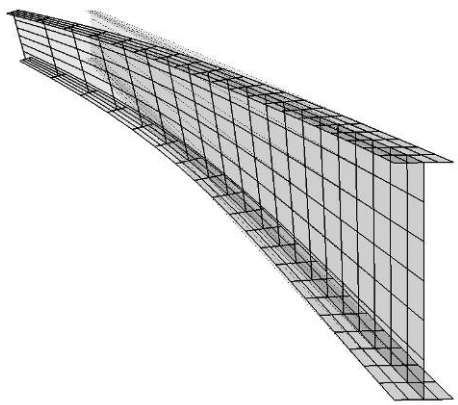

Figure 19. 1st buckling mode for web and flange-tapered cantilever

As a second example, one studies a cantilever with a different I-section and variable length for two tapering ratios applied to the member web (see Figure 20). Table 7 presents the values obtained by means of (i) GBT formulation, (ii) two-dimensional shell FEA and (iii) Andrade 1D analyses. It can be seen that the relative errors are under 5% with one exception concerning the prismatic cantilever (L = 4m) acted by a centroidal load. As it is explained in [26] this is due to the occurrence of a very localised web buckling phenomenon which was impossible to consider using the 1D model. The conventional GBT is theoretically able to represent any localised buckling by a combination of pure deformation modes but for this case, the number of these modes is extremely high and the analysis becomes similar with the ABAQUS FEA regarding the computational time. The value of P_{cr} given in Table 7 was obtained using 6 intermediate nodes for web and none for flanges, discretisation that yielded 13 deformation modes.

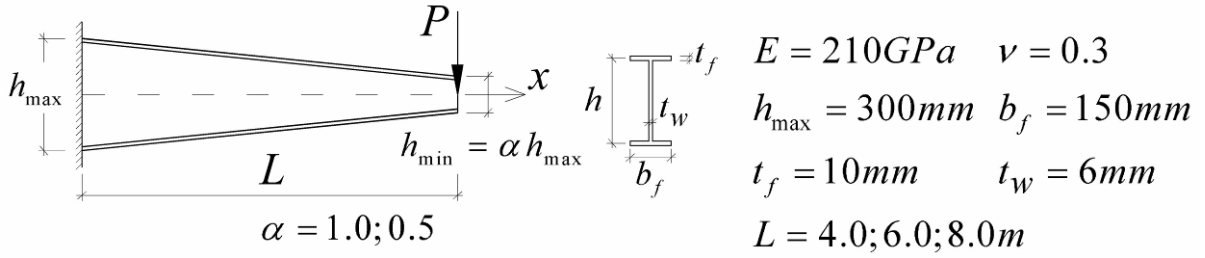

Figure 20. I-section cantilever: geometry, loading and material data

Table 7. Cantilever beams: linear critical loads (kN) and relative errors

Prismatic cantilever (α=1)				
L (m)	P_{cr}^{GBT}	P_{cr}^{FEM}	$\Delta(\%)$	P_{cr}^{1D}
4	53,6	47,4	13,08	58,8
6	20,8	20,2	2,97	21,3
8	10,5	10,4	0,96	10,6
Web-tapered cantilever (α=0,5)				
L	P_{cr}^{GBT}	P_{cr}^{FEM}	$\Delta(\%)$	P_{cr}^{1D}
4	53,7	53,5	0,28	56,6
6	20,3	20,3	0,15	20,5
8	10,0	10,2	2,51	10,2

(v) buckling analysis of a column with closed variable cross-section

This example studies the buckling of a tapered column with both ends fixed, rectangular hollow cross-section *b*x*h* and variable length for two tapering ratios applied to the cross-sectional height (see Figure 21). Figure 22 presents the first 10 most relevant deformation modes of the rectangular hollow cross-section. Table 8 presents the critical loads obtained by means of (i) GBT formulation, (ii) two-dimensional shell FEA using ABAQUS S4R finite shell elements and (iii) the relative differences. The deformation of the 1st buckling mode is a combination of deformation modes 6 (more than 90%) and 9. Figure 23 shows the buckling deformation obtained by FEA with L = 200mm and tapered ratio $b = 0.5$.

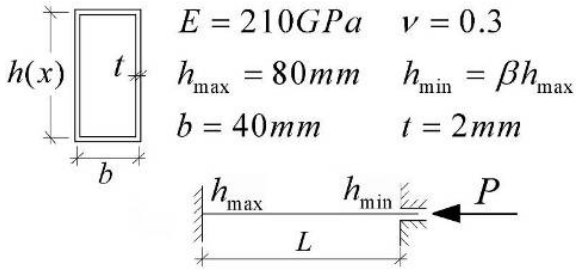

Figure 21. End fixed column

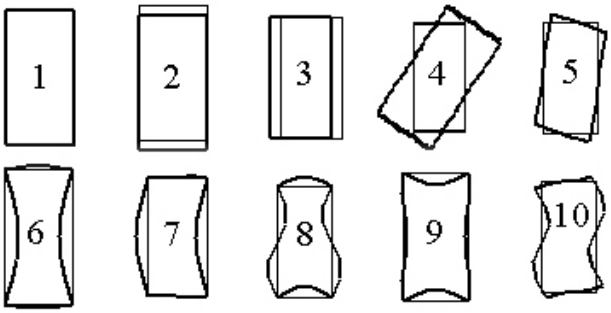

Figure 22. First 10 deformation mode shapes

Table 8. FEA vs. GBT results for the fixed member

L [mm]	b	P_{cr}^{FEA} [KN]	P_{cr}^{GBT} [KN]	Δ [%]
100	1	385,30	406,60	5,53
	0,5	493,15	516,40	4,71
200	1	321,50	326,77	1,63
	0,5	410,53	416,55	1,47
500	1	300,77	301,06	0,10
	0,5	362,18	368,80	1,83
1000	1	301,73	301,09	0,22
	0,5	351,41	358,96	2,15

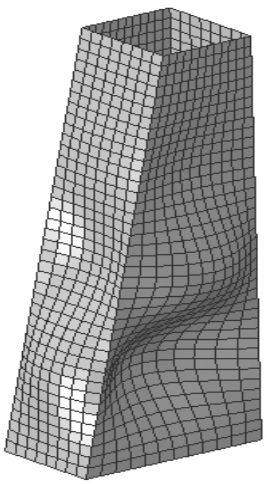

Figure 23. 1st buckling mode

(vi) buckling analysis of a hyperbolic tower

The formulation proposed by the candidate can be used to analyse truncated – conical and hyperbolic towers if their annular cross-section is approximated by a regular polygonal one.

For this example a concrete hyperbolic cooling tower was chosen, namely the Trojan tower, Portland Oregon USA, extensively analysed by Cole et al. [27]-[29] and presented in Figure 24. For the GBT approach, the annular cross-section was approximated by a regular dodecagon and each side had an intermediate node in its middle. This discretisation produced 25 unit deformation modes. Starting with a unit weight of $24\,kN/m^3$, the authors searched the concrete critical dead load for which the tower exhibits the bifurcation stability loss.

Recently, GBT formulations have been developed for thin-shells as circular and elliptical cylinders and tubes [30], [31] and conical shells (described in the next section). It was established that for axially loaded members, the critical shape is always described by one "shell-type" deformation mode characterized by a specific number of sine waves along the member cross-section. Using ABAQUS S4R finite shell elements, the buckling FEA of the Trojan Tower showed that the 1st buckling mode is described by 6 sine waves for a critical factor of λ = 26.7 (see Figure 24). Using the formulation described in this paper, a critical factor of λ = 27.4 emerged for the GBT mode 14 presented in Figure 25.

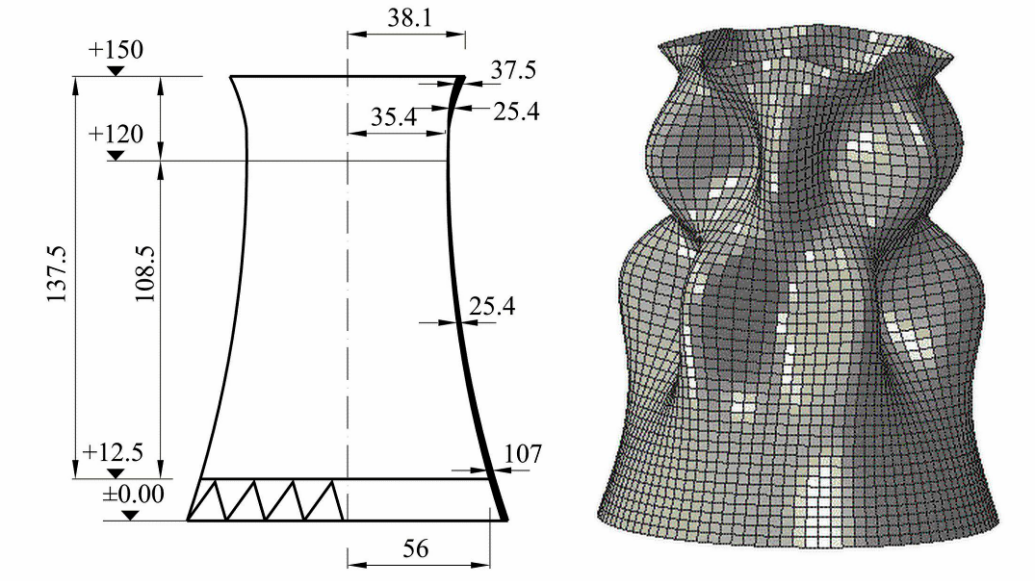

Figure 24. Trojan Tower and the 1st buckling mode

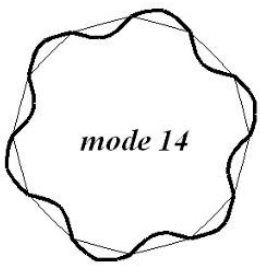

Figure 25. GBT cross-sectional mode no. 14

Conclusions

This section presented the GBT extension for bars with uniformly open and closed (one-cell) variable cross-section. The stiffness matrices are no longer constant along the bar length and because of that, the equilibrium differential equations gained new terms. For the 2nd order analysis only the effect of the pre-buckling longitudinal normal stresses was taken into account. The derivation of the variable stiffness matrices was made in two different ways: analytically for a special type of cross-section variation and numerically for a general variation law. For validation purposes, one investigated the structural response of a uniform

variable cross-section element subjected to torsion in a 1st order analysis, and the buckling behaviour of an element with different lengths and arbitrary cross-section variation. The obtained numerical values were compared to results already validated in the scientific community or obtained from FEM analysis. This formulation can be used to analyse truncated – conical and hyperbolic towers, if their annular cross-section is approximated by a regular polygonal one. In the end the candidate draws attention that the GBT extension presented here is applicable only for members with small tapering slopes (which, fortunately, cover a large amount of the thin-walled elements used in practice).

Personal Contribution

The candidate extended the GBT formulation in order to analyse *tapered* thin-walled members with small tapering slope, an achievement that changed the general accepted idea that GBT can analyse only prismatic members. This work improved the analysis of tapered thin-walled members, due to GBT's advantages: small number of DOF and buckling mode decomposition in pure deformation modes.

3.2 GBT formulation to analyse the buckling behaviour of isotropic conical shells

Introduction

Thin shells are widespread in many branches of engineering because of their efficient geometrical shape. Because of their thinness, the stability loss is often the main reason of failure. Extensive research on the buckling behaviour of cylindrical and conical shells is reported in literature. The solution of shell structures by linear theory has been widely investigated (Lorentz [32], Love [33], Donnell [34]). However, Donnell soon realized that in many problems the nonlinear effect is most significant and must be taken into account. Von Karman and Tsien [35] found the first accurate solution for geometrically 2nd order analysis.
Regarding the mechanical buckling of conical shells, numerous studies have been carried out. Seide [36], [37] studied the buckling of isotropic conical shells under the axial loading. Singer [38] considered the buckling of conical shells under the axisymmetrical external pressure. Baruch et al [39], [40], [41] studied the buckling of the stiffened/unstiffened conical shells under hydrostatic pressure and axial compression. Singer [42], [43] analyzed the buckling of orthotropic conical shells. Weigarten and Seide [44], [45] studied the stability of conical shells under the axial compression and external/internal pressure. Pariatmono and Chryssanthopoulos [46] and Spagnoli [47] showed that at a certain aspect ratio of an axially compressed conical shell, different buckling modes correspond to the same value of critical stress. Tong [48] suggested a simple formula for the critical buckling loads of laminated conical shells and assuming constant stiffness. Naj et al [49] studied the thermal and mechanical instability of conical shells made of functionally graded material.
Generally, the study of nonlinear behaviour of shell structures assumes large displacements and moderate rotations which is the case of the most common shell theories. (Donnell [50], Sanders [51], Love-Timoshenko [52]). Love [33] had presented the strain-displacement relations for a general shell from which Timoshenko and Woinowsky-Krieger [52], [53] derived the kinematic relations for a cylindrical shell. Recently, Goldfeld et al. [54] summarized the kinematic relations of these three shell theories and the differences between them can be easily detected. Goldfeld also made a valuable comparison between these shell theories in the context of buckling analysis of isotropic and laminated conical shells [55].
The author of GBT, R. Schardt studied the case of thin-walled members with circular hollow cross-section but only for 1st order (linear) analysis. Recently Silvestre [30], [31] developed a complete GBT methodology in order to analyse the buckling behaviour of circular and elliptical cylindrical shells and tubes.

In article 2 the candidate developed an original GBT-based formulation for the case of isotropic conical shells with constant thickness. Taking into account the member variable mechanical and geometric properties, new terms are added to the system of equilibrium differential equations. This new extended formulation will also accept members with constant cross-section (cylinders and tubes). The member stiffness matrices, variable along the longitudinal axis can be easily and efficiently computed.
In order to validate this new methodology, the buckling behaviour of thin-walled columns (compression members) having various boundary conditions is analysed. The GBT results obtained by the candidate are compared to values already presented in scientific literature or provided by shell finite element analyses.

Formulation proposed by the candidate

Consider the conical shell depicted in Figure 26, with length *L*, constant thickness *t* and semi-vertex angle α. Next we have the global coordinate system x_g, y_g, z_g and the local coordinate system x, θ, z, (meridional coordinate $x \in [0, L/\cos\alpha]$, circumferential coordinate $\theta \in [0, 2\pi]$ and normal coordinate $z \in [-t/2, +t/2]$). According to the local coordinate system we have the *u* (warping - meridional), *v* (transverse - circumferential) and *w* (flexural - normal) displacements. The conical shell radius has the expression $r = r_1 + x\sin\alpha$ ($r \in [r_1, r_2]$).

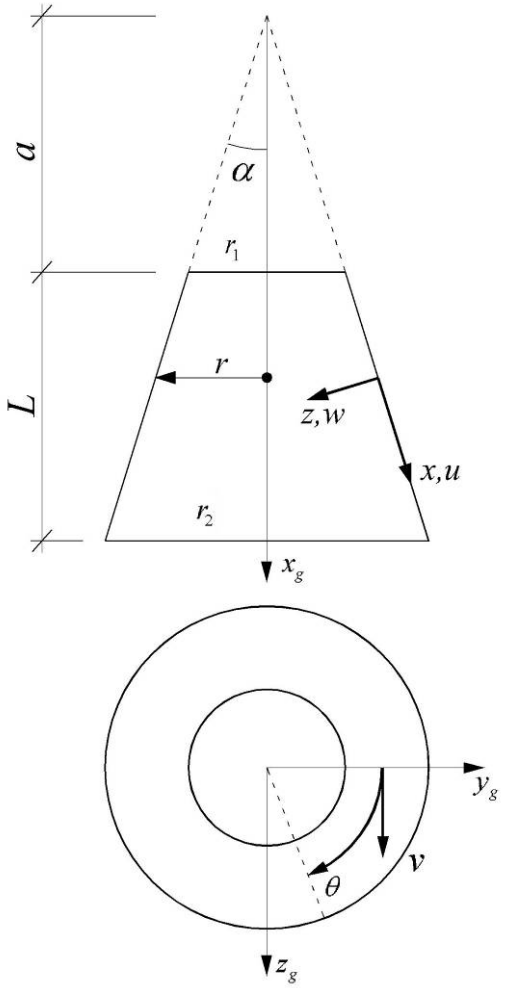

Figure 26. The geometry of the conical shell

The strain-displacement (kinematic) relation has the following form:

$$\{\varepsilon\} = \{\varepsilon^M\} + \{\varepsilon^B\} = \{\varepsilon^M\} + z\{\kappa\} \tag{47}$$

where $\{\varepsilon^M\}$ and $\{c\}$ are, respectively, the membrane strain (having linear and non-linear components) and change-of-curvature (bending) vectors of the reference surface, given as follows [54]:

$$\begin{aligned}
\varepsilon_{xx}^{M} &= \varepsilon_{xx}^{M,L} + \varepsilon_{xx}^{M,NL} = (u') + \left(\frac{w'^2}{2} + \delta_2 \frac{v'^2}{2} \right) \\
\varepsilon_{\theta\theta}^{M} &= \varepsilon_{\theta\theta}^{M,L} + \varepsilon_{\theta\theta}^{M,NL} = \left(\frac{\dot{v}}{r} + \frac{wc}{r} + \frac{us}{r} \right) + \left(\frac{1}{2} \left(\frac{\delta_1 vc - \dot{w}}{r} \right)^2 + \frac{\delta_2}{2} \left(\frac{\dot{v} + wc}{r} \right)^2 \right) \\
\gamma_{x\theta}^{M} &= \gamma_{x\theta}^{M,L} + \gamma_{x\theta}^{M,NL} = \left(\frac{\dot{u}}{r} + v' - \frac{vs}{r} \right) + \left(\frac{w'\dot{w}}{r} - \delta_1 \frac{vw'c}{r} + \delta_2 \frac{v'\dot{v}}{r} \right) \\
c_{xx} &= -w'' \\
c_{\theta\theta} &= -\frac{\ddot{w}}{r^2} - \frac{w's}{r} + \delta_1 \frac{\dot{v}c}{r^2} \\
c_{x\theta} &= 2\left[-\frac{\dot{w}'}{r} + \frac{\dot{w}s}{r^2} + \delta_1 \frac{c}{r} \left(\frac{v'}{2} - \frac{vs}{r} \right) \right]
\end{aligned} \tag{48}$$

where $c = \cos(\alpha)$, $s = \sin(\alpha)$, $()' = \partial()/\partial x$, $\dot{()} = \partial()/\partial\theta$.

The coefficients δ_1 and δ_2 represent specific shell theories ($\delta_1 = \delta_2 = 0$ for Donnell's [50], $\delta_1 = 1$ and $\delta_2 = 0$ for Sanders' [51], $\delta_1 = \delta_2 = 1$ for Love-Timoshenko [52]). Being the most *exact* theory, the last one was adopted by the candidate.

Using the GBT representation, the mid-surface displacements *u*, *v* and *w* are written as a combination of orthogonal functions:

$$u = \sum_{k=1}^{n} \bar{u}_k(x,\theta),\ v = \sum_{k=1}^{n} \bar{v}_k(x,\theta),\ w = \sum_{k=1}^{n} \bar{w}_k(x,\theta) \tag{49}$$

where *n* is the number of deformation modes. Each *k* function is expressed as a product of two functions:

$$\bar{u}_k(x,\theta) = u_k(\theta) f_k(x) \quad \bar{v}_k(x,\theta) = v_k(\theta) g_k(x) \quad \bar{w}_k(x,\theta) = w_k(\theta) h_k(x) \tag{50}$$

We introduce now the Vlasov's null membrane shear strain and transverse extension hypotheses.

$$\gamma_{x\theta}^{M,L} = 0 \Rightarrow \frac{\dot{u}}{r} + v' - \frac{vs}{r} = 0 \tag{51}$$

$$\varepsilon_{\theta\theta}^{M,L} = 0 \Rightarrow \frac{\dot{v}}{r} + \frac{wc}{r} + \frac{us}{r} = 0 \tag{52}$$

Now in order to obtain a GBT formulation we need to reduce the number of functions from Eq. (50) from six to only two (one function depending of θ and one depending of *x*). This is relatively easy for the cylindrical shell where the membrane shear strain and transverse extension are described only by the first two components of Eqs. (51) and (52). This is done by choosing the functions of Eq. (50) in the following manner:

$$f_k(x) = r(x)\mathsf{f}_k'(x) \qquad g_k(x) = h_k(x) = \mathsf{f}_k(x)$$
$$v_k(\mathsf{q}) = -\dot{u}_k(\mathsf{q}) \qquad w_k(\mathsf{q}) = \frac{\ddot{u}_k(\mathsf{q})}{c} \tag{53}$$

Using this approach, components $-vs/r$ and us/r are producing membrane strains and so the hypotheses of Eqs. (51) and (52) are no longer valid. To overcome this problem the formulation described here approximates the infinitesimal conical shell element (of length *dx*) with a cylindrical shell element from the point of view of the membrane strains. The radius varies no longer continuously but it has discrete values for any element of length *dx* as shown in Figure 27.

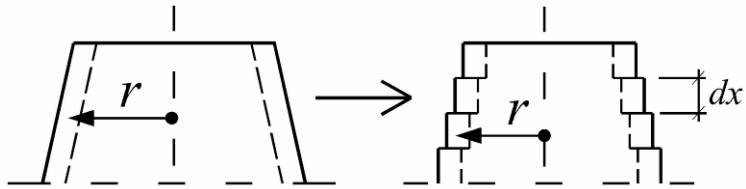

Figure 27. Geometry idealization of the conical shell for the membrane behaviour analysis

From Eqs. (50) and (53) the orthogonal functions of displacement become:

$$\bar{u}_k(x,\mathsf{q}) = u_k(\mathsf{q})r(x)\mathsf{f}_k'(x) \qquad \bar{v}_k(x,\mathsf{q}) = -\dot{u}_k(\mathsf{q})\mathsf{f}_k(x) \qquad \bar{w}_k(x,\mathsf{q}) = \frac{\ddot{u}_k(\mathsf{q})}{c}\mathsf{f}_k(x) \tag{54}$$

where $u_k(\mathsf{q})$ is a "unit warping function" defined along the cross-section circumference and $\mathsf{f}_k(x)$ is a "displacement amplitude function" defined along the member length *L*.

The kinematic relations (48) become:

$$\begin{aligned}
\mathsf{e}_{xx}^{L} &= u_k r\mathsf{f}_k'' - z\frac{\ddot{u}_k}{c}\mathsf{f}_k'' \\
\mathsf{e}_{\mathsf{qq}}^{L} &= -z\left(\frac{\dddot{u}_k/c + \ddot{u}_k c}{r^2}\mathsf{f}_k + \frac{\ddot{u}_k s}{rc}\mathsf{f}_k'\right) \\
\mathsf{g}_{x\mathsf{q}}^{L} &= 2z\left(\frac{-2\ddot{u}_k/c - \dot{u}_k c}{2r}\mathsf{f}_k' + \frac{\ddot{u}_k s/c + \dot{u}_k sc}{r^2}\mathsf{f}_k\right) \\
\mathsf{e}_{xx}^{NL} &= \frac{1}{2}\left[\frac{\ddot{u}_k\ddot{u}_i}{c^2} + \dot{u}_k\dot{u}_i\right]\mathsf{f}_k'\mathsf{f}_i' \\
\mathsf{e}_{\mathsf{qq}}^{NL} &= \frac{1}{2}\frac{\left(\dot{u}_k c + \ddot{u}_k/c\right)\left(\dot{u}_i c + \ddot{u}_i/c\right)}{r}\mathsf{f}_k\mathsf{f}_i \\
\mathsf{g}_{x\mathsf{q}}^{NL} &= \left(\frac{\ddot{u}_k}{c}\frac{\ddot{u}_i/c + \dot{u}_i c}{r} + \frac{\dot{u}_k\ddot{u}_i}{r}\right)\mathsf{f}_k'\mathsf{f}_i
\end{aligned} \tag{55}$$

The first variation of strain energy is now considered.

$$\mathsf{d}W = \int_L \oint \int_t \left(\mathsf{s}_{xx}^{L}\mathsf{de}_{xx}^{L} + \mathsf{s}_{\mathsf{qq}}^{L}\mathsf{de}_{\mathsf{qq}}^{L} + \mathsf{t}_{x\mathsf{q}}^{L}\mathsf{dg}_{x\mathsf{q}}^{L} + \mathsf{s}_{xx}^{o}\mathsf{de}_{xx}^{NL} + \mathsf{s}_{\mathsf{qq}}^{o}\mathsf{de}_{\mathsf{qq}}^{NL} + \mathsf{t}_{x\mathsf{q}}^{o}\mathsf{dg}_{x\mathsf{q}}^{NL}\right)dzrd\mathsf{q}\,dx = 0 \tag{56}$$

where s_{xx}^{o}, $\mathsf{s}_{\mathsf{qq}}^{o}$ and $\mathsf{t}_{x\mathsf{q}}^{o}$ are the pre-buckling meridional, circumferential and shear stresses due to the applied loads.

The constitutive relations related to the relevant stress components are written:

$$\mathsf{s}_{xx}^{M,L} = E\mathsf{e}_{xx}^{M,L} \tag{57}$$

$$\{\sigma^B\} = \begin{Bmatrix} s^B_{xx} \\ s^B_{qq} \\ t^B_{xq} \end{Bmatrix} = \frac{E}{1-m^2} \begin{bmatrix} 1 & m & 0 \\ m & 1 & 0 \\ 0 & 0 & \dfrac{1-m}{2} \end{bmatrix} \{\varepsilon^B\} \tag{58}$$

Using the kinematic relations Eq. (55) and the constitutive relations Eqs. (57), (58), the strain energy variation becomes:

$$\begin{aligned} dW = \int_L \Big[& C_{ik} f_k'' df_i'' + D^1_{ik} f_k' df_i' + D^2_{ik} f_k df_i'' + D^2_{ki} f_k'' df_i + B_{ik} f_k df_i + G_{ik} f_k df_i' + G_{ki} f_k' df_i \\ & + X^{sx}_{jik} f_k' df_i' + X^{sq}_{jik} f_k df_i + X^{t}_{jik} \left(f_k df_i' + f_k' df_i \right) \Big] dx \end{aligned} \tag{59}$$

The tensors of the above equation are the result of the integration on the conical shell circumference and thickness, of the corresponding displacement functions and their expressions are given below:

$$\begin{aligned} C_{ik} &= \oint \left(A_1^* u_k u_i r^2 + D_1^* \frac{\ddot{u}_k \ddot{u}_i}{c^2} \right) r dq \\ D^1_{ik} &= \oint \left(D_1 \frac{\ddot{u}_k \ddot{u}_i}{r^2} \frac{s^2}{c^2} + D_3 \frac{2\dddot{u}_k / c + \dot{u}_k c}{r} \frac{2\dddot{u}_i / c + \dot{u}_i c}{r} \right) r dq \\ D^2_{ik} &= \oint \left(D_2 \frac{\dddot{u}_k / c^2 + \ddot{u}_k}{r^2} \ddot{u}_i \right) r dq \\ B_{ik} &= \oint \left(D_1 \frac{\dddot{u}_k / c + \ddot{u}_k c}{r^2} \frac{\dddot{u}_i / c + \ddot{u}_i c}{r^2} + 4 D_3 \frac{\ddot{u}_k s / c + \dot{u}_k sc}{r^2} \frac{\ddot{u}_i s / c + \dot{u}_i sc}{r^2} \right) r dq \\ G_{ik} &= \oint \left(D_1 \frac{\dddot{u}_k / c + \ddot{u}_k c}{r^2} \frac{\ddot{u}_i s}{rc} + D_3 \frac{2\left(\ddot{u}_k s / c + \dot{u}_k sc\right)}{r^2} \frac{-2\ddot{u}_i / c - \dot{u}_i c}{r} \right) r dq \\ X^{sx}_{jik} &= \oint \left[s^o_{xx} \left(\frac{\ddot{u}_k \ddot{u}_i}{c^2} + \dot{u}_k \dot{u}_i \right) \right] t r dq \\ X^{sq}_{jik} &= \oint \left[s^o_{qq} \frac{\dot{u}_k c + \ddot{u}_k / c}{r} \frac{\dot{u}_i c + \ddot{u}_i / c}{r} \right] t r dq \\ X^{t}_{jik} &= \oint \left[t^o_{xq} \left(\frac{\ddot{u}_k}{c} \frac{\ddot{u}_i / c + \dot{u}_i c}{r} + \frac{\dot{u}_k \ddot{u}_i}{r} \right) \right] t r dq \end{aligned} \tag{60}$$

where $A_1^* = Et$, $D_1^* = Et^3/12$, $D_1 = D_1^*/(1-m^2)$, $D_2 = m D_1$ and $D_3 = E/2(1+m) \cdot t^3/12$.

C, D^1, D^2, G and B are mechanical stiffness matrices related with the generalized warping, twisting and transverse bending (cross-sectional distortion). X^{sx}_{jik}, X^{sq}_{jik}, X^{t}_{jik} are the elements of the geometric stiffness matrices taking into account the 2nd order effect of the pre-buckling meridional, circumferential and shear stresses, respectively, associated with the deformation mode *j*.

It is important to underline that the elements of the stiffness matrices are not *constant* along the member longitudinal axis as long as the value of the semi-vertex angle a is different of zero (the radius *r* is a function of *x*).

The expression of strain energy variation (Eq.(59)) contains the variation of $\delta f_i'$ and $\delta f_i''$. In order to eliminate these components several integrations by parts are performed. The variational equation receives the following form:

$$\begin{aligned}\delta W = \int_L \Big[& C_{ik} f_k^{IV} + 2C'_{ik} f_k''' + \left(C''_{ik} - D^1_{ik} + D^2_{ik} + D^2_{ki} - X^{sx}_{jik}\right) f_k'' + \\ & + \left(-D^{1\prime}_{ik} + 2D^{2\prime}_{ik} + G_{ki} - G_{ik} - X^{sx\prime}_{jik}\right) f_k' + \left(D^{2\prime\prime}_{ik} + B_{ik} - G'_{ik} + X^{sq}_{jik} - X^{t\prime}_{jik}\right) f_k \Big] \delta f_i dx \\ & + \left[-C_{ik} f_k''' - C'_{ik} f_k'' + \left(D^1_{ik} - D^2_{ik} + X^{sx}_{jik}\right) f_k' + \left(-D^{2\prime}_{ik} + G_{ik} + X^{t}_{jik}\right) f_k \right] \delta f_i \Big|_0^L \\ & + \left(C_{ik} f'' + D^2_{ik} f_k\right) \delta f_i' \Big|_0^L = 0\end{aligned} \tag{61}$$

The first term describes equilibrium along its length, and the other two describe the boundary conditions. The above expression would greatly simplify if all the mechanical stiffness matrices involved would be diagonal. This will assume that for any $k \neq i$, the set of warping functions $u_k(q)$ satisfy the orthogonality conditions:

$$\oint u_k u_i dq = 0, \quad \oint \ddot{u}_k \ddot{u}_i dq = 0, \quad \oint \ddot{u}_k \dot{u}_i dq = 0 \ etc. \tag{62}$$

Fortunately for the circular cross-section such functions exist and they are extensively used (ex. [7], [30]) (for other types of cross-sections the complete diagonalisation is not possible).

Shell-type modes

There are two independent sets of trigonometric functions:

$$u_k = \begin{cases} \sin(mq), \ m = k/2, & k = 2,4,6,....n \\ \cos(mq), \ m = (k-1)/2, & k = 3,5,7,....n+1 \end{cases} \tag{63}$$

which satisfy all the orthogonality conditions and define the so called *shell-type* deformation modes. Figure 28 presents the cross-sectional deformations of the first 12 shell-type modes:

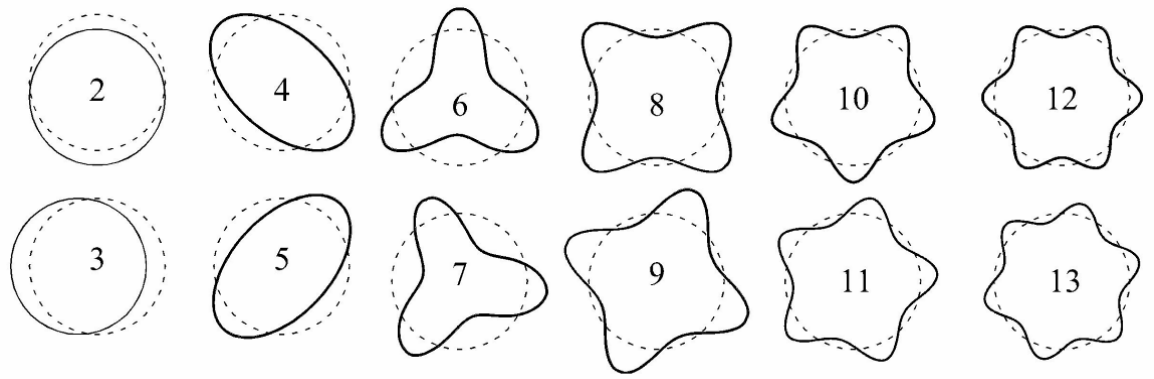

Figure 28. Shell-type deformation modes

Introducing the meridional displacement expressions of Eq. (63) into Eq. (60), the cross-section mechanical and geometric properties for each deformation mode are obtained, as well as their derivatives according to *x*:

$$
\begin{aligned}
&C_{kk} = A_1^* \pi r^3 + D_1^* \frac{\pi m^4}{c^2} r,\ C_{kk}' = 3A_1^* \pi r^2 s + D_1^* \frac{\pi m^4}{c^2} s,\ C_{kk}'' = 6A_1^* \pi r s^2 \\
&D_{kk}^1 = D_1 \frac{\pi m^4 (s/c)^2}{r} + D_3 \frac{\pi m^2}{r}\left(\frac{2m^2}{c} - c\right)^2 \\
&D_{kk}^1{}' = -D_1 \frac{\pi m^4 s^3/c^2}{r^2} - D_3 \frac{\pi s m^2}{r^2}\left(\frac{2m^2}{c} - c\right)^2 \\
&D_{kk}^2 = D_2 \frac{\pi m^4}{r}\left(1 - \frac{m^2}{c^2}\right),\ D_{kk}^2{}' = -D_2 \frac{\pi s m^4}{r^2}\left(1 - \frac{m^2}{c^2}\right),\ D_{kk}^2{}'' = D_2 \frac{2\pi s^2 m^4}{r^3}\left(1 - \frac{m^2}{c^2}\right) \\
&B_{kk} = D_1 \frac{\pi m^4}{r^3}\left(\frac{m^2}{c} - c\right)^2 + D_3 \frac{4\pi m^2}{r^3}\left(m^2 s/c - sc\right)^2 \\
&G_{kk} = D_1 \frac{\pi m^4 s/c}{r^2}\left(c - \frac{m^2}{c}\right) - D_3 \frac{2\pi m^2 s}{r^2}\left(\frac{2m^4}{c^2} - 3m^2 + c^2\right) \\
&G_{kk}{}' = -D_1 \frac{2\pi m^4 s^2/c}{r^3}\left(c - \frac{m^2}{c}\right) + D_3 \frac{4\pi m^2 s}{r^3}\left(\frac{2m^4}{c^2} - 3m^2 + c^2\right) \\
&X_{jkk}^{\sigma x} = \sigma_{xx}^{o} \pi m^2 tr\left(\frac{m^2}{c^2} + 1\right) \\
&X_{jkk}^{\sigma q} = \sigma_{qq}^{o} \frac{\pi m^2 t}{r}\left(\frac{m^2}{c^2} - c\right)^2 \\
&X_{jkk}^{\tau} = \tau_{xq}^{o} \frac{\pi m^3 t}{c}\left(\frac{m^2}{c} + c\right)
\end{aligned}
\tag{64}
$$

The derivatives of the geometric properties are not given because of the unknown nature of the pre-buckling stresses $\sigma_{xx}^{o}, \sigma_{qq}^{o}$ and τ_{xq}^{o}. These have to be calculated by a previous 1st order analysis and normally they introduce the bifurcation stress coefficient λ_b.

Extension mode

The extension mode is described by the following displacement field (see Figure 29a):

$$u_e = 1/r,\ v_e = 0,\ w_e = -s/(rc) \tag{65}$$

With these relations the extension mode is in agreement with the null membrane shear strain and transverse extension hypotheses.

$$\gamma_{xq}^{M,L} = 0\ ,\ \varepsilon_{qq}^{M,L} = \left(\frac{\dot{v}}{r} + \frac{wc}{r} + \frac{us}{r}\right) = 0 \tag{66}$$

Axisymmetric mode

Because of the of null transverse extension assumption ($\varepsilon_{qq}^{M,L} = 0$) the shell-type modes are inextensible in the circumferential direction. For the axisymmetric mode the assumption is no longer valid and the displacement field is given (see Figure 29b):

$$u_a = v_a = 0,\ w_a = 1 \tag{67}$$

Torsion mode

Because of the null transverse membrane shear strain ($\gamma_{xq}^{M,L} = 0$) the shell-type modes are shear undeformable. The torsion mode is introduced by the following displacement field (see Figure 29c):

$$u_t = w_t = 0,\ v_t = r \tag{68}$$

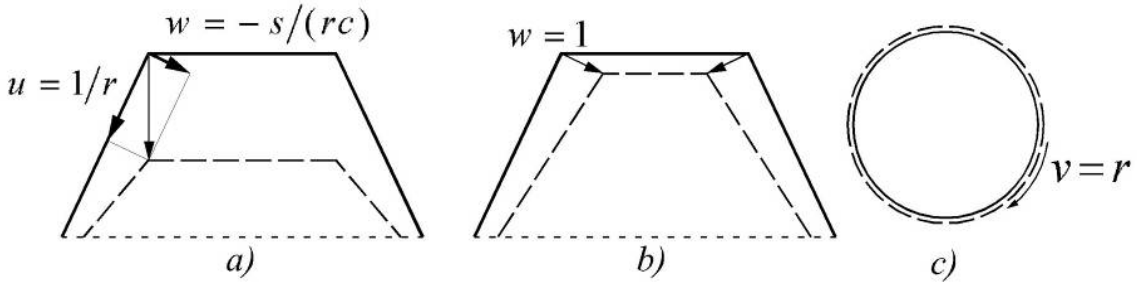

Figure 29. Displacement field for a)extension mode, b) axisymmetric mode, c) torsion mode

Numerical Solution

Knowing that δf_i are arbitrary kinematically admissible functions, the variational equation (61) leads to the following system of ordinary differential equilibrium equations:

$$\begin{aligned} &C_{kk} f_k^{IV} + 2C'_{kk} f_k''' + \left(C''_{kk} - D^1_{kk} + 2D^2_{kk} - X^{sx}_{jkk}\right) f_k'' + \left(-D^{1\prime}_{kk} + 2D^{2\prime}_{kk} - X^{sx\prime}_{jkk}\right) f_k' \\ &+ \left(D^{2\prime\prime}_{kk} + B_{kk} - G^{\prime}_{kk} + X^{sq}_{jkk} - X^{t\prime}_{jkk}\right) f_k = 0 \end{aligned} \tag{69}$$

Generally, the equation system is coupled because the geometric stiffness matrices don't have a diagonalised form. There is however the case of a conical shell under axial compression for which X^{sx} is a diagonal matrix while X^{sq} and X^{t} are zero matrices. The system presented above constitutes also a one-dimensional eigenvalue problem. The solution of this system leads to the value of bifurcation stress coefficient λ_b (the eigenvalues) and the corresponding buckling mode shapes (the eigenfunctions f_k). It is clear now that the theory uses bar elements instead of the two or three-dimension representations of the conical shell, a feature that is the main characteristic of GBT.

In the last two terms, Eq. (61) also describes the boundary conditions which are given below for different support conditions:

i) simply supported (locally and globally) end section:

$$f_k = 0, \quad C_{kk} f_k'' + D^2_{kk} f_k = 0 \tag{70}$$

ii) fixed end section:

$$f_k = f_k' = 0 \tag{71}$$

iii) free end section:

$$\begin{aligned} &-C_{kk} f_k''' - C'_{kk} f_k'' + \left(D^1_{kk} - D^2_{kk} + X^{sx}_{jkk}\right) f_k' + \left(-D^{2\prime}_{kk} + G_{kk} + X^{t}_{jkk}\right) f_k = 0 \\ &C_{kk} f_k'' + D^2_{kk} f_k = 0 \end{aligned} \tag{72}$$

The GBT eigenvalue problem can be solved by different methods like finite difference method [7], FEM [56], Galerkin method [30], etc. The results presented in this paper were obtained through the application of a Runge-Kutta numerical method, namely the collocation method Lobatto IIIA of fourth order [57]. This method uses a finite-dimensional space of

candidate solutions for $f_k(x)$ (usually, polynomials up to a certain degree) and a mesh of points ($0 < x_1 < x_2 < ... < L$) in the domain (the *collocation* points), and then selects the solution which satisfies the given differential equation at the collocation points.

Illustrative Examples

The GBT application is presented in this section through the buckling analysis of conical columns (compression members) with different end conditions. Consider the steel conical shell depicted in Figure 30, ($E = 210GPa, \nu = 0.3$) with a wall thickness $t = 1$ mm and length $L = 1200mm$. The starting radius is taken $r_1 = 50mm$ and the end radius r_2 is variable. The pre-buckling meridional stress is calculated in the classic manner:

$$\sigma_{xx}^{o} = P/(2\pi rtc) \tag{73}$$

where $P = \lambda_b P_0$. The minimum bifurcation load coefficient is introduced as $\lambda_c = \lambda_{b,\min}$ or critical load coefficient. The initial value of the axial load was taken as $P_0 = 2\pi r_1 \cdot 1kN/mm \simeq 314.16kN$.

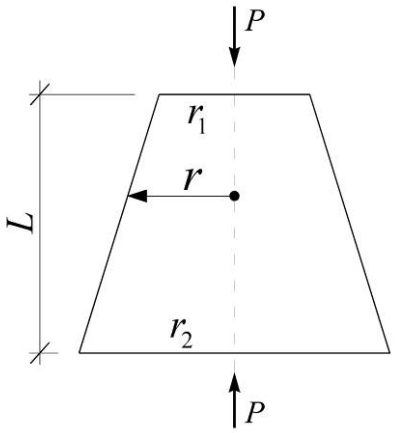

Figure 30. Conical shell under axial compression

The critical load coefficient ($\lambda_{c,FE}$) and the corresponding buckling mode shapes for several values of r_2 were obtained using ABAQUS code and a mesh of shell finite elements S4R.

(i) Simply supported members

The conical shell is locally and globally simply supported to both end sections, meaning the member is free to warp but the *v* and *w* displacements are locked. The critical buckling mode shape is given by means of two parameters: (i) *k* - the cross-sectional deformation mode and (ii) *n* - the number of longitudinal half-waves of $f_k(x)$. For a cylindrical shell ($r_1 = r_2 = 50mm$) the critical load coefficient was found as $\lambda_{c,GBT} = 1.564$ which gives a critical stress value of $\sigma_c = 1564N/mm^2$. These numerical results are in perfect agreement with the estimates obtained by Silvestre [30]. Table 9 shows a comparison between the critical load coefficients obtained by FEM and GBT for various values of r_2.

Table 9. FEM vs. GBT results for simply supported members

r_2	$l_{c,FEM}$	$l_{c,GBT}$	Error (%)	k/n
50	1.561	1.564	0.19	4/2
60	1.572	1.596	1.53	4/2
70	1.672	1.720	2.87	4/2
90	1.795	1.776	1.07	4/1
100	1.664	1.655	0.54	4/1
120	1.562	1.550	0.77	4/1
150	1.587	1.605	1.13	4/1
200	1.930	1.990	3.11	4/1
300	2.141	2.143	0.09	6/1
400	1.943	1.950	0.36	6/1
500	1.996	2.018	1.10	6/1
1000	1.531	1.485	3.10	8/1

Figure 31 presents the critical buckling mode shapes and the corresponding load coefficients obtained using shell FEA, for several values of r_2. Figure 32 presents the normalized modal amplitude functions.

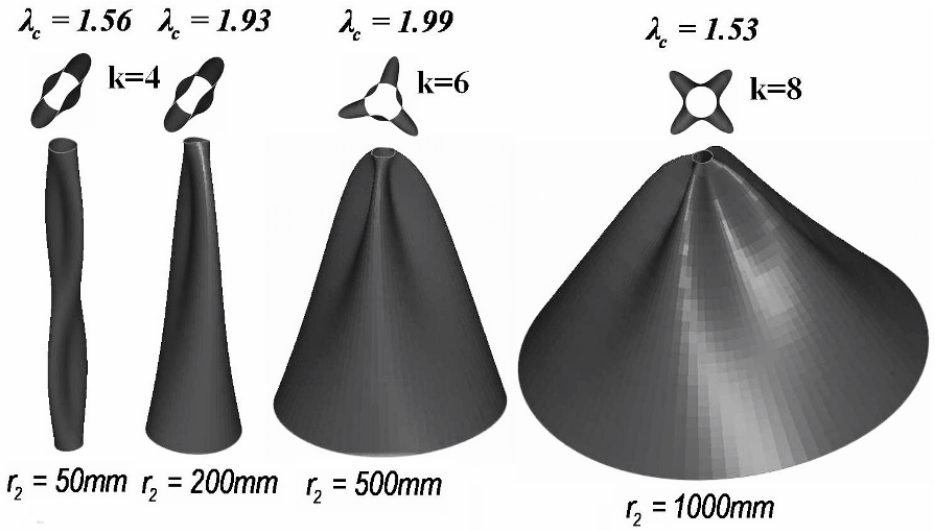

Figure 31. Simply supported members: critical buckling mode shapes, load coefficients

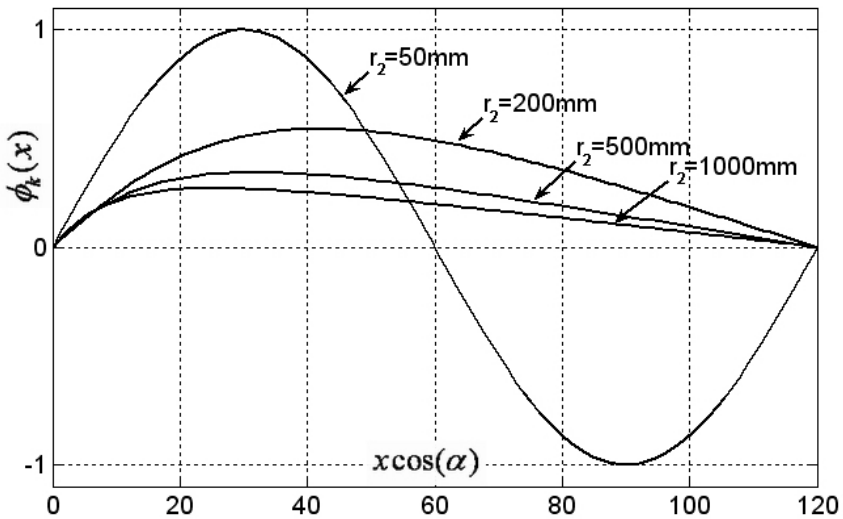

Figure 32. Simply supported members: modal amplitude functions

(ii) End fixed members

Both end section of the conical shell are fixed, meaning that all the displacements (*u, v, w*) are considered locked. Table 10 shows the good agreement between the GBT numerical results and the estimates obtained by FEM (four of them are shown in Figure 33).

Table 10. FEM vs. GBT results for fixed members

r_2	$\lambda_{c,FEM}$	$\lambda_{c,GBT}$	Error (%)	k
50	2.120	2.15	1.42	4
60	2.420	2.47	2.07	4
70	2.318	2.39	3.11	6
90	2.408	2.45	1.74	6
100	2.493	2.542	1.97	6
120	2.619	2.706	3.32	6
150	2.635	2.652	0.65	8
200	2.765	2.738	0.99	8
300	2.673	2.738	2.43	10
400	2.781	2.845	2.30	10
500	2.549	2.626	3.02	12
1000	1.876	1.955	4.21	14

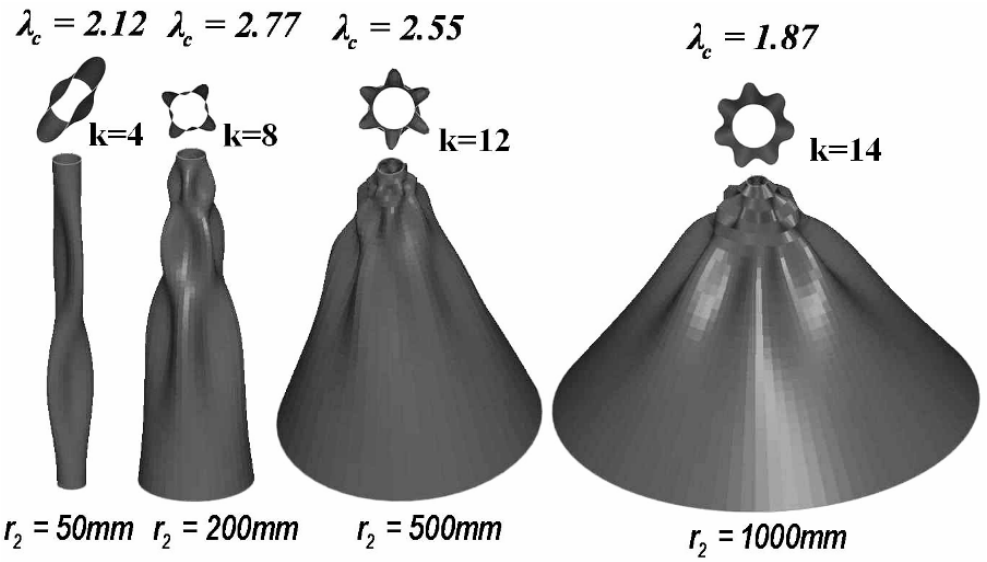

Figure 33. End fixed members: critical buckling mode shapes, load coefficients

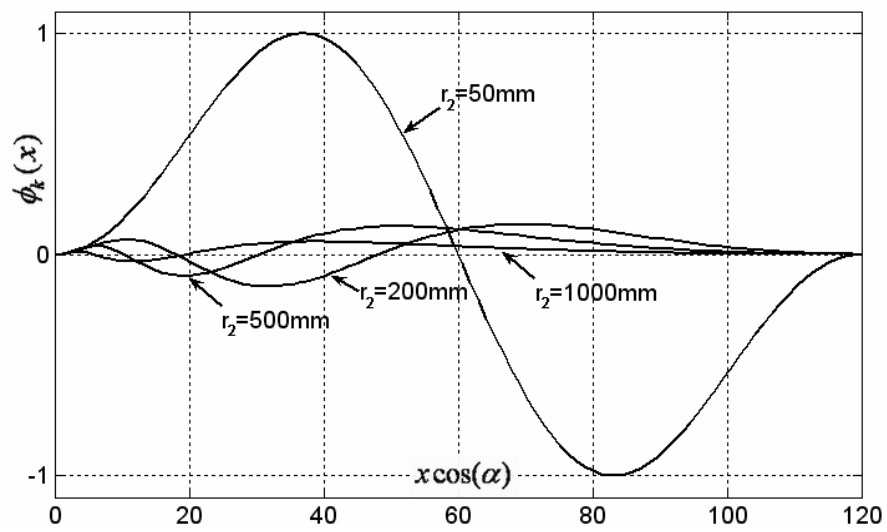

Figure 34. End fixed members: modal amplitude functions

(iii) Cantilever members

The conical shell is free at the end section of radius r_1 and fixed at the end section of radius r_2 as depicted in Figure 35. At the free end, the axial load P is applied by an uniformly distributed load $q_{xg} = P/(2\pi r_1)$. From this vertical load rise the pre-buckling meridional stress of Eq. (73) and also the lateral circumferential load $q_\theta = q_{xg} s/c$.

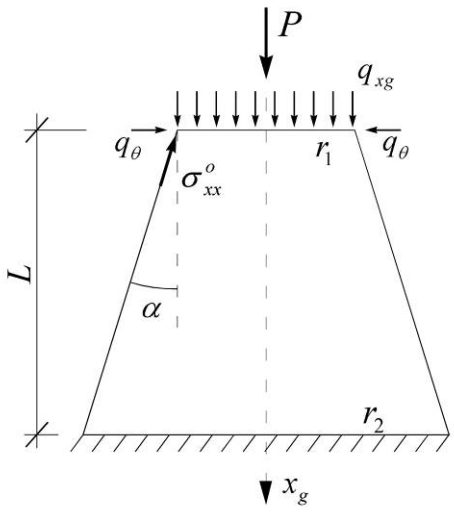

Figure 35. Cantilever member under axial compression

The effect of this load is the pre-buckling circumferential stress defined as [58]:

$$\sigma^o_{\theta\theta} = q_\theta \frac{r_1}{t} = \frac{Ps}{2\pi tc} \tag{74}$$

The local effect of $\sigma^o_{\theta\theta}$ is null for simply supported or fixed end section, but for the free end section can no longer be neglected. The new component of the strain energy variation at the end section $x = 0$ (see Figure 35) is given by:

$$\delta W_{\sigma^o_{\theta\theta}} = \oint\int_t \sigma^o_{\theta\theta}\delta\varepsilon^{NL}_{\theta\theta} dz r d\theta = X^{s\theta}_{jik}\varphi_k \delta\varphi_i\Big|_0 \tag{75}$$

This new component is added to the boundary conditions of Eqs. (61) and (72). From its expression given by Eq. (64) and using Eq. (74), the geometric stiffness matrix $X^{s\theta}_{jik}$ becomes:

$$X_{jik}^{sq} = \frac{Ps}{2r_1 c} m^2 \left(\frac{m^2}{c^2} - c \right)^2 \tag{76}$$

The comparison between the FEM and GBT critical stress values is given in Table 11, and once again four FEM buckling results are depicted in Figure 36 and Figure 37.

Table 11. FEM vs. GBT results for cantilever members

r_2	$l_{c,FEM}$	$l_{c,GBT}$	Error (%)	k
50	0.440	0.445	1.14	2
60	0.648	0.650	0.31	2
70	0.704	0.712	1.14	4
90	0.680	0.700	2.94	4
100	0.693	0.697	0.58	4
120	0.612	0.640	4.58	6
150	0.524	0.547	4.39	6
200	0.428	0.444	3.74	6
300	0.303	0.307	1.32	8
400	0.240	0.240	0.13	6
500	0.188	0.188	0.05	6
1000	0.115	0.111	3.60	6

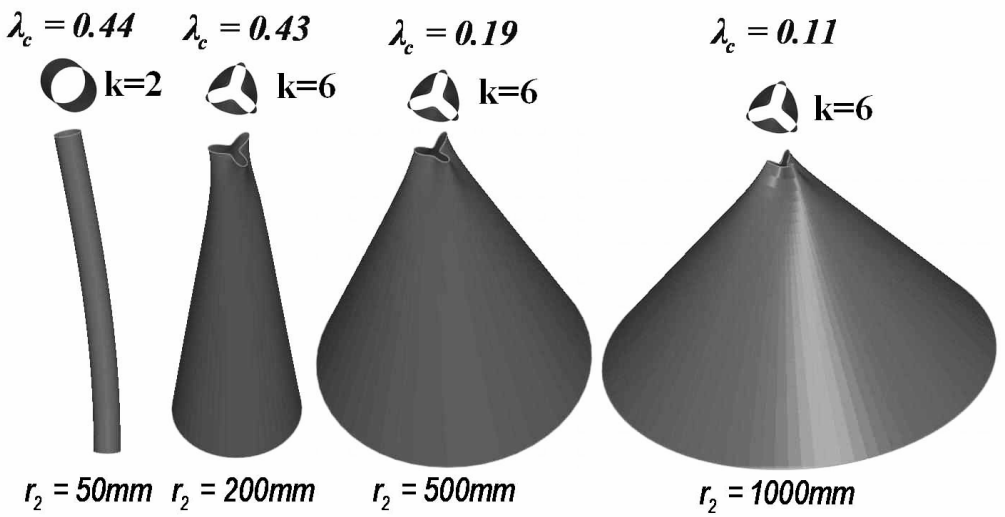

Figure 36. Cantilever members: critical buckling mode shapes, load coefficients

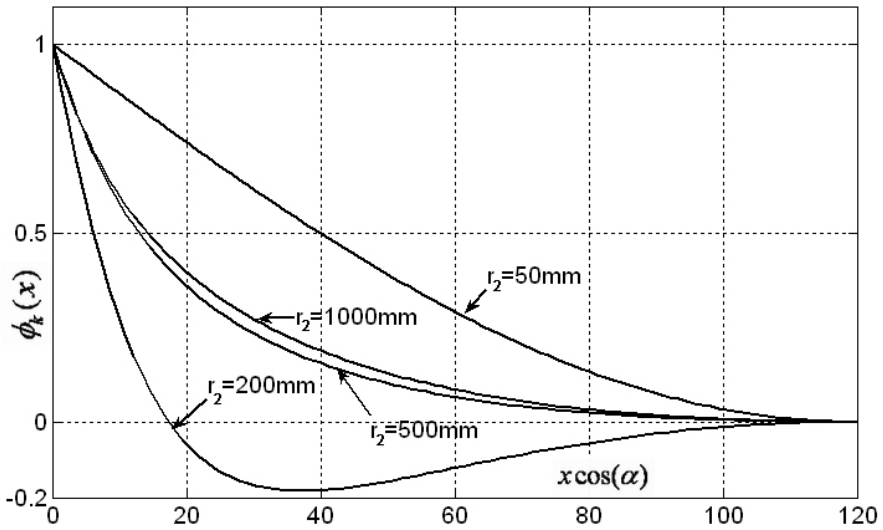

Figure 37. Cantilever members: modal amplitude functions

Until this point, the elastic buckling behaviour of isotropic conical shells with constant thickness under axial compression was presented here but the new GBT formulation also covers the buckling behaviour of conical shells in compression axisymmetric mode, or acting as beams (flexural members), beam-columns and shafts (torsion members). The GBT application for these cases was first presented in article 6 and is briefly given below.

The GBT application is presented through the buckling analysis of conical shell members subjected to i) compression, ii) bending, and iii) torsion (see Figure 38). The steel conical shell ($E = 210 GPa, \nu = 0.3$) has a wall thickness $t = 1$ mm , the starting radius is $r_1 = 50 mm$ and the end radius r_2 is variable. The loads were taken as:

$$P_0 = \lambda_c 2\pi r_1 t \cdot \sigma_0 , M_0 = \lambda_c \pi r_1^2 t \cdot \sigma_0 , M_{t0} = \lambda_c 2\pi r_1^2 t \cdot \tau_0 \tag{77}$$

where λ_c is the minimum bifurcation load coefficient and $\sigma_0 = \tau_0 = 1000 N / mm^2$.

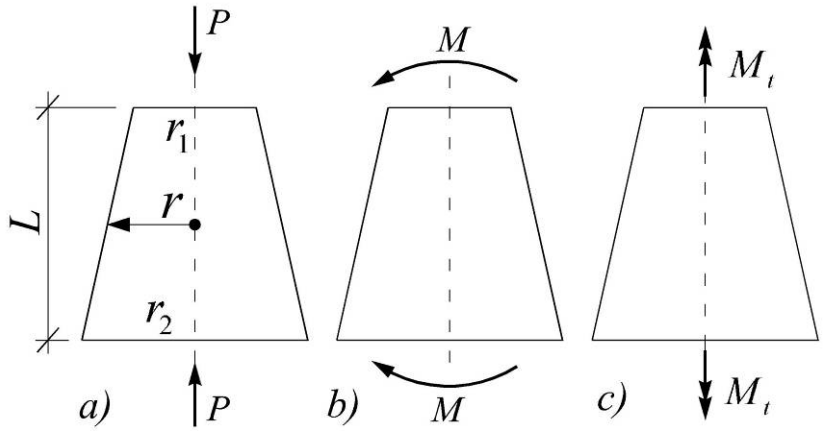

Figure 38. Conical shell members subjected to a) compression, b) bending, and c) torsion

The critical load coefficient ($\lambda_{c,FE}$) and the corresponding buckling mode shapes for several values of L and r_2 were obtained using ABAQUS code and a mesh of shell finite elements S4R. The comparison between the critical load coefficients obtained by FEM and GBT showed very good agreement (the maximum difference is less than 5%).

(iv) Compression axisymmetric mode

The conical shell is locally and globally simply supported to both end sections. For small length values the member buckles in a pure axisymmetric mode. The critical buckling mode

shape is characterized by n - the number of longitudinal half-waves of $\mathrm{f}(x)$. Figure 39 presents the critical buckling mode shapes, the corresponding load coefficients and the amplitude functions for several values of r_2 ($L = 48mm$).

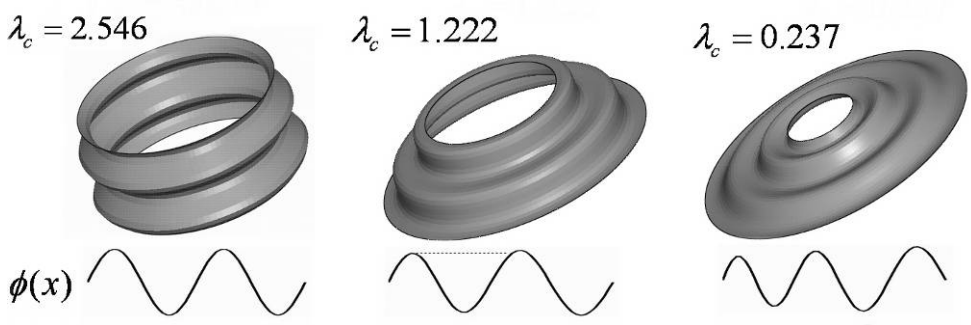

Figure 39. Axisymmetric mode: critical buckling mode shapes, load coefficients and amplitude functions

(v) Members under bending

The conical shell is locally and globally simply supported to both end sections. The member buckles in a combination of several shell-type modes (5+6+9+10+13+14+…) or (3+4+7+8+11+12+…) which leads to a localised "bubble" wave. Figure 40 presents the critical buckling mode shapes, the corresponding load coefficients and the amplitude functions for several values of r_2 ($L = 48mm$).

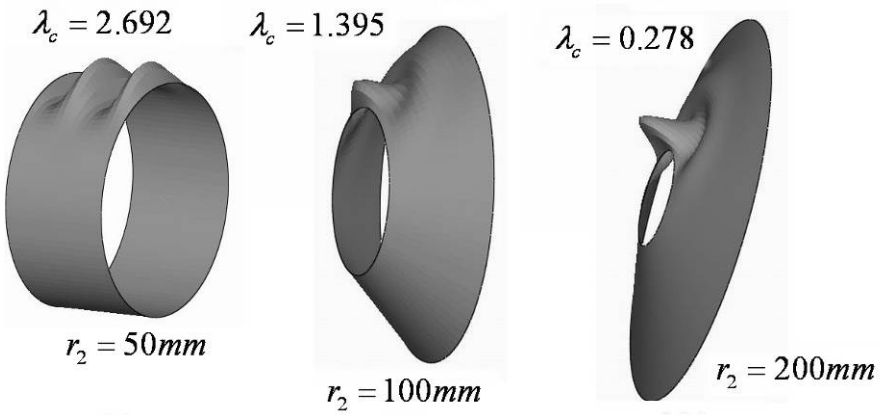

Figure 40. Members under bending: critical buckling mode shapes and load coefficients

(vi) Members under torsion

The conical shell has fully fixed end sections and is submitted to uniform torsion. The member always buckles in a combination of two shell-type modes with the same number of circumferential waves (10+11 or 8+9 etc.). Figure 41 presents the critical buckling mode shapes and the corresponding load coefficients for several values of r_2 ($L = 800mm$).

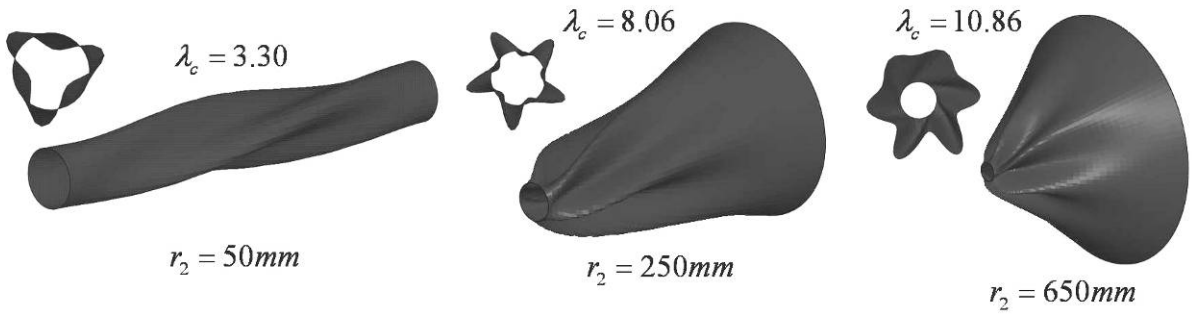

Figure 41. Members under torsion: critical buckling mode shapes, load coefficients and amplitude functions

Conclusions

As a *beam* theory GBT is an elegant and, computationally, a very efficient method for the investigation of conical shells buckling behaviour. The mechanical and geometric properties are no longer constant along the bar length but for conical shells they can be easily defined. The member deformed configuration (buckling mode) must be found among the pre-determined shell-type deformation modes, which have the characteristic of being fully orthogonal. In order to validate and show the application of the new GBT extension, the results obtained for conical shells with various loading and boundary conditions were compared with values obtained by shell finite element analyses.

Personal Contribution

For a long time it was thought that this method can be applied only for bars with constant cross-sections along the longitudinal axis (prismatic thin-walled members, cylindrical shells and tubes). The candidate's contribution consists in the introduction of a new GBT formulation for isotropic conical shells.

3.3 Buckling mode decomposition from FEA of thin-walled members

Introduction

Because of their slenderness, the design capacity of thin-walled members subjected to compressive stresses is usually governed by the buckling phenomena. As explained in section 3.1 there are three fundamental types which are defined based on the in-plane cross-sectional deformations *global*, *distortional* and *local* buckling (see Figure 1). Depending on its slenderness, the member instability may consist of a single *pure* buckling mode, but usually it is a combination of *pure* (and extremely important - *orthogonal*) modes of the same or different type. Each buckling type has its characteristic post-buckling behaviour; consequently, the derivation of the modal participation for a general buckling mode is a crucial step in assessing the real design resistance of the member.

The Generalised Beam Theory (GBT) is a method capable to carry out linear buckling analyses and to calculate modal participation. By using one-dimensional elements, GBT involves fewer DOF than Finite Strip Method (FSM) or Finite Element Method (FEM) which makes it more elegant and computationally efficient, but in the same time more restrictive to arbitrary boundary and loading conditions. Another specialized method on modal decomposition is the constrained Finite Strip Method (cFSM) which was created by Ádány et al. [18] by introducing the GBT assumptions into FSM. Even with the latest developments [59], cFSM still can not handle arbitrary boundary and loading conditions.

FEM has none of the above restrictions, it is a general method and nowadays, in spite of the large number of DOF, the linear buckling FEM analysis is no longer prohibitive due to the

rapid development of computer technology. Generally, for thin-walled members, shell elements are used and extremely efficient computer programs are capable to provide the critical load factors and buckling shapes. The major drawback is that FEA is not capable to provide the modal identification and for this reason two basic approaches were developed.
One approach is to implement constraints into FEM, similar to the technique used for creating cFSM, which forces FEM to calculate pure buckling modes (rather than general buckling modes), and the critical loads associated with these pure modes [60].
An alternative approach is to operate on the general FEM buckling modes, by identifying the participation of each pure mode in the existing buckling configuration. In [61], Ádány et al. used the cFSM modal *base functions* to approximate an arbitrary FEM buckling mode and to determine the contribution of each buckling type. The resulting pure buckling identification and its associated approximation error were investigated, including dependency on FEM discretisation, the number of cFSM functions considered, boundary and loading conditions.
The candidate followed the second approach, but the modal decomposition was done in a totally different manner. A conventional GBT analysis involves two steps: (i) a *cross-sectional analysis* leading to the GBT pure deformation modes and corresponding modal mechanical properties and (ii) a *member stability analysis* to obtain the critical loading factors and the associated mode shapes.
The method presented here performs only the first GBT step in order to obtain the *cross-sectional deformation modes,* which according to certain criteria are orthogonal along the member cross-section. Due to this feature, the cross-sectional deformation modes are next used to extract from any FEM buckling mode, the pure mode shapes in the form of the GBT displacement amplitude functions and finally the modal participation. There is no need of the second step which is by far the largest and the most time-consuming part of a conventional GBT analysis.

As presented in section 3.1, the GBT differential equations system describing the member equilibrium is given by the following equation:

$$C_{ik}\mathsf{f}_k^{IV} - D_{ik}\mathsf{f}_k'' + B_{ik}\mathsf{f}_k = \mathsf{l}\, X_{jik}\left(W_j^0\mathsf{f}_k'\right)' \tag{78}$$

The expressions of the stiffness matrices are given:

$$\begin{aligned}
&C_{ik} = C_{ik}^{Membrane} + C_{ik}^{Bending} = E\int_s tu_i u_k ds + \int_s Kw_i w_k ds \\
&D_{ik} = D_{1,ik} - \mathsf{m}\left(D_{2,ik} + D_{2,ki}\right) \quad D_{1,ik} = \frac{G}{3}\int_s t^3 \dot{w}_i \dot{w}_k ds \quad D_{2,ik} = \int_s K\ddot{w}_i w_k ds \\
&B_{ik} = \int_s K\ddot{w}_i \ddot{w}_k ds = \int_s \frac{1}{K} m_i m_k ds \\
&X_{jik} = \frac{E}{C_{jj}}\int_s u_j (v_i v_k + w_i w_k) t ds \quad j = 1..4
\end{aligned} \tag{79}$$

where C and B have diagonal form, proving the orthogonality characteristics of the pure deformation modes. The system is still coupled by the elements of D and X matrices, but the stiffness matrices have clear structural meaning and the functions $u_k(s), v_k(s), w_k(s)$ and $\mathsf{f}_k(x)$ describe orthogonal deformation modes. The vector W^0 ($j = 1..4$) contains the resultants of the applied pre-buckling stresses, namely (i) axial force ($W_1^0 = N$), (ii) major and minor axis bending moments ($W_2^0 = M_y$, $W_3^0 = M_z$), and (iii) bimoment ($W_4^0 = B$).
Together with the appropriate boundary conditions, the GBT differential equations system defines the buckling eigenvalue problem and the GBT 2nd step of the analysis, namely the

member stability analysis. Its solution yields the critical load factors (λ) and the corresponding modal amplitude functions ($f_k(x)$).

3.3.1 First formulation

This formulation was first presented in article 3 and also in the following conference paper:

- **Nedelcu M**, Chira N, Popa AG, Cucu HL (2012) „GBT-based buckling mode identification from Finite Element Analysis of thin-walled members", European Congress on Computational Methods in Applied Sciences and Engineering (ECCOMAS 2012), Vienna, Austria, 10-14 September 2012, e-Book Full Papers , pp. 1291-1304 (in Scopus).

A buckling analysis is first performed using any available FE code. Next, one considers for the finite element displacement components provided by a standard FEA, the GBT product formulation:

$$u_{FE}(s,x)=\sum_{k=1}^{n}u_k(s)f_k'(x) \quad v_{FE}(s,x)=\sum_{k=1}^{n}v_k(s)f_k(x) \quad w_{FE}(s,x)=\sum_{k=1}^{n}w_k(s)f_k(x) \tag{80}$$

where n is the number of pure deformation modes, $u_k(s), v_k(s), w_k(s)$ are known from the GBT cross-section analysis and $f_k(x)$ are the unknown amplitude functions.

Buckling mode decomposition using stiffness matrix B

Now if one introduces function $f_i(x)$ as the following cross-sectional integration for any $i=1..n$

$$f_i(x)=\int_s K\ddot{w}_i(s)\ddot{w}_{FE}(s,x)ds=\sum_{k=1}^{n}\left(\int_s K\ddot{w}_i(s)\ddot{w}_k(s)ds\right)f_k(x) \tag{81}$$

and taking into account the orthogonality condition that makes the transverse bending stiffness matrix B a diagonal matrix (see Eq. (79))

$$\int_s K\ddot{w}_i(s)\ddot{w}_k(s)ds=0 \quad for \quad i\neq k \tag{82}$$

one obtains

$$f_i(x)=\left(\int_s K\ddot{w}_i(s)\ddot{w}_i(s)ds\right)f_i(x)=B_{ii}f_i(x) \tag{83}$$

meaning that the amplitude functions can be obtained as following

$$f_i(x)=\frac{f_i(x)}{B_{ii}}=\frac{1}{B_{ii}}\int_s K\ddot{w}_i(s)\ddot{w}_{FE}(s,x)ds \tag{84}$$

Introducing the transverse bending moments as

$$m=-K\ddot{w} \tag{85}$$

from Eq. (79) the components of the transverse bending stiffness matrix are written

$$B_{ii}=-\int_s m_i\ddot{w}_i ds=\int_s\frac{1}{K}m_i m_i ds \tag{86}$$

and the amplitude functions become

$$f_i(x)=\frac{1}{B_{ii}}\int_s\frac{1}{K}m_i(s)m_{FE}(s,x)ds \tag{87}$$

It can be seen that matrix *B* contains the virtual work done by the transverse bending moments on the infinitesimal longitudinal element for unit values of the amplitude functions. For mode *i* the virtual work can be computed using the edge transverse moments ($m_{i,r}$) and the relative rotations of the plates. The absolute and relative rotations are considered using straight lines between nodes. The stiffness matrix components are written

$$B_{ii} = -\sum_{r=1}^{p} m_{i,r} \Delta \mathsf{q}_{i,r} \tag{88}$$

where *p* is the number of member longitudinal edges, $\Delta \mathsf{q}_r$ is the relative rotation between two adjacent plates at node *r*.

For a branched section it is easier to multiply each end plate bending moment with the plate absolute rotation. As it can be seen in Figure 42, the free edges have no transverse bending moments and this is also true for their most nearby edges.

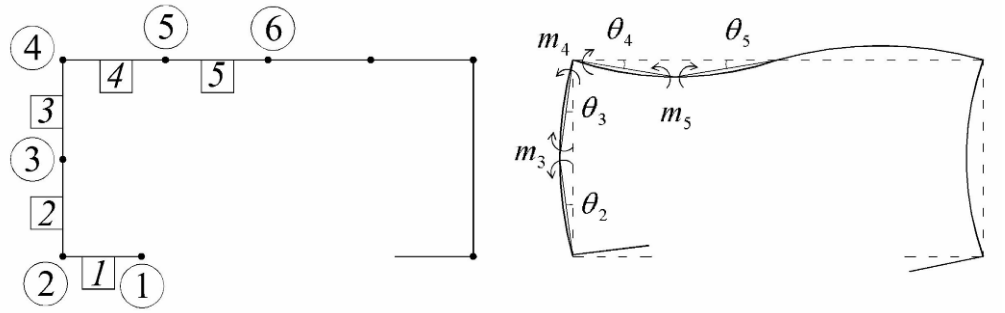

Figure 42. Lipped channel deformation mode: edge transverse moments and plate rotations

The computation of the edge transverse moments $m_{i,r}$ is a necessary step in the GBT cross-section analysis and it is extensively presented in [7] and [12]. The procedure is based on the *compatibility* between the membrane and transverse displacements across the individual plate element. Starting with the displacement components of the edges, the force or displacement method is used on the infinitesimal member element (length *dx*) and edge transverse moments $m_{i,r}$ are computed together with the transverse displacement components $w(s)$.

From Eq. (87), (88) one obtains the amplitude functions as following

$$\mathsf{f}_i(x) = -\frac{1}{B_{ii}} \sum_{r=1}^{p} m_{i,r} \Delta \mathsf{q}_{FE,r}(x) \tag{89}$$

The relative rotations $\Delta \mathsf{q}_{FE,r}(x)$ can easily be extracted from any FEM computer program using a mesh of points along the member length and therefore the amplitude functions can be calculated on each mesh point. Once again it must be underlined that all the plate rotations are extracted by considering straight lines between nodes. The values of $\mathsf{f}_i(x)$ between the mesh points can next be calculated by simple interpolation.

The above described procedure can be used to identify all the pure buckling modes which involve cross-sectional distortions. This is not the case of the first four pure deformation modes involving axial extension, major axis bending, minor axis bending and torsion. These four *global* modes produce rigid-body displacements of the cross-section in its plane. Therefore there are no flexural plate deformations, no transverse moments and the *B* components are null ($B_{ii} = 0$, for $i = 1..4$). In order to find the amplitude functions, a similar procedure is introduced, one which uses the stiffness matrix *C* instead of *B*.

Buckling mode decomposition using stiffness matrix C

We introduce function $g_i(x)$ as the following cross-sectional integration for $i = 1..n$

$$g_i(x) = E\int_s t u_i(s) u_{FE}(s,x) ds = E\sum_{k=1}^{n}\left(\int_s t u_i(s) u_k(s) ds\right)\mathsf{f}'_k(x) \tag{90}$$

Using Eq. (79) we can rewrite the above expression by introducing the components of the membrane warping stiffness matrix.

$$g_i(x) = \sum_{k=1}^{n} C_{ik}^M \mathsf{f}'_k(x) \tag{91}$$

The matrix $C^M = C - C^B$ is not a diagonal matrix, because the GBT diagonalisation process is done over the warping matrix *C*. However, for the global deformation modes, the influence of the bending stiffness is extremely small compared to the membrane stiffness and consequently it is neglected in this paper. Making the approximation $C \simeq C^M$ and knowing that *C* is a diagonal matrix one obtains

$$E\int_s t u_i(s) u_k(s) ds = 0 \quad for \quad i \neq k \tag{92}$$

Eq. (90) becomes

$$g_i(x) = \left(E\int_s t u_i(s) u_i(s) ds\right)\mathsf{f}'_i(x) = C_{ii}^M \mathsf{f}'_i(x) \tag{93}$$

meaning that the amplitude functions derivatives according to *x* can be obtained as following

$$\mathsf{f}'_i(x) = \frac{E}{C_{ii}^M}\int_s t u_i(s) u_{FE}(s,x) ds, \text{ for } i = 2..4 \tag{94}$$

The extension mode ($i = 1$) was eliminated because it is not a valid buckling deformation mode. One considers the warping functions $u(s)$ to have linear variation over the cross-section, a GBT assumption that, in this procedure, greatly simplifies the computation of the cross-sectional integral, using only the nodal values of *u*. As in the preceding section, the FEM warping displacements at each edge can be easily extracted for a given mesh of points along the member length, the vector u_i is given by the GBT cross-section analysis and so the derivatives of the amplitude functions can be computed on each mesh point.
Next, one has to compute the amplitude functions knowing their derivatives, an easy task if the member has classical bar boundary conditions: (i) simply supported (S-S), (ii) clamped-free (or cantilever, C-F), (iii) clamped-clamped (C-C) and (iv) clamped – simply supported (C-S). They all involve, at least at one member end, the boundary condition

$$\mathsf{f}_i(0) = 0 \tag{95}$$

and so the integration constant is null and the integration can be done by any numerical method. Once again the values of $\mathsf{f}_i(x)$ between the mesh points can be calculated by simple interpolation.

Modal Participation Calculation

Regarding modal participation the candidate used the same procedure proposed by Silvestre et al. in [13]. It is an easy and intuitive method to specify the contribution of each pure deformation mode to the final buckling configuration. The modal participation factor (P_i) is introduced with the following expression

$$P_i = \frac{\int_L \left|\mathsf{f}_i(x)\right| dx}{\sum_{k=1}^{n}\int_L \left|\mathsf{f}_k(x)\right| dx} \tag{96}$$

where the numerator and denominator are (i) the sum of the contributions of that deformation mode *i* and (ii) all the *n* deformation modes included in the analysis of the member deformed configurations associated with the buckling mode under consideration.
This procedure was chosen here on one hand because of its easy-to-apply and intuitive features and on the other hand because it is already implemented in the computer program GBTUL [17]. In the next section the modal participations extracted from FEA are compared to the values obtained using GBTUL. Therefore, any differences between the general buckling modes found by two approaches can not be attributed to the use of different procedures at the level of modal participation calculation.
A more refined procedure would involve the computation of the modal participation factor depending on the strain energy produced by each pure mode included in the analysis. This approach, which is currently under work, will also detect if the number of considered pure modes is too small by comparing their total strain energy with the value of the strain energy provided by FEA. It could also detect the influence of other deformation modes (containing membrane transverse extensions and shear strains) neglected by GBT.

Illustrative Examples - I

The proposed decomposition method is presented in this section through the buckling analysis of simple columns and beams with different end conditions. A parametric study is completed on a symmetric steel lipped channel (C-shape) column also studied in [18], with a Young's modulus of 210000MPa and Poisson's ratio of 0.3. The column length is 1200mm, with a web height of 100mm, flange width of 60 mm, lip lengths of 10mm and thickness of 2 mm. Note, the dimensions are for the mid-line, and sharp corners are employed.
The cross-section discretisation introduced in GBTUL is made with 3, 5, and 1 intermediate nodes between the corners, respectively in the flanges, web and flange lips. This gives a number of 21 pure deformation modes and their in plane shapes are presented in Figure 43 together with the cross-section discretisation. Modes 1 to 4 are *global* deformation modes (characterized by in-plane rigid-body cross-section displacements), modes 5 and 6 belong to the *distorsional* type (the cross-section exhibits edge displacements and also plate flexural deformations) and the rest of them are *local* deformation modes (the cross-section exhibits only flexural plate deformation).

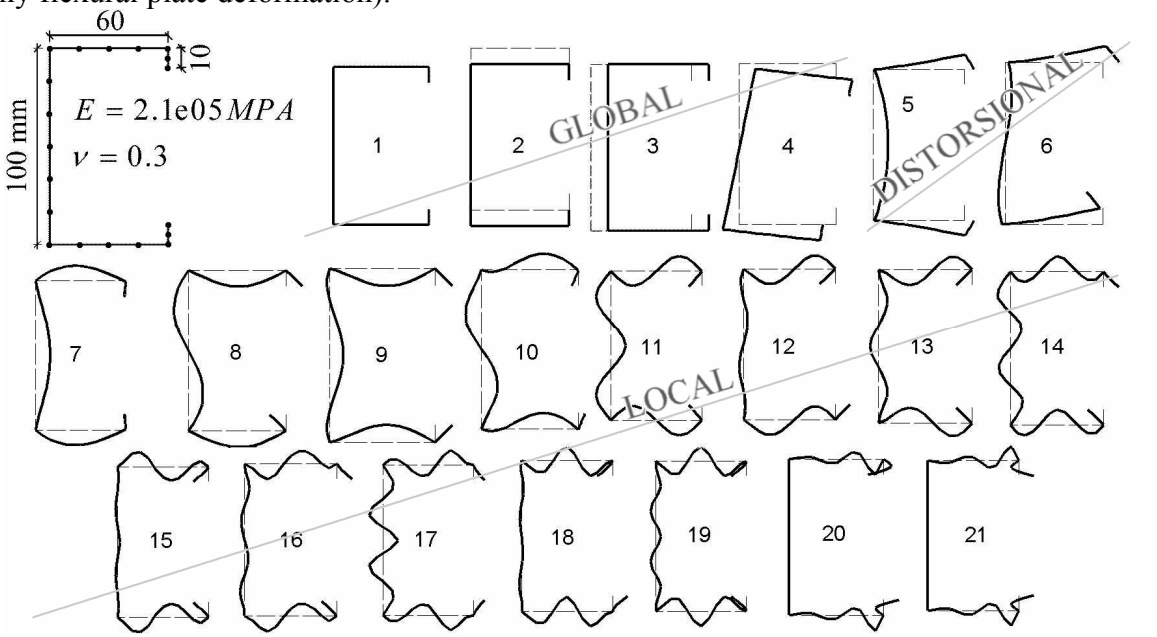

Figure 43. In-plane shapes of the lipped channel deformation modes

The FEM calculations are conducted in ABAQUS, using S8R5 shell elements (8-node doubly curved thin shell elements, using 5 DOF per node and reduced integration) in a highly regular rectangular mesh (see Figure 44). Both the cross-section discretisation and element longitudinal dimension are constant along the member length. There are 32 elements on the longitudinal direction and 9 elements in the element cross-section thus giving a number of 19 nodes on the cross-section and a total number of 947 nodes while the total number of displacement degrees of freedom (DOF) is 4735.

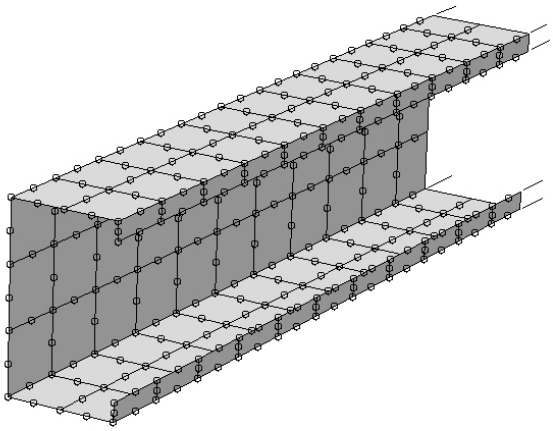

Figure 44. Member FE discretisation

To compute the GBT-based modal participation described in Section 3, a Matlab program was written. It uses the displacement field of 33 cross-sections (defined by the shell elements edges normal to the member longitudinal axis) resulted from an ABAQUS "buckle" type analysis.

The first 10 buckling modes are calculated in ABAQUS for a simple column (pure compression member) and also a simple beam (pure bending member). In order to investigate the effect of boundary conditions, numerical studies have been completed using all four bar classical boundary conditions (S-S, C-F, C-C and C-S). Comparison is made between the modal participation factors extracted from FEM analysis (*FEM modal participation*) and those given by GBTUL (*GBT modal participation*). The choice of FEM shell element type and discretisation has an important influence on the critical loading factors and also on the buckling mode shape. In the same time, GBTUL analysis was performed by using the *numerical solution* which involves a longitudinal discretisation of the member into GBT-based finite elements. The number of bar finite elements also has an important effect on the final solution. In this study a number of 20 GBT finite elements along the bar length was used. Even if, generally, there is good agreement between FEM and GBT results, there are few exceptions which will be discussed in the next sections. Tables 12-15 present the FEM and GBT numerical results in the form of critical loading factors and modal participations for the first 10 buckling modes of the simple column problem. Each table is dealing with one of the four bar classical boundary conditions. Table 16 gives the same data, but for a simple beam having S-S boundary conditions. It was observed that the last 12 pure modes have a modal contribution of less then 4% of the total; for this reason their combined contribution is given in the last column.

Numerical results for simply supported columns

The S-S boundary conditions correspond to pinned–pinned (both locally and globally) and free to warp end supports, sometimes also referred to as *fork supports*. Moreover, during FEM analysis the longitudinal translation was restrained at the middle of the member.

Table 12. FEM vs. GBT results for the simply supported member

Mode no.	l_{cr} FEM/GBT	Modal participation - *FEM/GBT* (%)								
		2	3	4	5	6	7	8	9	10-21
1	146.04	30.21	0.00	43.45	0.00	25.36	0.00	0.66	0.00	0.32
	147.76	30.19	0.00	43.47	0.00	25.37	0.00	0.70	0.00	0.27
2	159.89	0.00	0.79	0.00	92.38	0.00	5.69	0.00	1.02	0.12
	159.90	0.00	0.78	0.00	92.41	0.00	5.67	0.00	1.08	0.06
3	***178.48***	0.00	0.94	0.00	84.22	0.00	12.99	0.00	1.66	0.19
	163.07	0.00	0.44	0.00	87.54	0.00	10.11	0.00	1.80	0.10
4	187.45	0.00	0.32	0.00	76.08	0.00	20.89	0.00	2.39	0.31
	189.13	0.00	0.34	0.00	77.84	0.00	18.93	0.00	2.71	0.19
5	189.40	0.00	0.28	0.00	8.75	0.00	84.35	0.00	5.22	1.40
	193.46	0.00	0.06	0.00	4.26	0.00	88.17	0.00	5.92	1.59
6	189.56	0.00	0.20	0.00	**39.16**	0.00	**55.36**	0.00	4.21	1.08
	194.08	0.00	0.05	0.00	**3.56**	0.00	**87.97**	0.00	6.61	1.80
7	192.73	0.00	0.08	0.00	7.48	0.00	85.67	0.00	5.27	1.51
	194.98	0.00	0.07	0.00	5.23	0.00	88.16	0.00	5.16	1.38
8	192.94	0.00	0.34	0.00	5.30	0.00	86.46	0.00	6.21	1.69
	196.55	0.00	0.05	0.00	3.06	0.00	87.65	0.00	7.23	2.02
9	196.32	0.00	0.07	0.00	5.51	0.00	84.81	0.00	7.54	2.07
	198.98	0.00	0.09	0.00	6.67	0.00	87.77	0.00	4.30	1.17
10	196.71	0.00	0.31	0.00	4.80	0.00	89.63	0.00	4.04	1.23
	200.63	0.00	0.04	0.00	2.68	0.00	87.23	0.00	7.81	2.24

For buckling mode 3 there is a difference of 9.45% between the critical loading factors. Visual inspection showed good correlation between modal shapes and this can also be seen from the good agreement between modal participations. The reason for this difference is given by the FEM longitudinal restraining at the middle of the member which increases the member stiffness. Figure 45 shows the warping displacements resulted from the GBT analysis on this position. Mode 3 is also the only mode with asymmetric longitudinal shape regarding the middle of the member and therefore the other buckling modes are not affected by the FEM longitudinal restraining.

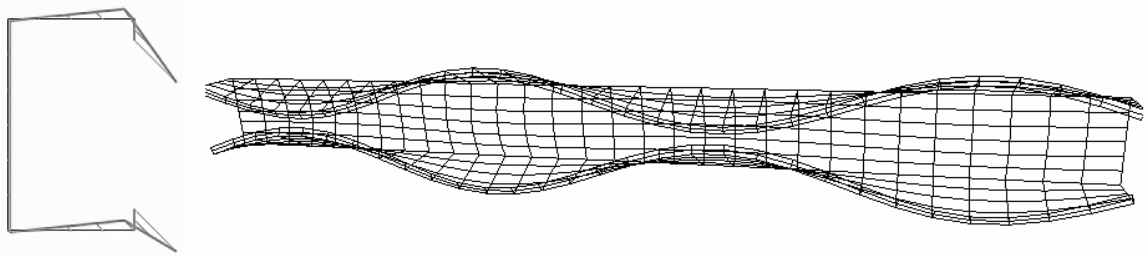

Figure 45. Buckling mode 3: warping deformation at $x = l/2$ and mode shape

Buckling mode 6 displays important differences from the modal participation point of view. The method proposed by the candidate is not responsible for this disagreement. Figure 46 presents a comparison between the modal shapes obtained from the two buckling analyses. It can be seen that buckling mode 6 is from FEM analysis a mixture of distortional and local pure modes (modes 5 and 7) but from GBT analysis is mainly the local mode 7.

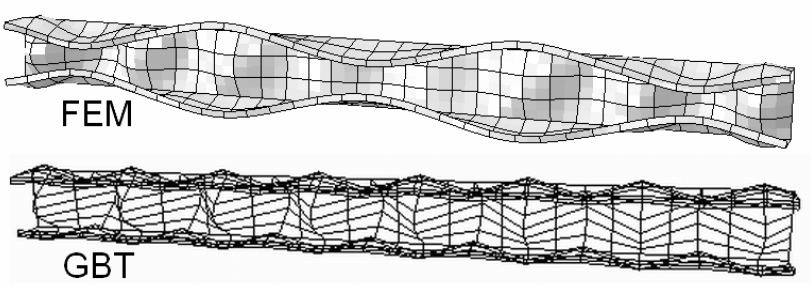

Figure 46. Buckling mode 6: FEM and GBT modal shapes

The C-C boundary conditions correspond to globally and locally fixed supports at both ends. Table 13 shows very good agreement between the two decomposition methods as critical loading factors and also as modal participation.

Table 13. FEM vs. GBT results for the clamped-clamped member

Mode no.	l_{cr}	Modal participation - FEM/GBT (%)								
	FEM/GBT	2	3	4	5	6	7	8	9	10-21
1	172.41	0.00	1.40	0.00	87.72	0.00	9.30	0.00	1.43	0.15
	172.77	0.00	1.30	0.00	87.22	0.00	9.83	0.00	1.56	0.10
2	178.59	0.00	0.96	0.00	85.17	0.00	11.94	0.00	1.75	0.19
	179.39	0.00	0.93	0.00	84.84	0.00	12.25	0.00	1.85	0.14
3	192.22	0.00	0.10	0.00	5.18	0.00	86.90	0.00	6.11	1.71
	194.45	0.00	0.06	0.00	4.32	0.00	87.82	0.00	6.13	1.66
4	192.31	0.00	0.08	0.00	5.28	0.00	86.76	0.00	6.15	1.73
	194.48	0.00	0.09	0.00	4.94	0.00	87.31	0.00	6.02	1.65
5	194.85	0.00	0.07	0.00	6.90	0.00	85.37	0.00	5.96	1.70
	197.49	0.00	0.08	0.00	5.86	0.00	86.07	0.00	6.24	1.75
6	195.27	0.00	0.16	0.00	9.88	0.00	82.37	0.00	5.90	1.69
	197.67	0.00	0.17	0.00	9.15	0.00	83.28	0.00	5.77	1.63
7	199.32	0.00	0.30	0.00	12.43	0.00	80.73	0.00	5.01	1.53
	202.54	0.00	0.12	0.00	7.03	0.00	84.57	0.00	6.41	1.87
8	200.13	0.00	0.10	0.00	9.87	0.00	82.94	0.00	5.46	1.63
	202.86	0.00	0.10	0.00	9.38	0.00	83.22	0.00	5.66	1.65
9	205.48	0.00	0.29	0.00	21.59	0.00	72.64	0.00	4.16	1.32
	209.39	0.00	0.25	0.00	16.73	0.00	75.81	0.00	5.50	1.71
10	206.71	0.00	0.24	0.00	18.27	0.00	73.76	0.00	6.00	1.73
	209.64	0.00	0.26	0.00	17.21	0.00	74.50	0.00	6.16	1.86

The C-F (cantilever) boundary conditions correspond to globally and locally fixed conditions at one end and free support conditions at the other. Table 14 shows good agreement between the two decomposition methods, except for buckling modes 4 and 5. This is the same problem as previously described for the *S-S* member (buckling mode 6). The differences between modal shapes can be seen in Figure 47 and Figure 48 and one can also notice an interesting situation. There is an inversion between the two buckling modes: the FEM buckling mode 4 is similar with the GBT buckling mode 5 and vice versa.

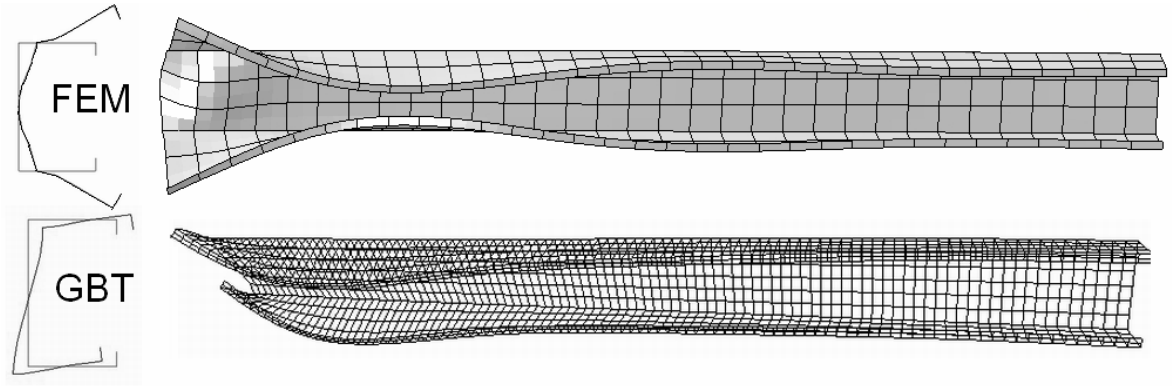

Figure 47. Buckling mode 4: FEM and GBT free end warping deformations and modal shapes

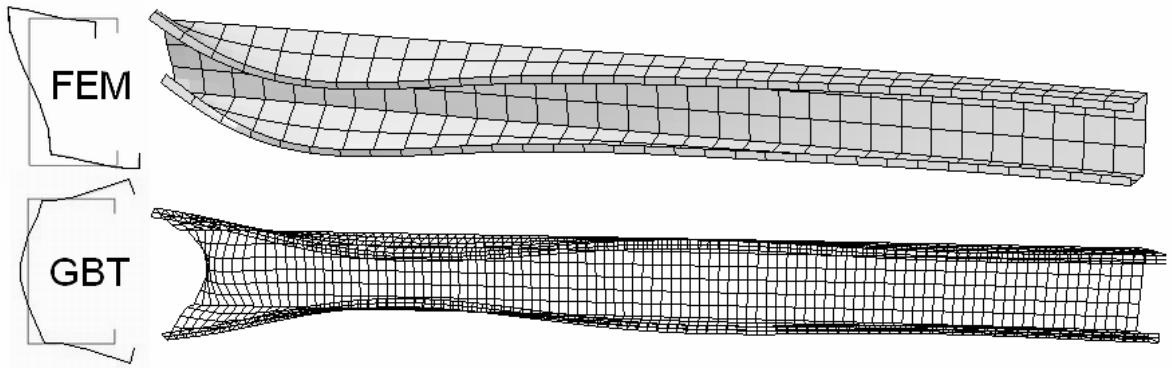

Figure 48. Buckling mode 5: FEM and GBT free end warping deformations and modal shapes

Table 14. FEM vs. GBT results for the clamped-free member

Mode no.	l_{cr} FEM/GBT	Modal participation - FEM/GBT (%)								
		2	3	4	5	6	7	8	9	10-21
1	44.31	44.46	0.00	52.22	0.00	3.02	0.00	0.19	0.00	0.12
	44.38	42.96	0.00	50.40	0.00	6.07	0.00	0.29	0.00	0.27
2	72.59	0.00	91.28	0.00	7.42	0.00	1.15	0.00	0.10	0.05
	79.47	0.00	88.60	0.00	9.90	0.00	1.33	0.00	0.10	0.07
3	96.74	0.00	91.11	0.00	7.88	0.00	0.80	0.00	0.17	0.04
	100.96	0.00	75.64	0.00	22.21	0.00	1.53	0.00	0.52	0.10
4	**126.12**	**0.00**	**61.26**	**0.00**	**30.15**	**0.00**	**7.20**	**0.00**	1.13	0.27
	138.60	**4.58**	**0.00**	**28.20**	**0.00**	**61.69**	**0.00**	**3.83**	0.00	1.70
5	**132.81**	**8.88**	**0.00**	**32.82**	**0.00**	**54.06**	**0.00**	**3.27**	0.00	0.97
	144.29	**0.00**	**49.11**	**0.00**	**32.16**	**0.00**	**15.73**	**0.00**	2.25	0.75
6	171.66	0.00	17.61	0.00	72.47	0.00	8.18	0.00	1.54	0.20
	173.29	0.00	13.49	0.00	74.52	0.00	10.01	0.00	1.78	0.19
7	178.10	0.00	8.46	0.00	80.46	0.00	9.36	0.00	1.52	0.19
	178.95	0.00	8.49	0.00	78.91	0.00	10.62	0.00	1.78	0.20
8	192.32	0.00	1.89	0.00	9.75	0.00	80.99	0.00	5.74	1.62
	194.39	0.00	1.49	0.00	7.21	0.00	83.92	0.00	5.80	1.59
9	192.38	0.00	3.47	0.00	6.12	0.00	82.76	0.00	5.99	1.67
	194.55	0.00	1.66	0.00	7.31	0.00	83.59	0.00	5.83	1.61
10	194.91	0.00	1.13	0.00	24.09	0.00	68.78	0.00	4.67	1.33
	197.19	0.00	0.69	0.00	19.99	0.00	72.79	0.00	5.10	1.43

The C-S boundary conditions correspond to globally and locally fixed conditions at one end and fork support at the other. Table 15 shows good agreement between the two decomposition methods, as critical loading factors and modal participation, except for modes 3 and 9. Again the visual inspection of the modal shapes showed that the differences are due to the solutions of the buckling analyses and not to the proposed modal decomposition method.

Table 15. FEM vs. GBT results for the clamped-simply supported member

Mode no.	l_{cr}	Modal participation - FEM/GBT (%)								
	FEM/GBT	2	3	4	5	6	7	8	9	10-21
1	161.30	0.00	0.85	0.00	90.34	0.00	7.39	0.00	1.28	0.14
	161.39	0.00	0.84	0.00	90.15	0.00	7.56	0.00	1.37	0.08
2	174.71	0.00	0.96	0.00	85.65	0.00	11.52	0.00	1.70	0.18
	175.33	0.00	0.92	0.00	85.52	0.00	11.60	0.00	1.84	0.12
3	189.31	0.00	0.39	0.00	**19.08**	0.00	**73.80**	0.00	5.32	1.42
	193.68	0.00	0.07	0.00	**4.50**	0.00	**87.78**	0.00	6.03	1.62
4	192.29	0.00	0.05	0.00	4.85	0.00	87.01	0.00	6.34	1.76
	194.48	0.00	0.08	0.00	5.19	0.00	87.08	0.00	6.02	1.63
5	192.73	0.00	0.09	0.00	6.47	0.00	85.87	0.00	5.90	1.67
	195.72	0.00	0.16	0.00	7.49	0.00	84.85	0.00	5.88	1.63
6	195.06	0.00	0.18	0.00	8.42	0.00	83.30	0.00	6.34	1.77
	197.61	0.00	0.18	0.00	10.94	0.00	81.59	0.00	5.68	1.61
7	196.30	0.00	0.72	0.00	47.84	0.00	46.63	0.00	3.75	1.06
	199.57	0.00	1.04	0.00	54.97	0.00	40.41	0.00	2.81	0.77
8	198.50	0.00	1.52	0.00	67.49	0.00	28.65	0.00	2.01	0.34
	200.33	0.00	1.35	0.00	69.68	0.00	26.26	0.00	2.25	0.45
9	199.62	0.00	0.68	0.00	**33.62**	0.00	**59.48**	0.00	4.88	1.34
	202.76	0.00	0.23	0.00	**10.96**	0.00	**80.93**	0.00	6.10	1.77
10	202.31	0.00	0.44	0.00	19.76	0.00	73.18	0.00	5.11	1.50
	205.99	0.00	0.44	0.00	19.93	0.00	72.65	0.00	5.38	1.61

Numerical results for a simple beam

The same member was subjected to pure major axis bending and S-S boundary conditions. During FEA the longitudinal translation was restrained in the middle of the member, but only for the tensioned flange and lip. The GBTUL buckling analysis was carried out by both *analytical and numerical solution*. The last one is available only for S-S boundary conditions but is much faster than its numerical equivalent. A maximum number of 10 halfwaves appeared from FEM analysis and for this reason the same number was introduced in GBTUL *analytical solution*. The maximum number of halfwaves appears at buckling mode 10 (see Figure 49). As Table 16 shows, all the buckling modes are a mixture of distortional (5 and 6) and local (7, 8 and 9) pure modes and there is very good agreement between the two decomposition methods.

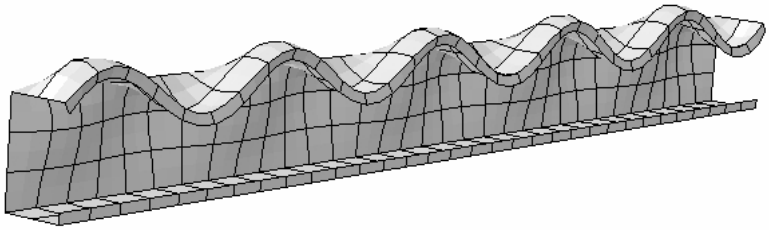

Figure 49. Buckling mode 10: FEM shape

Table 16. FEM vs. GBT results for the simply supported beam

Mode no.	l_{cr} FEM/GBT	Modal participation - FEM/GBT (%)								
		2	3	4	5	6	7	8	9	10-21
1	760.89	0.21	0.56	0.23	51.46	42.29	1.34	2.06	1.35	0.51
	768.47	0.22	0.07	0.23	51.63	42.25	1.46	2.18	1.44	0.51
2	794.22	0.41	1.02	0.47	54.58	40.33	0.78	1.28	0.81	0.32
	801.51	0.44	0.06	0.46	55.27	40.38	0.84	1.37	0.87	0.29
3	853.22	0.14	0.12	0.16	48.25	42.21	2.66	3.37	2.29	0.80
	864.80	0.15	0.06	0.16	48.01	41.92	2.89	3.55	2.42	0.85
4	1007.30	0.11	0.07	0.14	44.44	40.09	4.92	5.33	3.70	1.19
	1027.37	0.12	0.05	0.13	43.89	39.64	5.36	5.61	3.91	1.30
5	1112.90	1.42	1.33	1.85	58.23	34.81	0.72	0.84	0.60	0.21
	1118.26	1.45	0.81	1.61	59.01	34.66	0.73	0.89	0.63	0.18
6	1188.30	0.18	1.90	0.48	39.09	35.62	7.94	7.71	5.42	1.66
	1220.06	0.10	0.04	0.11	38.93	35.77	8.94	8.39	5.91	1.82
7	1271.70	3.80	42.90	9.93	37.77	4.50	0.47	0.13	0.37	0.12
	1239.68	4.22	39.73	11.13	38.91	4.90	0.49	0.11	0.42	0.10
8	1368.30	0.08	0.64	0.13	34.54	31.70	12.01	10.92	7.72	2.25
	1411.68	0.08	0.04	0.09	33.23	30.78	13.42	11.74	8.31	2.33
9	1522.90	0.09	0.98	0.21	28.71	26.55	16.25	14.21	10.10	2.91
	1572.93	0.07	0.03	0.07	27.27	25.33	18.26	15.33	10.87	2.75
10	1635.40	0.04	0.25	0.05	23.78	21.89	20.32	17.48	12.50	3.69
	1683.66	0.05	0.02	0.06	21.67	20.11	22.66	18.69	13.29	3.44

3.3.2 Second formulation

This formulation was first presented in article 4. The drawbacks of the previous formulation are: (i) it is restricted to bar classical boundary conditions and (ii) the amplitude functions and their derivatives are extracted on a mesh of points along the member's axis, usually a regular one. If the mesh is not sufficiently dense, the numerical integration might introduce significant errors.

To overcome these problems, the amplitude functions for the global modes are extracted in a different manner described in the following section. Nevertheless, matrix C is still in use because the warping displacements depend on the derivatives of the amplitude functions $\mathsf{f}_k'(x)$ (see Eq. (80)); consequently the computation of these values is absolutely necessary.

For the torsion deformation mode, it is only natural to use the torsion stiffness matrix D, having the expression given by Eq. (79).

This matrix doesn't have a diagonal shape but it has zero values for the first four rows and columns, except for D_{44} corresponding to the torsional moment of inertia (Saint Venant torsion constant). It can be seen from Eq. (79) that the amplitude functions $\mathsf{f}_k(x)$ can be extracted with the aid of matrix D, in their *original* form and not through their derivatives. Until present time, the procedure neglects the elements of D_2 and writes the expression of the torsion stiffness matrix as follows [7]:

$$D_{ik} = \frac{G}{3}\sum_{r=1}^{np} \mathsf{q}_{i,r}\mathsf{q}_{k,r} b_r t_r^3 \tag{97}$$

where *np* is the number of finite elements (plates) over the cross-section, q_r is absolute rotation of plate *r* considering straight lines between nodes (see Figure 42), b_r is the width of the plate *r*, and the thickness t_r is considered constant for each plate. Following the procedure briefly described in the previous section, the amplitude function of the torsion deformation mode receives the expression

$$\mathsf{f}_4(x)=\frac{G}{D_{44}}\left(\frac{1}{3}\sum_{r=1}^{np}\mathsf{q}_{4,r}\mathsf{q}_{FE,r}b_r t_r^3-\frac{1}{G}\sum_{k=5}^{n}D_{4k}\mathsf{f}_k(x)\right) \tag{98}$$

The cross-sectional absolute rotations of the plates ($\mathsf{q}_k(s)$) for each pure mode are provided by the GBT 1st step. For pure torsion, they are all equal, describing a rigid-body rotation. The FE absolute rotations $\mathsf{q}_{FE,r}(s,x)$ are provided by the shell FEA as previously discussed. The amplitude functions for $k\geq 5$ are already known from the previous section.

The second and third global deformation modes are next discussed, namely the major/minor axis bending. One uses the geometrical stiffness matrix *X*, which stands for the stiffness degradation due to pre-buckling membrane longitudinal stresses and has the expression given by Eq. (79). For the method described in this paper it is enough to use only the first geometrical stiffness matrix X_1. Knowing that all unit warping displacements for the first deformation mode (axial extension) are introduced by GBT as $u_1(s)=-1$, the expression of X_1 can be approximately written:

$$X_{1ik}=-\frac{E}{C_{11}}\sum_{r=1}^{np}\left(v_{i,r}v_{k,r}+\overline{w}_{i,r}\overline{w}_{k,r}\right)b_r t_r=-\frac{1}{A}\sum_{r=1}^{np}\left(v_{i,r}v_{k,r}+\overline{w}_{i,r}\overline{w}_{k,r}\right)b_r t_r \tag{99}$$

where *A* is the cross-section area, and $\overline{w}_r$ are the average displacements of plate *r*, calculated as the semi-sum of the plate end displacements. Based on Vlasov's hypothesis ($\mathsf{e}_s^{M,L}=0$), the displacements v_r are considered constant along each cross-sectional segment *r*. Eq. (99) uses only the first two terms of the original expression of matrix *X* given in [8], because the other terms proved to have negligible effect concerning the global deformation modes.

Once again, taking into consideration Eq. (79), the amplitude functions $\mathsf{f}_k(x)$ can be directly extracted with the aid of matrix X_1 on a longitudinal mesh of points. Finally, the expressions of the amplitude functions for the major/minor axis bending deformation modes are given

$$\begin{aligned}\mathsf{f}_2(x)&=\frac{1}{A}\left(\sum_{r=1}^{np}\left(v_{2,r}\overline{v}_{FE,r}+\overline{w}_{2,r}\overline{w}_{FE,r}\right)t_r b_r+\sum_{k=4}^{n}X_{12k}\mathsf{f}_k(x)\right)\\ \mathsf{f}_3(x)&=\frac{1}{A}\left(\sum_{r=1}^{np}\left(v_{3,r}\overline{v}_{FE,r}+\overline{w}_{3,r}\overline{w}_{FE,r}\right)t_r b_r+\sum_{k=4}^{n}X_{13k}\mathsf{f}_k(x)\right)\end{aligned} \tag{100}$$

where $\overline{w}_r$ are the average transversal cross-sectional displacements provided by GBT, $\overline{v}_{FE,r}$ and $\overline{w}_{FE,r}$ are the average displacements of finite element *r* provided by FEA, and the amplitude functions for $k\geq 4$ are already found.

Finding the amplitude function of the axial extension deformation mode (which for some special loading and boundary conditions, appears in coupled instabilities) is a subject still under work.

Validation Method

The candidate used the procedure proposed by Ádány et al. [18]. Once the amplitude functions $\mathsf{f}_k(x)$ are extracted from FEA, the displacement field is recreated using Eq. (2). The

error vector d_{err} is computed as the difference between the Finite Element displacement vector d_{FE} and its GBT-based approximation. Finally, the global approximation error (err_{uvw}) can be measured as the norm of the error vector relative to the norm of the FE displacement vector.

$$err_{uvw} = \frac{\sqrt{d_{err}{}^T d_{err}}}{\sqrt{d_{FE}{}^T d_{FE}}} \tag{101}$$

The only drawback of this procedure is that the norm of the warping displacements is usually 1 or 2 orders of magnitude smaller than the norm of the transversal displacements, and consequently this approach will not detect possible significant errors regarding the warping displacement field, if the recreated transversal displacements are very close to the corresponding values provided by FEA. For this reason in section 4, a *warping approximation error* (err_u) concerning only the warping displacement field was calculated and presented parallel with the global approximation error (err_{uvw}).
To compute the GBT-based modal participation a computer application was written using the Matlab programming language. By obtaining very low values of the global approximation errors for arbitrary cross-sections, loading and support conditions, the candidate proved that the described theoretical formulations are correct.

Illustrative Examples - II

Cantilever I-section member

The buckling identification method is used for the buckling analysis of a branched steel section (I-shape), with bar length $L = 1200mm$ and thickness $t = 2mm$. The rest of the dimensions together with Young's modulus and Poisson's ratio are given in Figure 50. The GBT cross-section discretisation is made with 2 and 5 intermediate nodes between edges, respectively in the flanges and web. This gives a number of 17 pure deformation modes and their in-plane shapes are presented in Figure 50. The first four are Global deformation modes, all the rest are, according to GBT definition, Local deformation modes (the cross-section exhibits only flexural plate deformation).

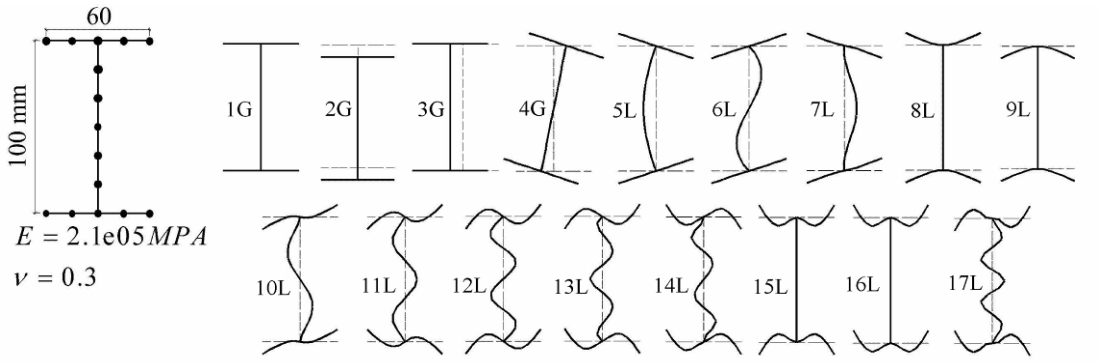

Figure 50. I-section: cross-sectional deformation modes

The member is a cantilever subjected to axial compression and bending by an edge uniform load of intensity $q = 10N/mm$, and two concentrated forces of intensity $P = 50N$ placed at the member free end, in the extremities of the upper flange (see Figure 51). Both loads are variable, depending of the same loading coefficient λ.

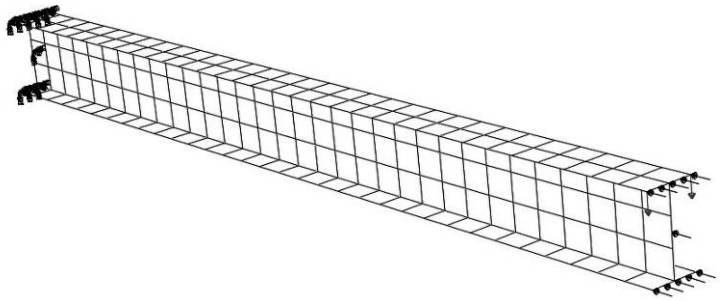

Figure 51. I-section: member FE discretisation, boundary conditions and loading

A shell FE buckling analysis of the thin-walled member was performed in ABAQUS, using S8R5 shell elements (8-node doubly curved thin shell elements, 5 DOF per node and reduced integration) in a highly regular rectangular mesh (see Figure 51). The cross-section discretisation is identical with the one used by GBT and it is constant along the member length, having 32 elements on the longitudinal direction. In order to compute the modal participation, the procedure uses the displacement field of 33 cross-sections, defined by the shell elements edges normal to the member longitudinal axis.

Figure 52 presents the modal participation and the approximation errors calculated by the presented validation method, for the first 50 buckling modes provided by the shell FEA. The presented method is able to provide the amplitude functions of the pure deformation modes for any general buckling mode. Figure 53 presents the deformation shapes of the first 5 buckling modes given by FEA and the corresponding amplitude functions of the first 5 most significant pure modes, provided by the presented method.

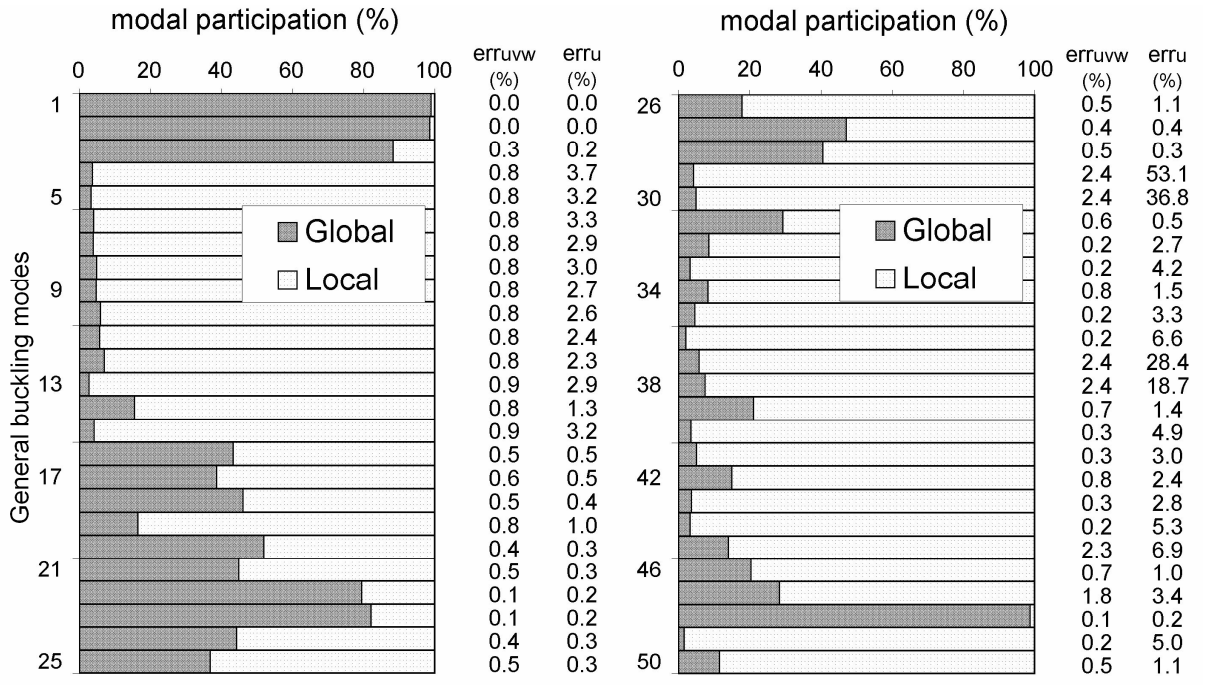

Figure 52. I-section: modal participation, approximation errors

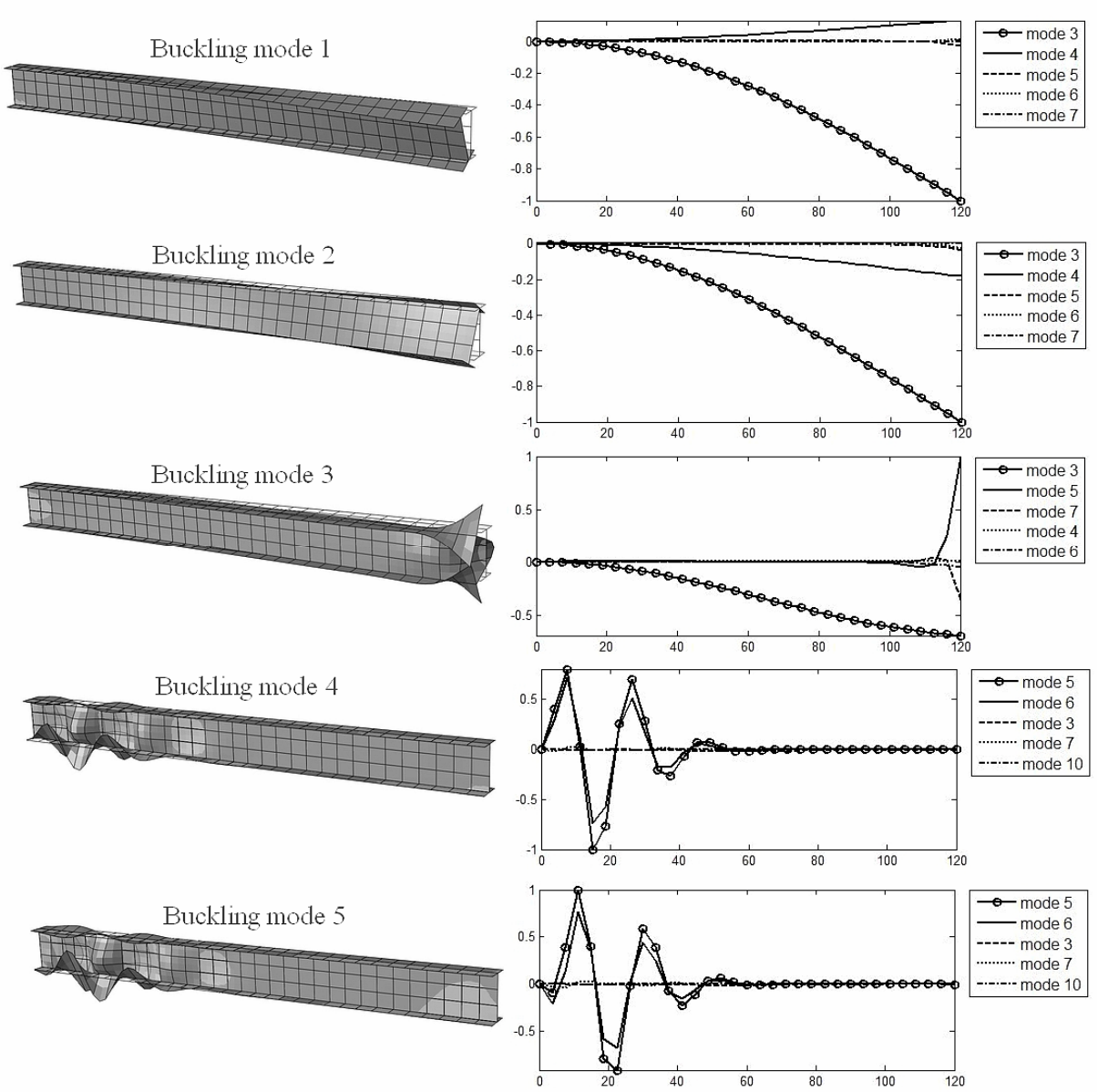

Figure 53. I-section: first 5 FEM buckling modes and the amplitudes of the pure modes

Discussion

As specified in the section "Validation Method", the warping approximation error (err_u) can have significant values, as it can be seen for buckling modes 29, 30, 37 and 38. This is due mainly to the simplifying assumption that the warping displacements *u(x,s)* are linear according the *s* axis. For buckling modes where the local deformations are localized on very small regions (see Figure 54), the errors introduced by this assumption are no longer negligible. On the other hand, the transversal displacements field is very well approximated, a fact proven by the small values of the global approximation error (err_{uvw}) in which the warping displacements have very small contribution. Several tests were made with a finer discretisation, both cross-sectional and longitudinal. Theoretically, by increasing the number of intermediate nodes on the member's cross-section, one introduces new pure modes, which may be in some cases necessary to describe the general buckling deformation. However, for this example, the new pure modes showed negligible contribution to the general deformation. Regarding the longitudinal discretisation, there is always the possibility of localised deformations on a very small region which will not be properly detected using a sparse mesh. However, for this example, tripling the number of FE in longitudinal direction didn't produce a significant improvement, because: (i) the transversal displacement field was already very

well approximated and (ii) for the buckling modes with very localised deformations, the warping approximation errors decrease only by 3-5%.
It can be concluded that the errors introduced by considering linear warping displacements can not be eliminated by an increase of the FE number and new theoretical improvements are needed.

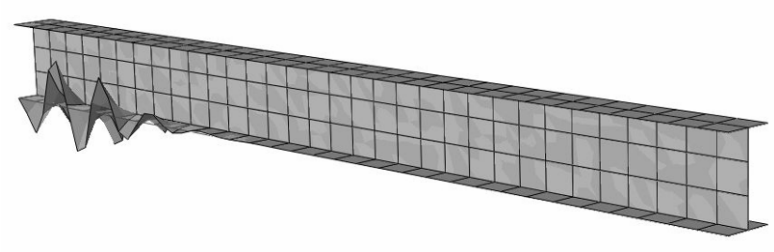

Figure 54. I-section: buckling mode 29 from FEA

C-section member

The second parametric study is completed on a symmetric steel lipped channel (C-shape) already described in section "Illustrative Examples - I". The GBT cross-section discretisation started with 3, 5 and 1 intermediate nodes between the corners, respectively in the flanges, web and flange lips, a configuration named C351. The differences are introduced by the boundary and loading conditions presented in Figure 55 and also by the previously used validation method. The inferior flange is simply supported at midspan (according the vertical axis) and hinged at one member's end. The superior flange of the opposite end is subjected to a uniform vertical load of value q = 10N/mm.

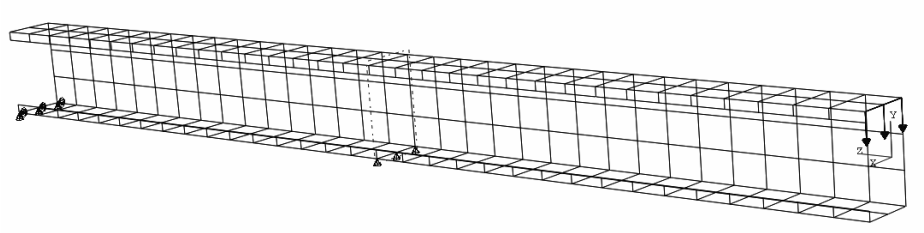

Figure 55. C-section: Member FE discretisation, boundary conditions and loading

The analysis provides the modal participation for the first 50 buckling modes and also the approximation error which had a maximum value of 4.72% for mode no. 42. Figure 56 presents the modal participation and the approximation errors, for the first 50 buckling modes provided by FEA. Figure 57 presents the deformation shapes of the first 5 buckling modes given by the shell FEA and the corresponding amplitude functions of the first 5 most significant pure modes, provided by the presented method.

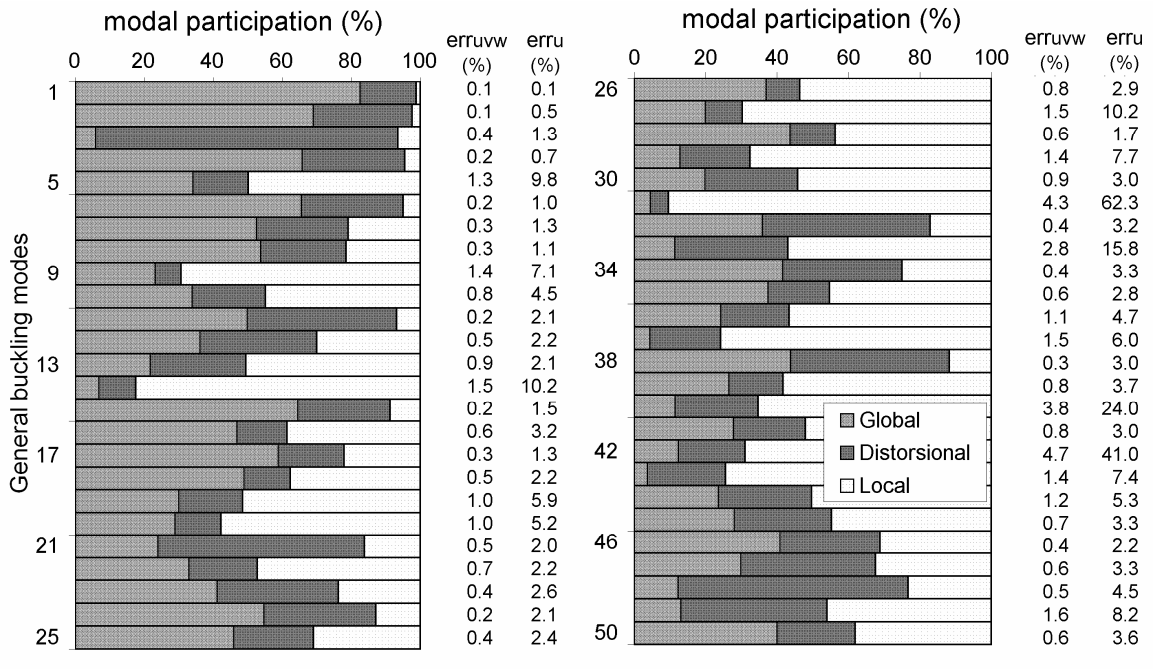

Figure 56. C-section: modal participation, approximation errors

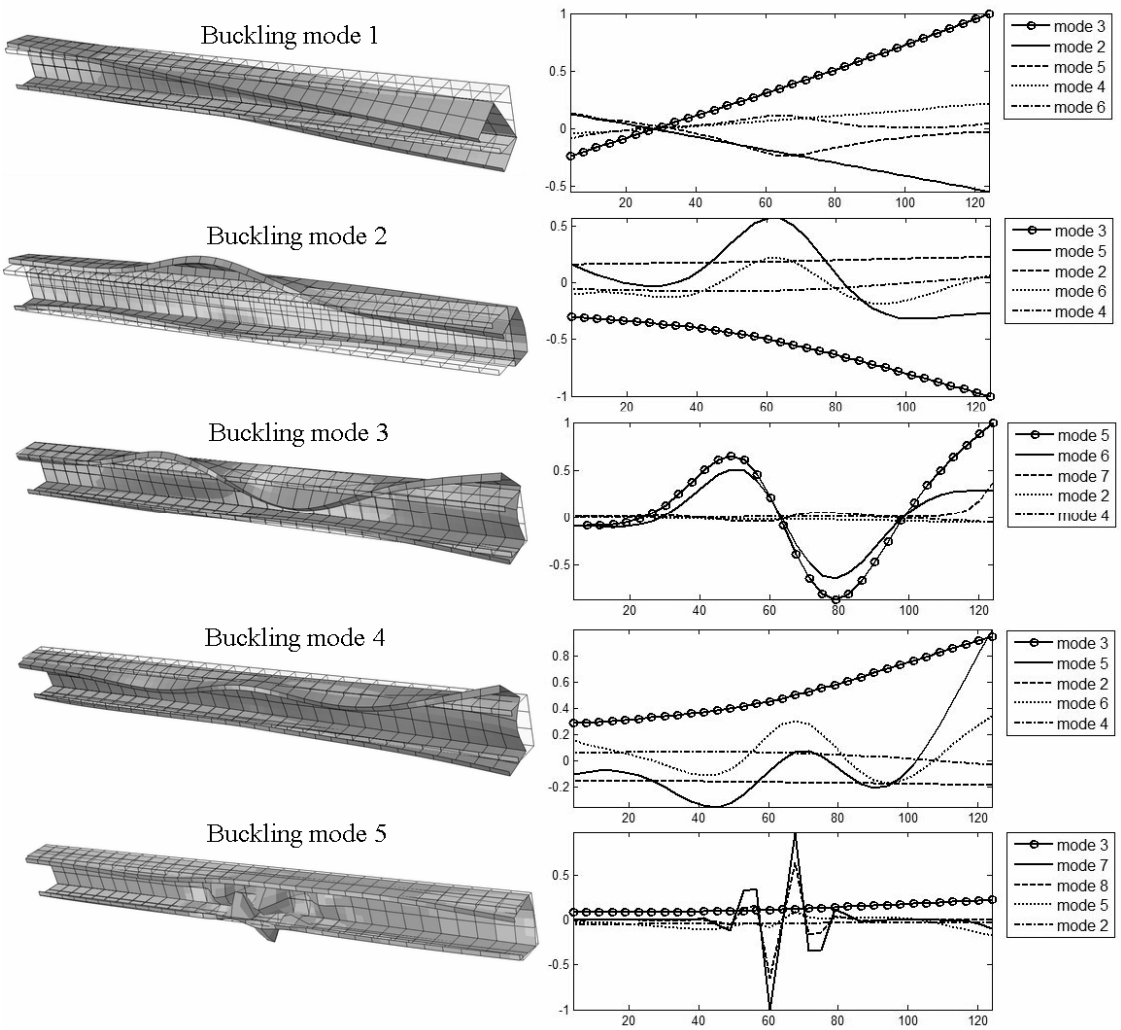

Figure 57. C-section: first 5 FEM buckling modes and the amplitudes of the pure modes

Discussion

In order to assess the effect of the FE discretisation, several analyses were carried out, changing only the number of cross-sectional and longitudinal nodes. Three different configurations were analysed: C571 – 1536FE, C771 – 1792FE and finally C772 – 2048FE. One has to remember the special FE type (S8R5 – 8 nodes/FE) used in this numerical simulation. However, refining the member's discretisation produced no significant improvements regarding the buckling modes with very localised deformations (for this example, modes 14, 27, 31, 33, 40, 42), due to reasons explained in the previous example. The deformed shape of buckling mode 42 is presented in Figure 58.

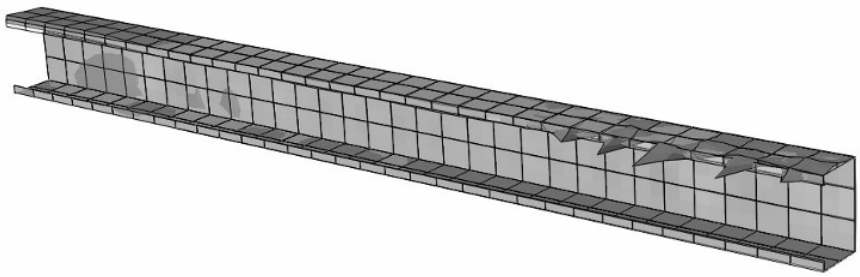

Figure 58. C-section: buckling mode 42 from FEA

3.3.3 Third formulation - members with and without holes

This formulation was not yet published but a paper entitled "Buckling mode identification from shell FEA of perforated thin-walled members" was sent to Journal Computers and Structures and is currently under review.

Perforated cold-formed steel members are often used in civil engineering as structural elements for residential buildings and storage rack systems. The new formulation proposed by the candidate and described in this section can be applied for both members with and without holes.

An extensive literature review is given in [62] where the authors concluded that perforated sections and non-standard restraint conditions make the numerical analysis too complicated to be used in the design of storage rack structures. Consequently, current design of these structures is based on test procedures. Nevertheless, extensive research is currently under work, to overcome these difficulties. The spline FSM [63] is an elegant tool capable to analyze perforated members but it is not yet developed to quantify the participation of pure deformation modes.

Regarding GBT and cFSM, considering that these methods were initially developed for unperforated compression members, special adjustments and approximations had to be introduced. Davies et al. [64] investigated the local buckling in rack sections. He carried out tests on stub column members and compared the results to the ones obtained numerically with GBT and FEM. Recently, Moen & Schafer [65] reported the use of cFSM and Direct Strength Method (DSM) for perforated thin-walled sections. Both methods take into account the effect of the holes by introducing the concept of *reduced thickness* of the perforated strip.

Even if satisfactory results have been obtained, this procedure could be criticized for using an unperforated model, disregarding the stress concentrations around the holes. It would be also impossible to apply this procedure for the case of uneven distribution or size of the holes.

This section presents the theoretical extension of the GBT-based modal identification method developed by the author, for the special case of isotropic perforated thin-walled members. In principle, the method uses the same technique as for the case of unperforated elements and it starts with a classic buckling shell FEA. The GBT cross-sectional analysis is used *only* to define the cross-sectional deformation modes, each one corresponding to a pure Global,

Distorsional or Local (GDL) buckling type. Next, they are used to extract from buckling shell FEA, discrete values of the amplitude functions of each pure buckling mode on a regular grid of points along the member's axis. For the points lying in the perforated regions, special assumptions and theoretical developments are introduced, thus taking into account the effect of holes. Based on the obtained amplitude functions, the modal participation is computed. For validation, the displacement field provided by shell FEA is compared with the one recreated using the extracted amplitude functions and the GBT cross-sectional deformation modes. This last step leads to the approximation error of the entire procedure.

Thin-walled members without holes

In this formulation, new improvements have been made, consequently only two stiffness matrices were used - the warping stiffness matrix C and the geometrical stiffness matrix X (see Eq. (79)). The stiffness matrices B and D are no longer used, since the candidate discovered that all the amplitude functions $\mathsf{f}_k(x)$ can be extracted by using only the geometrical stiffness matrix X. Considering Eq. (79), only the first matrix is used, namely X_1 standing for the stiffness degradation due to pre-buckling axial compression. The cross-section warping mode is constant along cross-section and has the expression $u_j = -1$. The corresponding component of the warping matrix has the expression $C_{11} = EA$, where A is the cross-sectional area. Introducing the simplified notation X_{ik}, the expression of X_{1ik} becomes:

$$X_{ik} = X_{1ik} = -\frac{1}{A}\int_s (v_i v_k + w_i w_k) t ds \tag{102}$$

The first term inside the integral is easy to calculate, considering the first Vlasov's hypothesis ($\mathsf{e}_s^{M,L} = 0$) which gives constant displacements v along each plate. Using the discrete values given in Figure 6b that approximate the element deformation, the above integral becomes:

$$\begin{aligned} X_{ik} = -\frac{1}{A}\sum_{r=1}^{np} b_r t_r \Bigg[& v_{i,r} v_{k,r} + \overline{w}_{i,r}\overline{w}_{k,r} + \mathsf{q}_{i,r}\mathsf{q}_{k,r}\frac{b_r^2}{12} + \left(\overline{w}_{i,r}\overline{m}_{k,r} + \overline{m}_{i,r}\overline{w}_{k,r}\right)\frac{b_r^2}{12K} + \dots \\ & + \left(\mathsf{q}_{i,r}\hat{m}_{k,r} + \hat{m}_{i,r}\mathsf{q}_{k,r}\right)\frac{b_r^3}{360K} + \left(\overline{m}_{i,r}\overline{m}_{k,r} + \frac{1}{63}\hat{m}_{i,r}\overline{m}_{k,r}\right)\frac{b_r^4}{120K^2}\Bigg] \end{aligned} \tag{103}$$

where np is the number of segments considered along the cross-section, delimitated by the fold-lines and the considered intermediate nodes. For a segment r, $\overline{w}_r$ is the middle transversal displacement, q_r is the plate absolute rotation, $\overline{m}_r$ and $\hat{m}_r$ are the semi-sum and the semi-difference, respectively, of the end transversal moments m_r. During the 1st GBT step, the components of matrix X are computed based on the above equation.

Next, a buckling shell FEA of a thin-walled member is performed and the cross-sectional displacement field is extracted on a mesh of points along the member's axis ($0 \le x_1 < x_2 < \dots < x_g < \dots \le L$, with L being the bar's length) and the GBT product formulation is considered according to Eq. (80). From the transversal displacements v_{FE} and w_{FE} one can easily derive the values of the absolute rotations q_{FE}. Next, one recreates the matrix X, by introducing the FE displacement field instead of the cross-section deformation modes, index k. Here the method uses an approximation, by using only the transversal displacements and the absolute rotations, which can be easily extracted from a shell FEA. Even if the neglected terms are known to have very small effect [8], they should be taken into account and research is currently under work on this subject. The result is a column matrix having the following expression:

$$X_{FE,i} = -\frac{1}{A}\sum_{r=1}^{np} b_r t_r \left[v_{i,r} v_{FE,r} + \overline{w}_{i,r}\overline{w}_{FE,r} + \mathsf{q}_{i,r}\mathsf{q}_{FE,r}\frac{b_r^2}{12} + \overline{m}_{i,r}\overline{w}_{FE,r}\frac{b_r^2}{12K} + \hat{m}_{i,r}\mathsf{q}_{k,r}\frac{b_r^3}{360K} \right] \tag{104}$$

Looking again at Eq. (80) and Eq. (102) one can see the following relation

$$X_{FE,i} = -\frac{1}{A}\int_s (v_i v_{FE} + w_i w_{FE})tds = \sum_{k=1}^{n}\left(-\frac{1}{A}\int_s (v_i v_k + w_i w_k)tds \right)\mathsf{f}_k(x_g) = \sum_{k=1}^{n} X_{ik}\mathsf{f}_k \tag{105}$$

which, written in matrix formulation, becomes

$$X\mathsf{f} = X_{FE} \tag{106}$$

Next, the column vector f containing the discrete values of the amplitude functions for any specified point x_g ($0 \le x_g \le L$), is calculating by solving the above system of linear equations. By interpolation, the amplitude functions can be found on the entire domain.

Having the amplitudes functions, one can recreate the transversal displacements *v* and *w* using the last two formulas of Eq. (80) of the entire member. In order to recreate also the warping displacements *u,* using first formula of Eq. (80), one has to extract the derivatives of the amplitude functions $\mathsf{f}_k'(x)$.

The procedure is similar with the previously described; the difference stays in using matrix *C* instead of *X*. Starting with Eq. (79), the membrane components are calculated using the nodal warping values (see Figure 6a), considering linear warping along the cross-section.

$$C_{ik}^{M} = E\sum_{r=1}^{np} t_r b_r \left(\frac{u_{i,r1}u_{k,r1} + u_{i,r2}u_{k,r2}}{3} + \frac{u_{i,r1}u_{k,r2} + u_{i,r2}u_{k,r1}}{6} \right) \tag{107}$$

The bending components are written introducing the same discrete values used in Eq. (103):

$$\begin{aligned} C_{ik}^{B} = \sum_{r=1}^{np} K_r b_r \Bigg[& \overline{w}_{i,r}\overline{w}_{k,r} + \mathsf{q}_{i,r}\mathsf{q}_{k,r}\frac{b_r^2}{12} + \left(\overline{w}_{i,r}\overline{m}_{k,r} + \overline{m}_{i,r}\overline{w}_{k,r}\right)\frac{b_r^2}{12K} + \dots \\ & + \left(\mathsf{q}_{i,r}\hat{m}_{k,r} + \hat{m}_{i,r}\mathsf{q}_{k,r}\right)\frac{b_r^3}{360K} + \left(\overline{m}_{i,r}\overline{m}_{k,r} + \frac{1}{63}\hat{m}_{i,r}\overline{m}_{k,r}\right)\frac{b_r^4}{120K^2} \Bigg] \end{aligned} \tag{108}$$

One recreates matrix *C*, by introducing the displacement field extracted from shell FEA

$$C_{FE,i} = C_{FE,i}^{M} + C_{FE,i}^{B} = E\int_s t u_i u_{FE} ds + \int_s K w_i w_{FE} ds \tag{109}$$

and the final matrix equation yields:

$$C^{M}\mathsf{f}' + C^{B}\mathsf{f} = C_{FE} \tag{110}$$

from which the column vector f' containing the discrete values of the derivatives of the amplitude functions in any specified point x_g ($0 \le x_g \le L$), is calculated, keeping in mind that the column vector f was already found in the previous stage.

The effect of the bending components is very small, comparing with the membrane components, so an extra approximation could be introduced, considering for this step, only the warping membrane stiffness matrix ($C \simeq C^{M}$). Eq. (110) becomes

$$C^{M}\mathsf{f}' = C_{FE}^{M} \tag{111}$$

which significantly reduces the computational cost.

Having the amplitude functions and their derivatives, the approximation error of the entire procedure is done according to Eq.(101). Finally, the method provides the modal identification and participation, the goal of the entire procedure, using Eq. (96).

Thin-walled members with holes

The main goal of this section is to present the application of the above described formulation to the special case of perforated thin-walled members. First, the member is divided in two regions along its length as shown in Figure 59: continuous regions given by the intervals *d*, and regions with holes given by the intervals d_h. These intervals don't have to be equal, there are no theoretical limitations concerning the shape, size and distribution of the holes. Of course a regular pattern will increase the speed of this procedure and it will ease its implementation in a computer application, but not to a significant extent. The buckling shell FEA is performed. For any point $x_g\ (0 \le x_g \le L)$ situated inside and at the borders of the continuous regions, the method described in the previous section can be directly applied.

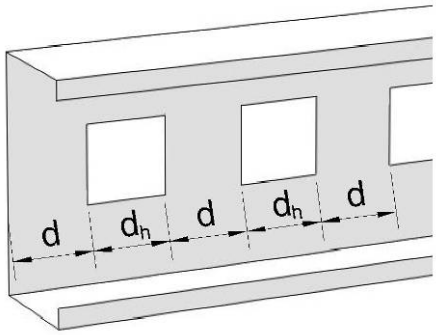

Figure 59. Thin-walled member: continuous and perforated regions

For the perforated regions, the method can be applied if a minor modification is performed, taking into account the missing segments along the cross-section. The cross-section deformation modes for the example given in Figure 43, remain the same, so the GBT 1st step is still applied for the continuous cross-section. Working from the start with a perforated cross-section will introduce an entire different set of cross-section deformation modes, difficult to classify as GDL modes, and not compatible with the one obtained for the continuous cross-section. Actually the GBT will "see" the perforated cross-section of the C-section given in Figure 59 as two distinct cross-sections. The modification is introduced with respect the stiffness matrices. Basically, the components of these matrices are given by the virtual work produced by unit values of the amplitude functions, or their derivatives. So, for each missing segment, the virtual work is eliminated. Eqs. (103), (104), (107) and (108) are modified only by the number of segments *np*, which is now the initial number of segments minus the ones corresponding to the hole. The simplest example is of the warping matrix component $C_{11} = EA_h$, where A_h is now the area of the perforated cross-section. Next the procedure is applied for any point $x_g\ (0 \le x_g \le L)$ situated inside (and not at the borders) of the perforated regions.

Illustrative Examples - III

The parametric study is completed on a perforated symmetric steel lipped channel; dimensions referred for the mid-line together the material properties are given in Figure 60. The thickness for all walls is t = 2mm and the bar's length is L = 1240mm. As shown in Figure 59, the holes are square (side d_h = 40mm), have equal size and they are placed in a regular pattern (distance between holes d = 40mm) at the middle of the web height. The GBT cross-section discretisation is made with 7, 11 and 1 intermediate nodes between the corners, respectively in the flanges, web and flange lips. The GBT 1st step provides a number of 35 pure deformation modes, a step performed as explained in the previous section, on the continuous cross-section. The derivation of the stiffness matrices used by this method

(namely C and X) and also of the cross-section deformation modes ($u_k(s)$, $v_k(s)$, $w_k(s)$) can be done with the help of the free available and user friendly software GBTUL.

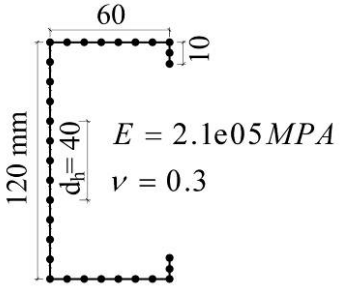

Figure 60. C-section: mid-line dimensions and material properties

A buckling shell FEA of a thin-walled member was performed using ABAQUS for the first 50 eigenvalues. 3728 shell elements of type S4 were considered, in a highly regular rectangular mesh (see Figure 61). The cross-section discretisation is constant along the member length and identical with the one used by the GBT 1st step. In longitudinal direction, all the elements have the same size of 10mm. In order to implement the described method of buckling identification and to calculate the modal participation, a MATLAB application was written. It uses the FE displacement field of 125 cross-sections given by the shell elements sides normal to the member longitudinal axis.

Numerical results for a simple supported column

The simple supported (SS) boundary conditions correspond to pinned–pinned, both locally and globally, and free to warp end supports, sometimes also referred to as *fork supports*. Moreover, during FEM analysis the longitudinal translation was restrained approximately at the middle of the member, as shown in Figure 61. The member is axially compressed by an edge uniform load of intensity $q = 3.846 N/mm$ which gives a resultant force of 1000N.

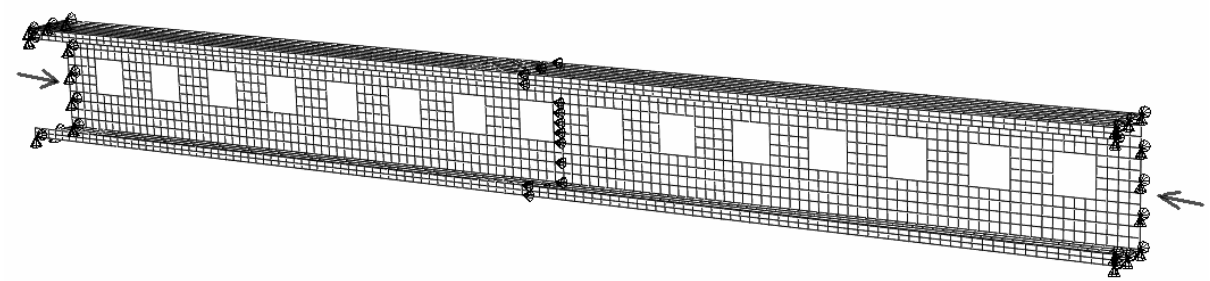

Figure 61. SS Member: FE discretisation, boundary conditions and loading

The analysis provides the modal participation for the first 50 buckling modes and also the approximation error which had a maximum value of 1.62% for mode no. 49. Table 17 shows these results for the first 10 buckling modes. It can be concluded that the first 10 buckling modes are of Distortional-Local type, except the 5th one which is a Global-Distortional coupled instability. Figure 62 presents the deformation shapes of the first 5 buckling modes given by shell FEA and the corresponding amplitude functions of the first 5 most significant pure modes, provided by the presented method.

Table 17. SS Member: Modal participation and approx. error for the first 10 buckling modes

Buckling mode	2G	3G	4G	5D	6D	7-35L	error (%)
1	0.00	0.48	0.00	86.64	0.00	12.87	0.26
2	0.00	0.63	0.00	85.55	0.00	13.82	0.27
3	0.00	0.44	0.00	82.19	0.00	17.37	0.30
4	0.00	0.69	0.00	84.60	0.00	14.71	0.27
5	23.15	0.00	35.51	0.00	38.78	2.56	0.10
6	0.96	0.00	0.67	0.00	91.07	7.30	0.34
7	2.77	0.00	4.00	0.00	86.12	7.11	0.32
8	1.38	0.00	1.05	0.00	91.45	6.11	0.32
9	0.00	0.84	0.00	73.74	0.00	25.42	0.39
10	0.00	0.71	0.00	74.21	0.00	25.08	0.39

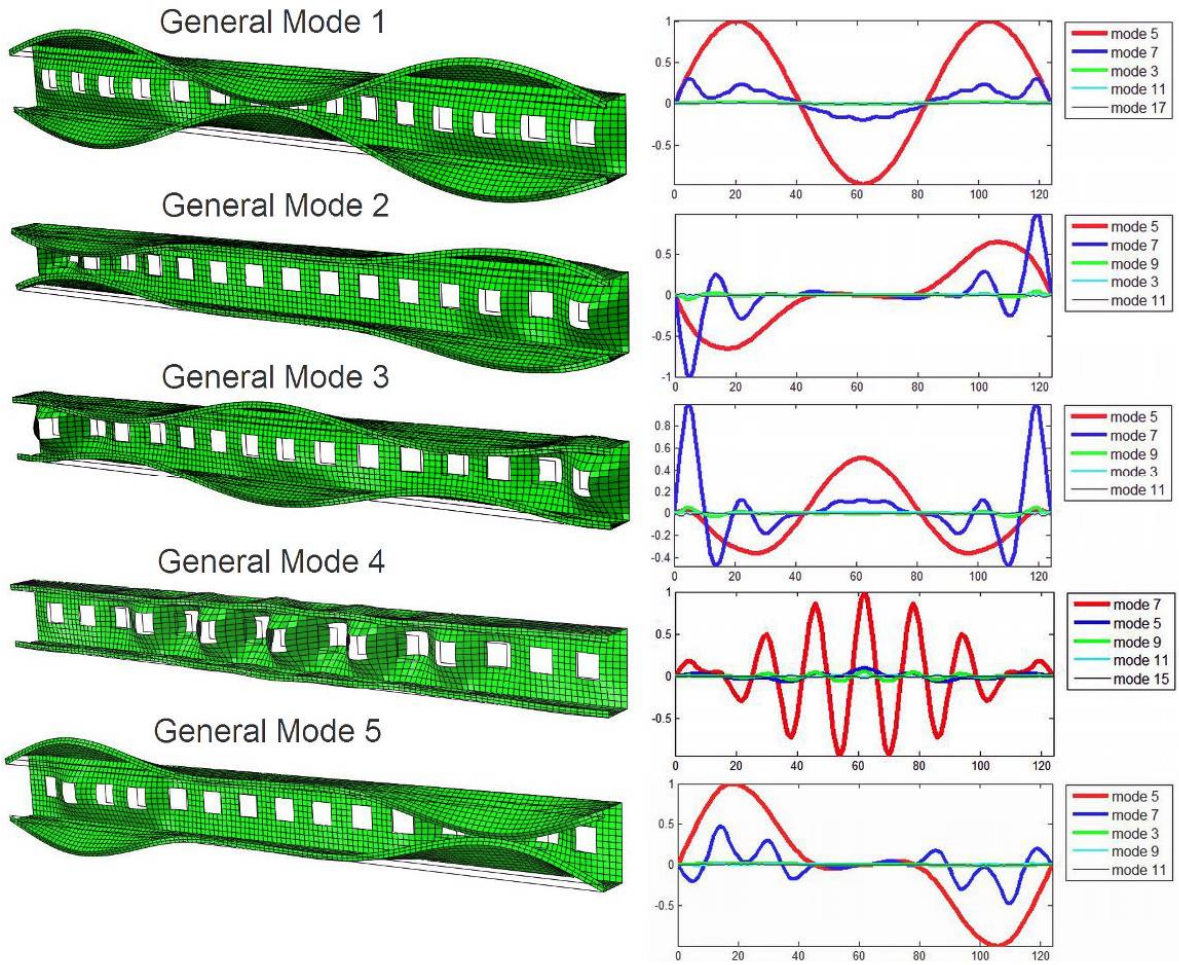

Figure 62. SS Member: first 5 FEM buckling modes and the amplitudes of the pure modes

Numerical results for a cantilever column with concentrated loads

The member of the previous example is now analysed using clamped-free (CF) boundary conditions. The loading is also replaced with 2 longitudinal, equal forces of intensity $P = 500N$, placed at the end at the intersection between the upper flange with the web and lip, as shown in Figure 63.

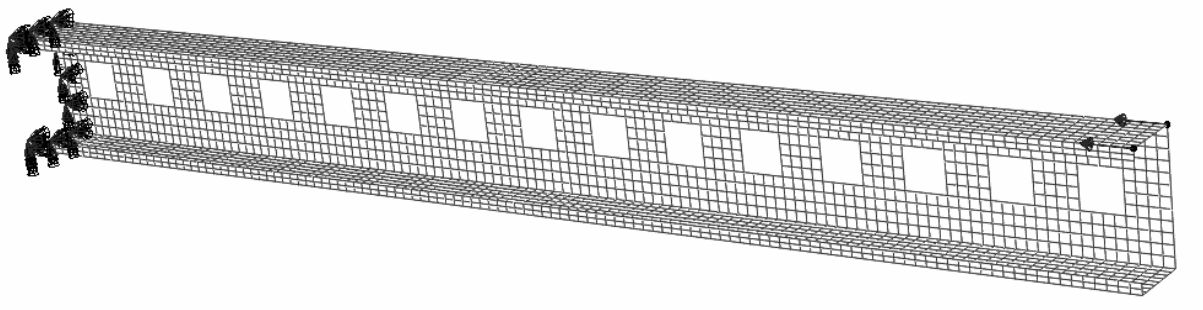

Figure 63. CF Member: FE discretisation, boundary conditions and loading

Once again the first 50 buckling modes are analysed and the maximum approximation error is now 2.24% for mode no. 41. Table 18 shows the modal identification and the approximation error of the proposed method for the first 10 buckling modes.
Figure 64 presents the deformation shapes of first 5 buckling modes given by shell FEA and the corresponding amplitude functions of the first 5 most significant pure modes, provided by the presented method.

Table 18. CF Member: Modal participation and approx. error for the first 10 buckling modes

Buckling mode	2G	3G	4G	5D	6D	7-35L	error (%)
1	9.96	51.17	16.11	14.56	5.89	2.31	0.06
2	1.71	59.61	10.36	16.16	9.30	2.85	0.05
3	1.62	16.30	1.17	45.72	25.45	9.75	0.25
4	1.26	15.45	1.48	46.77	25.31	9.72	0.25
5	2.66	23.48	1.28	40.13	21.88	10.56	0.24
6	6.09	34.83	0.69	33.77	15.73	8.89	0.19
7	9.32	42.73	1.68	28.75	10.89	6.63	0.15
8	9.47	36.31	2.77	25.62	13.60	12.23	0.18
9	10.76	36.04	3.25	18.60	12.67	18.69	0.21
10	8.26	22.68	3.48	19.55	14.23	31.79	0.34

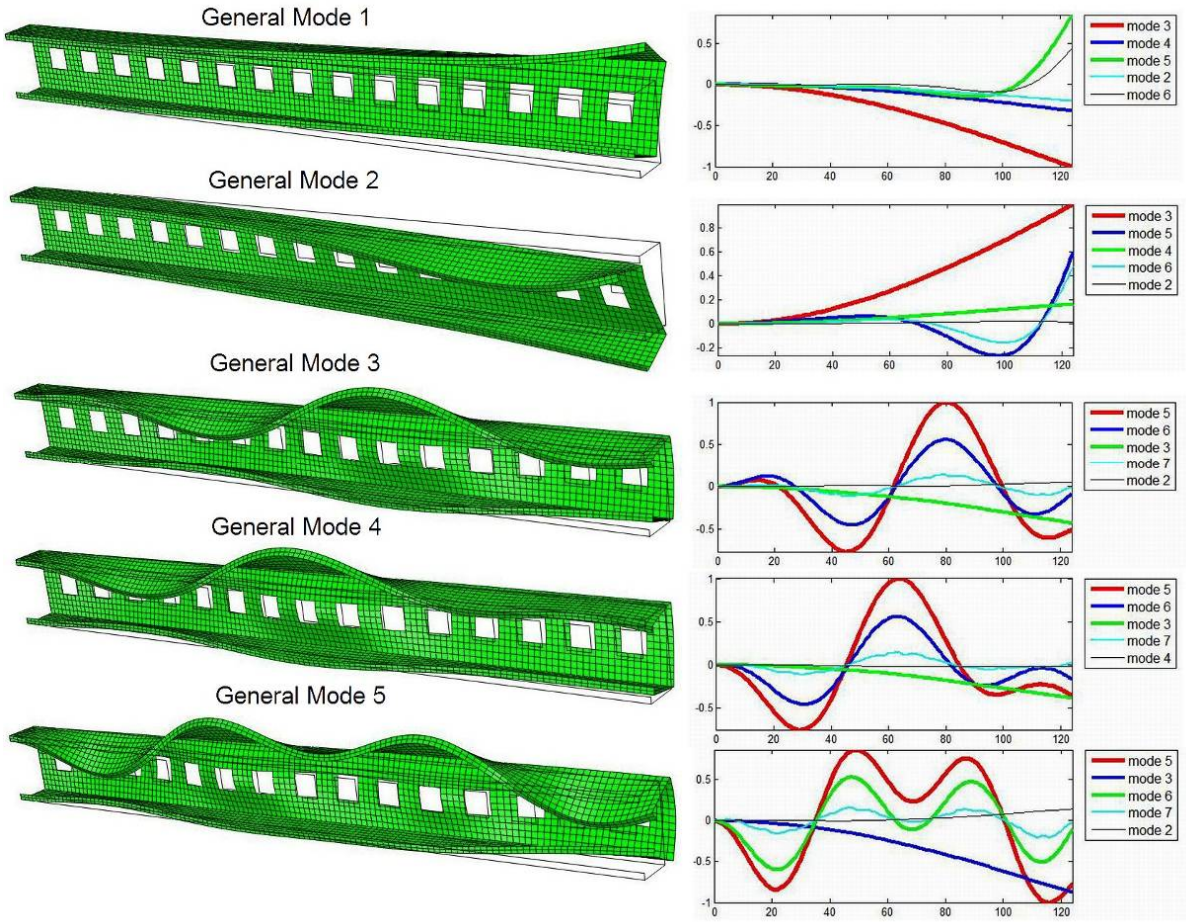

Figure 64. CF Member: first 5 FEM buckling modes and the amplitudes of the pure modes

Discussion

Other numerical simulations showed that the approximation errors strongly depend on the GBT and FEM discretisation, meaning that the refining of the longitudinal mesh and of the GBT cross-sectional discretisation improve the accuracy of the presented method. One has to keep in mind the basic assumptions introduced by the classic GBT, especially the Vlasov's hypotheses and the linearity of the warping displacements $u(x,s)$ according the s axis. Nowadays GBT is capable to handle non-linear variation of the warping displacements along the cross-section wall midline, and also can take into account the cross-section deformations due to the wall transverse extensions [66]. New pure modes are introduced, namely shear modes and transverse extension modes. The implementation of these two features will further improve the precision of the presented method, and is currently under work.

Numerical results for a cantilever column with two rows of holes

The following study was fully described in the following conference article:

- **Nedelcu M**, Chira.N, Cucu HL, Popa AG (2013). "Buckling mode decomposition of thin-walled members with holes", SEMC 2013, The Fifth International Conference on Structural Engineering, Mechanics and Computation, 2-4 September 2013, Cape Town, South Africa.

The parametric study is completed on a perforated symmetric steel lipped channel with boundary conditions of type clamped-free (cantilever member). Figure 65 presents the cross-sectional dimensions referred for the mid-line, the size and distribution of the holes, and the

material properties (Young's modulus and Poisson's ratio). The thickness for all walls is t = 2mm and the bar's length is L = 1240mm. The holes are rectangular, have equal size and they are placed in a regular pattern. The GBT cross-section discretisation is made with 5, 9 and 1 intermediate nodes between the corners, respectively in the flanges, web and flange lips. The GBT 1st step provides a number of 29 pure deformation modes.

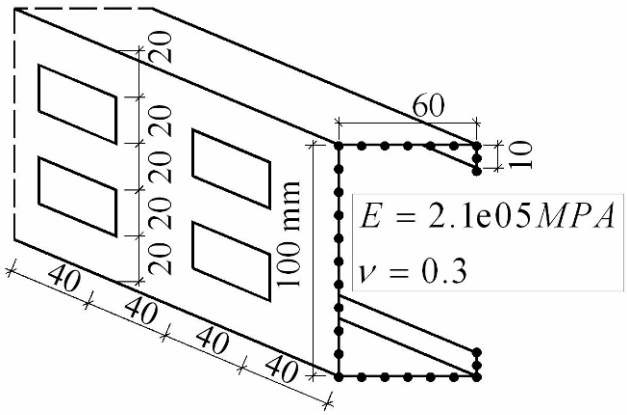

Figure 65. Lipped channel

A buckling SFEA of a thin-walled member was performed using ABAQUS (for the first 50 eigenvalues. 2984 shell elements of type S4 were considered, in a highly regular square mesh (see Figure 66). The cross-section discretisation is constant along the member length and identical with the one used by the GBT 1st step. In longitudinal direction, all the elements have the same size of 10mm. The method used the FE displacement field of 125 cross-sections given by the shell elements sides normal to the member longitudinal axis. The member is axially compressed by edge uniform loads applied on the free end and also on one edge of the six holes indicated in Figure 66. For the free end, the loading magnitude is q_1 = 4.1667N/mm and for the holes q_2 = 12.5N/mm.

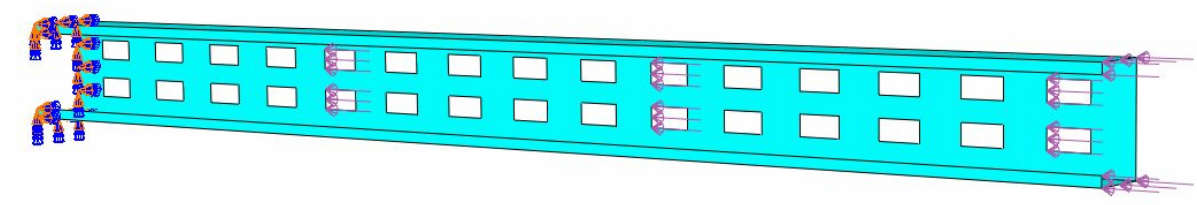

Figure 66. Loading and boundary conditions

The analysis provides the modal participation of the Global, Distortional and Local deformation modes for the first 50 buckling modes and also the approximation error which had a maximum value of 5.89% for mode no. 38. A better approximation can be achieved by refining the GBT cross-sectional discretisation and also the member longitudinal mesh, but not significant changes were observed regarding the modal participation. Figure 67 shows these results for the first 50 buckling modes. Figure 68 presents the deformation shapes of the first 5 buckling modes given by the shell FEA and the corresponding amplitude functions provided by the buckling decomposition method.
It can be concluded that the first buckling mode is a Global mode of flexural-torsional type. Modes 2, 3 exhibit a Global-Local behaviour, mode 4 is a global mode (flexural over the minor axis) and the rest are coupled instabilities of GDL type.

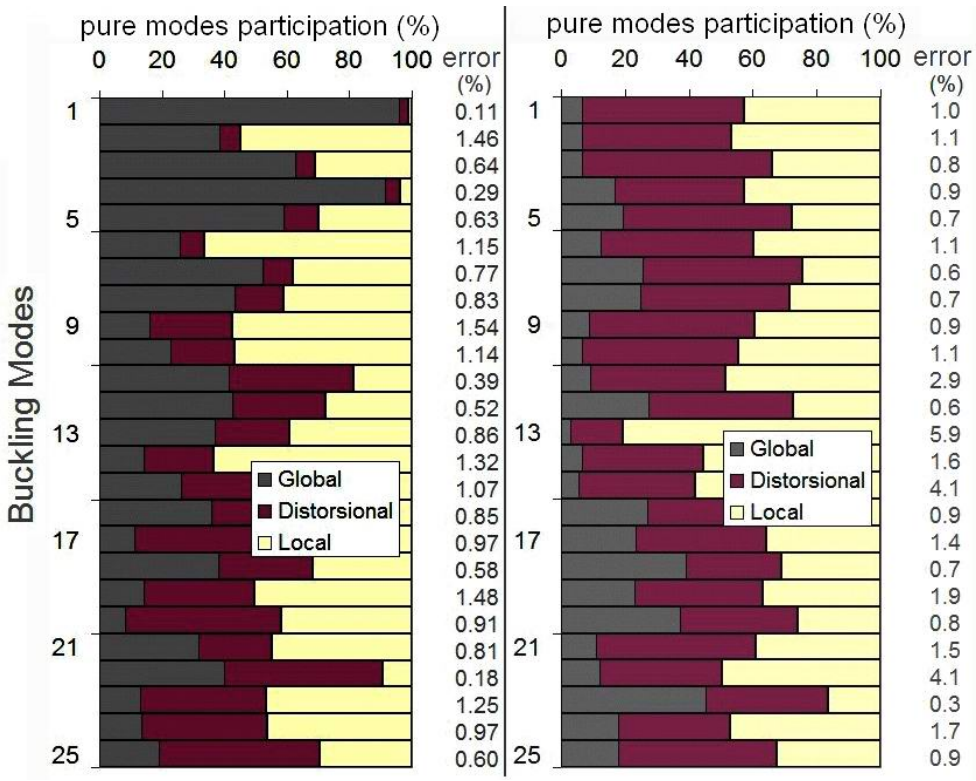

Figure 67. Modal participation and approximation error for the first 50 buckling modes

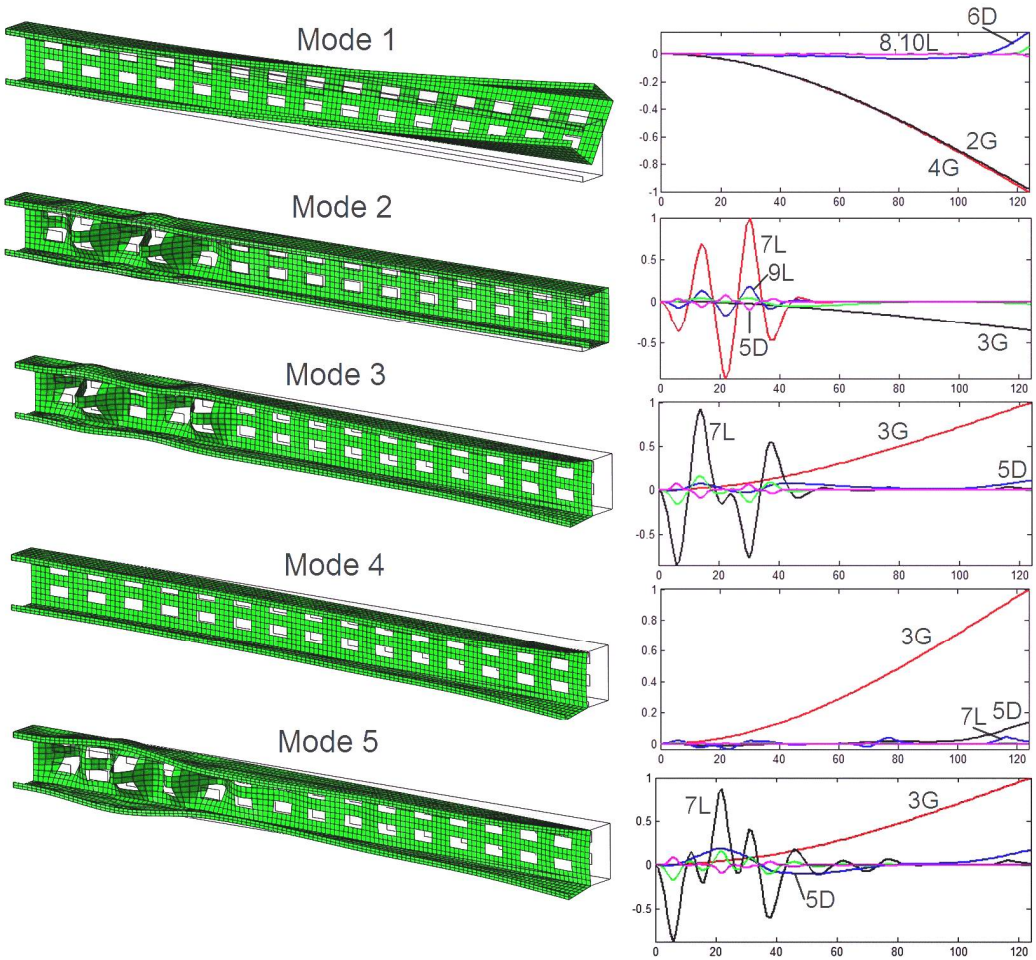

Figure 68. First 5 buckling modes and the corresponding amplitude functions

Conclusions

This section presented a GBT-based method capable of decomposing any thin-walled member deformations (such as buckling modes) into global, distortional and local pure deformation modes and of computing their quantitative participation. The deformations to be decomposed can be determined by FEM or any similar numerical methods.
Only the GBT first step is used (the cross-section analysis) in order to have the modal cross-section deformation components, edge transverse moments, warping and transverse bending stiffness matrices. Using the modal orthogonality, the GBT amplitude functions are extracted from the FEM deformations. Finally, the modal participation factors are computed based on the amplitude functions. Several numerical examples are presented, in which the GDL deformation modes participation is identified in the general buckling modes calculated by FEM, applying shell finite elements. Both column and beam problems are solved by using arbitrary loading and boundary conditions.
The last formulation presented the theoretical extensions and the applicability of the proposed method for the special case of thin-walled members with holes. In theory, there are no restrictions concerning the shape, size and distribution of the holes. However, writing a computer application for an arbitrary pattern of holes is not yet finished, due to some technical difficulties, so the presented examples display a highly regular distribution of identical holes. Fortunately, in practice the vast majority of perforated thin-walled members have this property.
Regarding the method limitations, following the GBT classical assumptions, the membrane transverse extensions and shear strains are neglected, together with the pure deformation modes which may contain these deformations.
Regarding the method advantages, there are no restrictions regarding the cross-section shape, loading and boundary conditions. In principle, the method is not restricted to prismatic members or cross-sections made of straight segments, so it can be applied to any member GBT can handle. Nowadays, GBT was extended to cover tapered thin-walled members, conical shells, circular and elliptical cylindrical shells and tubes.
Its high speed must also be mentioned. The GBT cross-analysis involves an eigenvalue problem of small dimensions, a relatively small number of matrix computations and there is no need for the second GBT step (the member stability analysis). This second step is by far the most time-consuming one in a GBT analysis, except for the use of analytical solutions, which are restricted to simply supported members. Also, the computation of the amplitude functions and modal participation follows an analytical and simple procedure. Another advantage is the possibility of working with a limited number of GBT pure modes. After a first analysis, the user can choose a set of the most significant pure modes, and if the approximation errors are satisfactory, maintain this set for future analyses, thus further increasing the speed of this method.
For all these reasons, the proposed method is elegant, extremely fast and a promising candidate to providing buckling mode decomposition for arbitrary thin-walled members modelled in general purpose finite element codes.

Personal Contribution

Starting from classical GBT, the candidate succeeded in formulating an original modal decomposition method and proved its capabilities by several numerical examples. Presently, the method is continuously optimised, a fact proved by the three different formulations presented here. In the last formulation, the candidate extended the method for the buckling analysis of thin-walled members with holes.

4. Vibration analysis of civil engineering structures

This section covers two main research directions followed by the candidate, both related with the vibration analysis. First deals with the applicability of the modal decomposition method described in section 3.3 to the modal shapes derived from FEA associated with the natural frequencies. The second involves the experimental vibration analyses performed by the candidate on real-world structures and also on small elements inside laboratory.

4.1 Vibration mode decomposition from FEA of thin-walled members

In order to properly assess the buckling and dynamic behaviour of thin-walled members, one must identify the relevant deformation modes involved and their contribution to the general buckling/vibration modes. Section 3 described the theoretical research of the candidate related with the buckling analysis of thin-walled members. None the less, one has to take into account that a high mathematical resemblance exists between the stability and vibration analyses (solutions of similar eigenvalue problems). Indeed, extensive research has been performed by Camotim, Silvestre et al. in this area using GBT, and their software GBTUL is able to perform both analyses [67]-[69]. In addition, the method proposed in article 3, and fully described in section 3.3, was applied by the candidate to FEM vibration analyses on thin-walled members with and without holes, in order to extract the contribution of each pure deformation mode of Global, Distortional or Local nature. The contribution of each pure GDL deformation mode can be calculated, allowing a better understanding of their variation depending on the thin-walled member natural frequencies, modal shapes, loading level and supports. Similar with the buckling analyses, there are no restrictions regarding the element cross-sectional shape, loading and boundary conditions.
The applicability of the modal decomposition method proposed by the candidate is briefly presented below and it is fully covered by article 9 and also by the following conference article:

- **Nedelcu M**, Popa AG, Cucu HL, Chira N (2013). "Vibration mode decomposition from Finite Element Analysis of thin-walled members with holes", 11th International Conference on Vibration Problems, 9-12 September 2013, Lisbon, Portugal.

4.1.1 Members without holes

The parametric study is completed on a simple supported axially compressed steel column (C-shape); mass density $\rho = 7850\, daN/m^3$, bar length $L = 100cm$, thickness $t = 2mm$ and the rest of dimensions together with Young's modulus, Poisson's ratio and GBT discretisation are given in Figure 43. The pure deformation modes are also presented in Figure 43 (through their in-plane shapes) and their deformation *nature* (global, distortional or local) is clearly established. A buckling combined with a "Frequency" FEA of the thin-walled member was performed in ABAQUS, using S4 shell elements in a highly regular rectangular mesh. In order to compute the modal participation, the procedure uses the displacement field of all cross-sections defined by the shell elements edges normal to the member longitudinal axis.
The 1st step provides the critical loads given in Table 19 for the first 5 buckling modes. Next, the vibration analyses are carried out applying different levels of the compression force, from 0 (load-free case) till $0.99P_{cr}$, where P_{cr} is the critical load of the 1st buckling mode. Table 20 presents the fundamental vibration modes for each loading step with the corresponding angular frequencies and modal participations. The last column of both tables shows the

approximation error (calculated by Eq. (101)) of the modal decomposition given by the proposed method.
Figure 69 presents the 1st buckling mode and two vibration mode shapes together with the corresponding amplitude functions of the deformation modes which proved to have the most significant contribution.

Table 19. Modal participation for the first 5 buckling modes

Buckling mode	FEA	Modal participation (%)									Error
	P_{cr} (kN)	2	3	4	5	6	7	8	9	10-21	(%)
1	158.3	0.0	0.5	0.0	90.0	0.0	8.0	0.0	1.4	0.1	0.4
2	183.9	0.0	0.8	0.0	87.4	0.0	10.3	0.0	1.4	0.1	0.4
3	195.1	0.0	0.2	0.0	7.4	0.0	85.8	0.0	5.5	1.1	0.9
4	195.8	0.0	0.2	0.0	18.9	0.0	74.4	0.0	5.4	1.1	0.9
5	199.4	23.7	0.0	32.8	0.0	42.0	0.0	1.1	0.0	0.3	0.1

Table 20. Modal participation for the fundamental vibration mode using 5 loading levels

Vibration mode	FEA	Modal participation (%)									Error
	ω(rad/s)	2	3	4	5	6	7	8	9	10-21	(%)
0.00Pcr	722.9	23.8	0.0	33.0	0.0	41.8	0.0	1.1	0.0	0.3	0.1
0.10Pcr	693.8	23.8	0.0	33.0	0.0	41.8	0.0	1.1	0.0	0.3	0.1
0.50Pcr	562.7	23.7	0.0	32.9	0.0	41.9	0.0	1.1	0.0	0.3	0.1
0.90Pcr	390.1	23.6	0.0	32.7	0.0	42.2	0.0	1.1	0.0	0.3	0.1
0.99Pcr	192.4	0.0	6.4	0.0	84.9	0.0	7.4	0.0	1.3	0.1	0.7

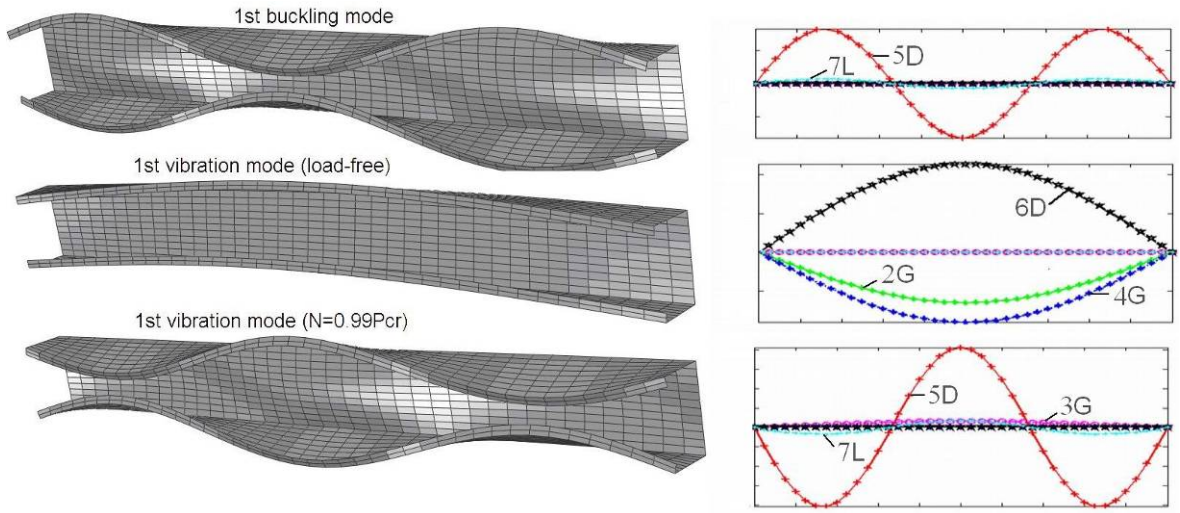

Figure 69. 1st buckling mode (P_{cr}=158.3 kN), 1st vibration mode (load-free and N = 0.99P_{cr}); corresponding amplitude functions of the pure deformation modes

4.1.2 Members with holes

The parametric study is completed on a perforated symmetric steel lipped channel; dimensions referred for the mid-line together with GBT cross-section discretisation and the material properties are given in Figure 70. The thickness for all walls t = 2mm, the bar's length L = 1240mm and the mass density $\rho = 7850\,daN/m^3$. As shown in Figure 72, the holes are square (side d_h = 40mm), have equal size and they are placed in a regular pattern (distance between holes d = 40mm) at the middle of the web height. The GBT 1st step provides a number of 35 pure deformation modes from which the first 21 are presented in Figure 70.

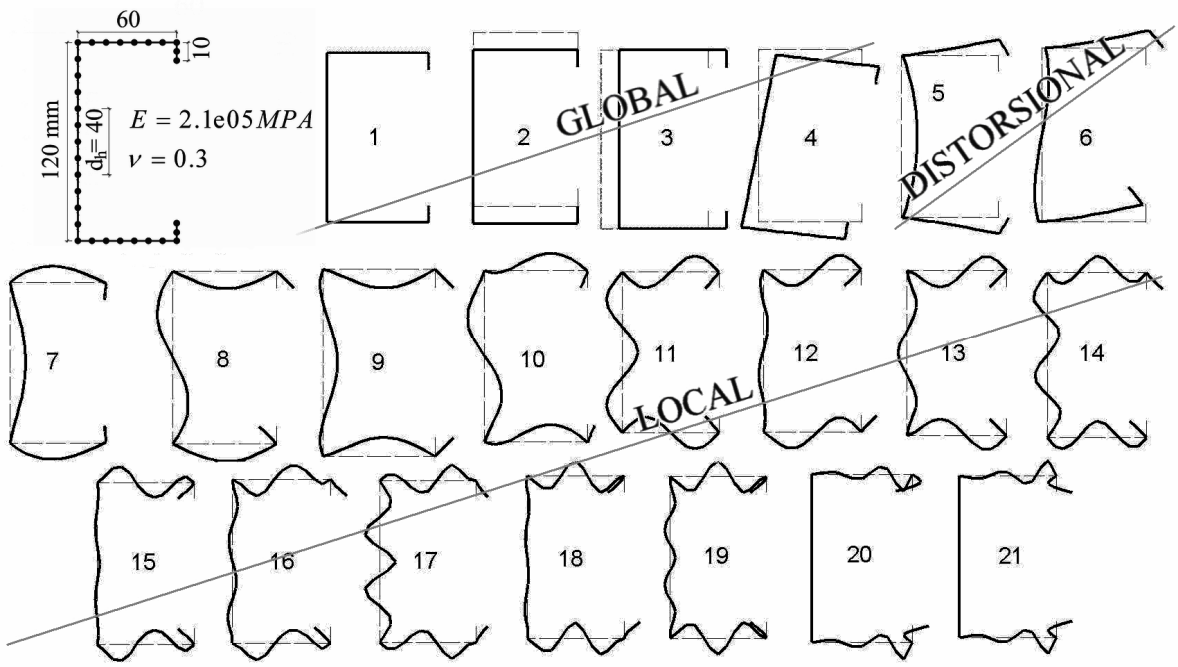

Figure 70. C-section: first 21 deformation modes given by their in-plane shapes.

The member is fixed at one end, simply supported (fork support) at the other, and axially compressed by an edge uniform load of intensity q = 3.846N/mm which gives a resultant force of 1kN. First, a buckling shell FEA was performed using ABAQUS. Next, vibration analyses are carried applying 8 loading levels of the compression force, from 0 (load-free case) till 0.99Pcr, where P_{cr} is the critical load of the 1st buckling mode. The method was applied on 29 modal shapes (the first 5 buckling modes + the first 3 vibration modes for each loading level). The approximation errors calculated according to Eq.(101) had a maximum value of 1.08%.

Figure 71 presents the GDL modal participation for the fundamental vibration modes given by the 8 loading levels and also for the 1st buckling mode. Figure 72 presents the FEM modal shapes of 4 fundamental vibration modes and also of the 1st buckling mode. Great similarities can be observed for the first 4 loading levels (the fundamental vibration mode is a combination of GD deformation modes) and also for the last 4 loading levels together with the 1st buckling mode (mainly DL deformations). Figure 72 also presents the normalized amplitude functions of the first more relevant 5 GDL deformation modes, chosen according to their participation (Eq.(96)).

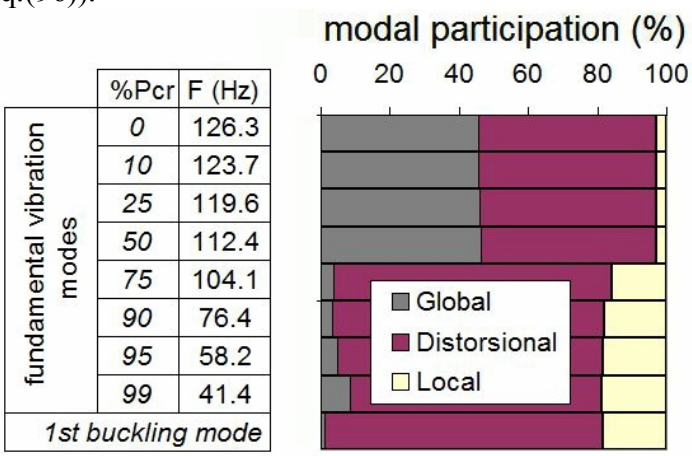

Figure 71. GDL modal participation for the fundamental vibration and buckling modes

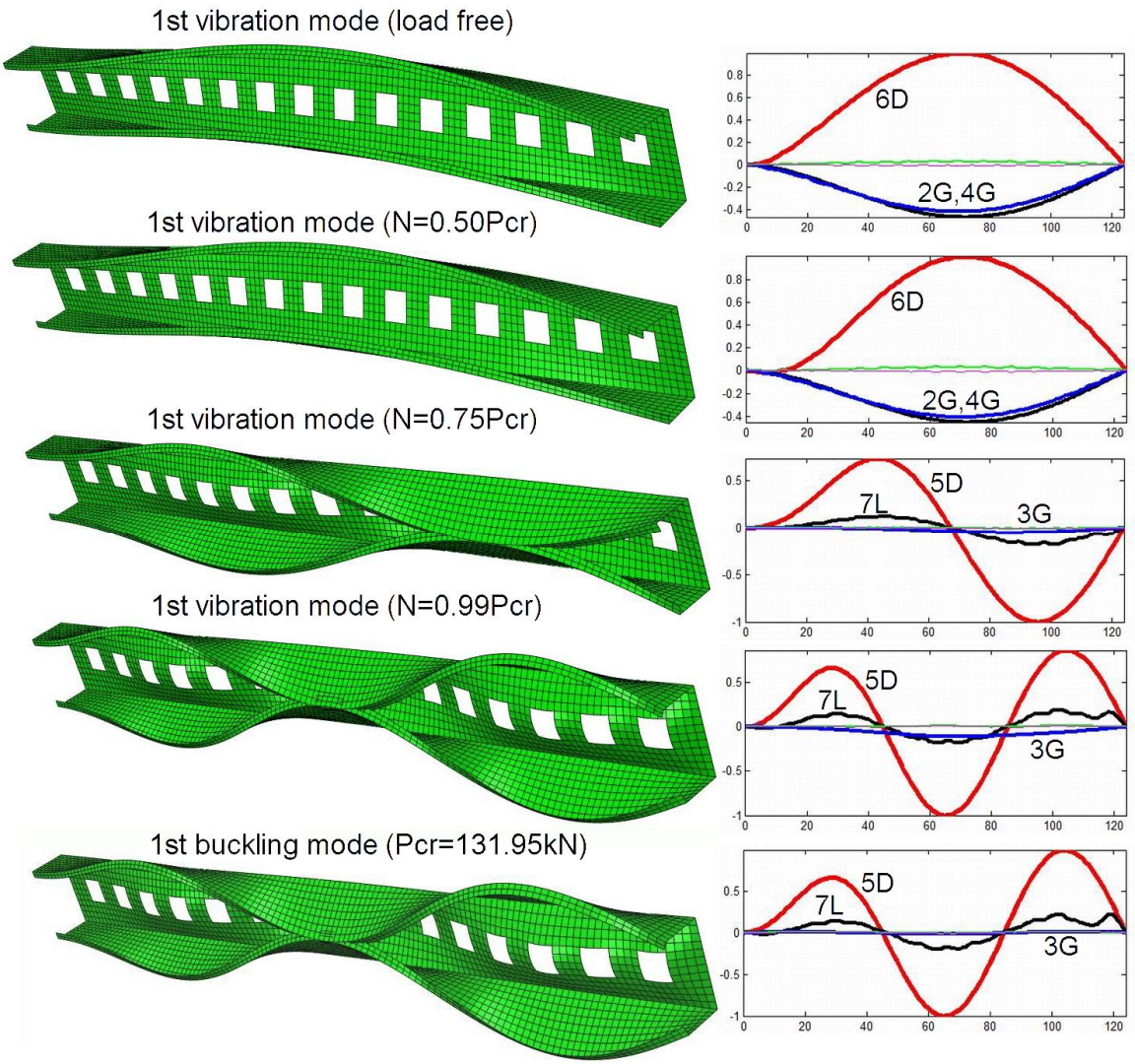

Figure 72. FEM vibration/buckling modes and the corresponding amplitudes of the GDL pure modes

4.2 Experimental modal analysis

Regarding the experimental part of the research activity, the candidate was recently (2011) nominated as coordinator of the laboratory „Actions in Buildings and Structures", Department of Structural Mechanics, Faculty of Civil Engineering, Technical University of Cluj-Napoca. The laboratory contains Bruel&Kjaer [70] and PCB Piezotronics [71] equipment suited to perform experimental vibration analyses. At present time, under the candidate supervision, successful experimental modal analyses were performed on real-world structures and also on small elements inside laboratory (see http://users.utcluj.ro/~mnedelcu/index_en.htm, section "Research Activity"). All the experiments were performed with the help of MS and PhD students and part of these experimental analyses were presented in articles 7 and 8.

4.2.1 Estimation of dynamic properties of a partially-fixed beam

Complex and ambitious civil structures, like large cable-stayed or suspension bridges, dams, tall residential buildings, or other special structures compelled structural engineers to create new experimental methods to enable the accurate identification of the most relevant static and

dynamic properties. This section presents some general aspects regarding modal analysis and experimental methods for the estimation of the modal frequencies of a structure, followed by an experimental modal testing of a partially-fixed beam, conducted in order to calibrate the computer FE model.

Introduction

The experimental modal analysis has become a widespread means of finding the natural modes of vibration of a machine or structure. In every development of a new or improved mechanical product, structural dynamic testing on product prototypes is used to assess its real dynamic behaviour.
Essential dynamic parameters such as the natural frequencies, modal shapes and damping coefficients are required in FE modelling to predict the response of the structure to a variety of dynamic loadings. The interaction between the inertial and elastic characteristics of the materials within a structure causes the phenomenon called resonant vibration. Structures can resonate and damage can be induced even by small dynamic forces, thus giving abnormally large vibrations. Experimental modal testing is based on estimating a set of Frequency Response Functions (FRF) relating the applied force and corresponding response at several points along the structure. The measured time data is transformed from time domain to frequency domain using Fast Fourier Transform algorithm [72]. The Fourier transform accomplishes this by breaking down the original time-based waveform into a series of sinusoidal terms, each with a unique magnitude, frequency, and phase. This process, in effect, converts a waveform from the time domain into a more manageable series of sinusoidal functions that when added together, exactly reproduce the original waveform. Plotting the amplitude of each sinusoidal term versus its frequency creates a power spectrum, which is the response of the original waveform in the frequency domain. Figure 73 illustrates this time to frequency domain conversion concept.

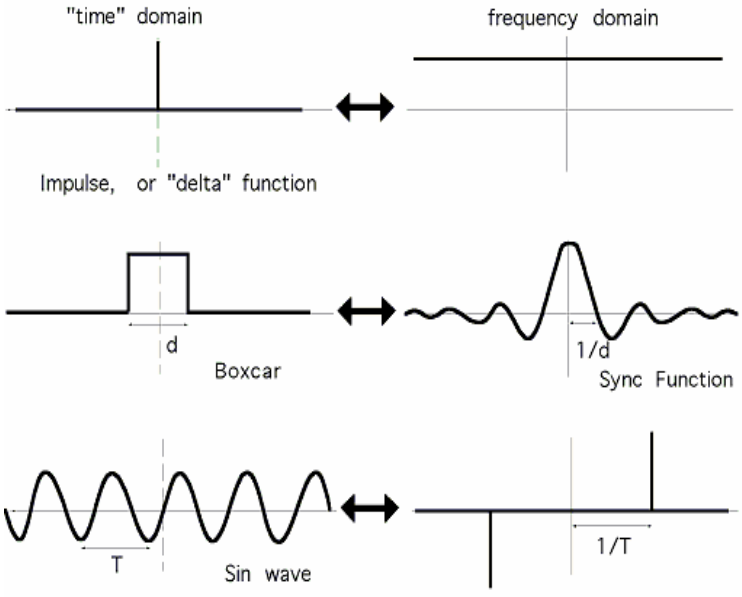

Figure 73. The Fourier transform

Objectives

Measured time data is transformed from the time domain to the frequency domain using a Fast Fourier Transform algorithm found in any signal processing analyzer and related computer software packages. Due to this transformation, the functions end up being complex thus, containing real and imaginary components or magnitude and phase components to describe the function. One could evaluate a simple freely supported plate (Figure 74)

subjected to a dynamic force with constant peak and changing rate of oscillation in sinusoidal fashion [73]. There are peaks in this function which occur at the resonant frequencies of the system. And we notice that these peaks occur at frequencies where the time response was observed to have maximum values corresponding to the rate of oscillation of the input excitation (Figure 75). We can use either the time trace to determine the frequency at which maximum amplitude increases occur or the frequency response function to determine where these natural frequencies occur (Figure 76).

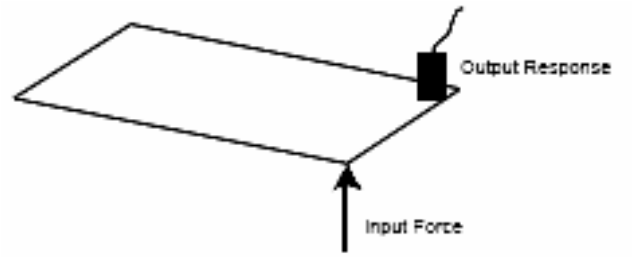

Figure 74. Excitation/response testing

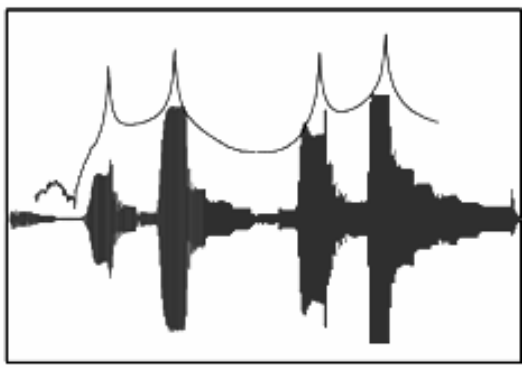

Figure 75. Overlay of time and frequency response functions

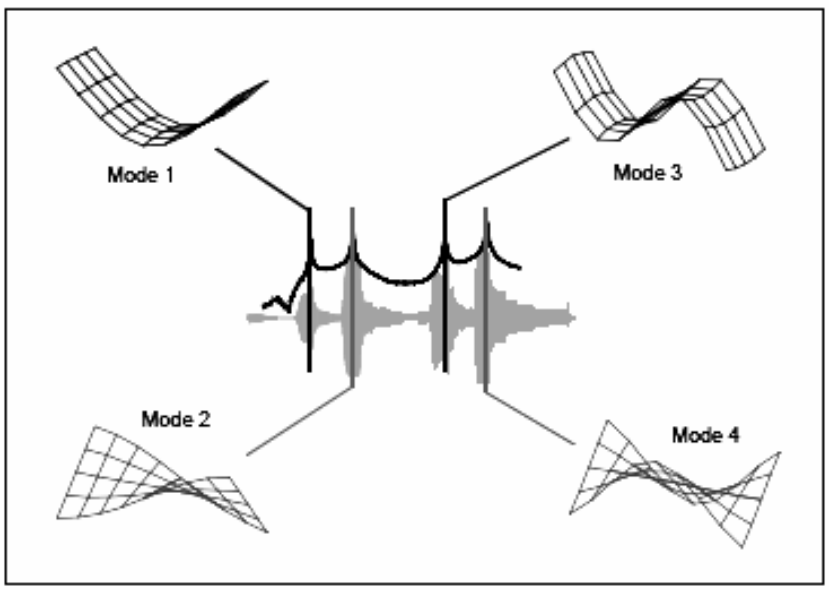

Figure 76. Simple plate sine dwell responses

Experimental modal analysis obtains the modal model from FRF data or measured free vibration response data. Thus, it is a path from response data to modal model. Once the modal model is derived, a number of applications can be investigated. Some applications of modal analysis involve direct use of modal data from measurement while others use these data for further analysis. Troubleshooting using experimental modal analysis is to gain an insight into

a dynamic structure which is problematic [74]. An essential approach is to take a measurement of the structure, derive its modal model and use it to correlate with the existing FE model in order to update it. The philosophy behind this model correlation is that the modal model derived from measurement, though incomplete due to lack of sufficient numbers of vibration modes and measured locations, truly represents the structure's dynamic behaviour. Thus, it can be used to "correct" the FE model, should any discrepancies occur between them. Structural modification analysis, sensitivity analysis, response prediction, substructure coupling, structural damage detection and active vibration control are the other applications of modal parameters and the derived model from thereof.

Experimental method

Conventional modal analysis is based on estimating a set of FRFs relating the applied force and corresponding response at several pairs of points along the structure. The construction of FRFs requires use of an instrumentation chain for structural excitation, data acquisition, and signal processing. Remarkable technological progress in transducers and analog-to-digital converters has supported experimental modal analysis of large structures exclusively based on measuring the structural response to ambient excitations and applying suitable stochastic modal identification methods (the operational modal analysis). In small and medium-size structures, the excitation can be induced by an impact hammer similar to those currently used in mechanical engineering. This device has the advantage of providing a wide-band input that is able to stimulate different modes of vibration. The main drawbacks are the relatively low frequency resolution of the spectral estimates (which can compromise the accurate estimation of modal damping factors) and the lack of energy to excite some relevant modes of vibration. An alternative, also derived from mechanical engineering, is the use of large electrodynamic shakers, which can apply a large variety of input signals (random, multi-sine, etc.) when duly controlled both in frequency and amplitude using a signal generator and a power amplifier. The dynamic response of a structure is usually measured with piezoelectric, piezoresistive, capacitive or force balance accelerometers, due to their relatively low cost and high sensitivity [76]. A particular feature of piezoelectric accelerometers is that they don't need a power supply and operate well over a wide frequency range. The data acquisition and storage of dynamic data requires the use of an analog-to-digital (A/D) converter in the measurement chain.

Equipments used in the presented experiment:

- Impact hammer 8206C03 – PCB Piezotronics
- Accelerometer Brüel&Kjær (4507)
- Software PULSE™ Labshop
- Pulse Type 3560-C Portable Data Acquisition unit, Brüel&Kjær
- Connectors, calibration system, accesories
- Laptop computer

In this laboratory study, the tested specimen is a S235 steel bar, type UPN80 with the following dimensions: web height h = 8cm, flange width b = 4.5cm, web thickness t_w = 0.6cm, flange thickness t_f= 0.8cm, bar length L = 126.5 cm (Figure 77).

Figure 77. The tested member UPN80

Experimental set up

The beam was divided into a grid of points along the bar axis, by 7 cross-sections and 5 points on each cross-section, thus generating 35 points on the beam that will be the nodal points. The accelerometer was fixed in one of these points, leaving his position unchanged throughout the trial (Figure 78). The impact hammer was prepared so that the induced force has a common optimal value to stimulate measurable frequencies of the beam, and on this basis, the hammer tip and the additional weight at the opposite end were chosen. Figure 79 shows all selected nodal points for hammer excitation and the striking directions. The member was fixed at both ends; the restraints were made by spot welding between the profile and two metal plates which were fixed by adding weights on each one. The accelerometer was fixed at one side to the beam at the test node among all the nodal points on the beam. The impact hammer was kept ready to excite the beam at each point. On each strike, the structural response was obtained in frequency domain. For each point an average of three measurements was saved, provided that good correlation between measurements was achieved. At the time of the striking with the impact hammer, precautions were taken whether the striking should have been perpendicular to the steel beam surface. The above procedure was repeated for all the nodal points. The FRF plots were saved after assigning the direction and the position of extracted data from the nodal points. The values (i.e., natural frequencies and modal shapes) obtained from the experimental modal analysis were compared with the values obtained from a FEM analysis, created in Autodesk Robot Structural Analysis Professional code [75].

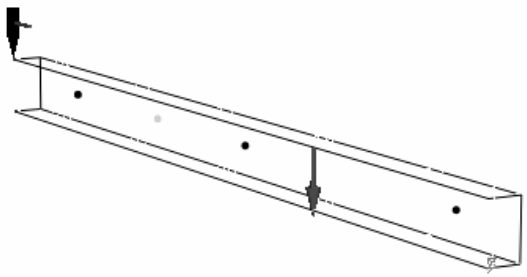

Figure 78. Accelerometer position and first striking position

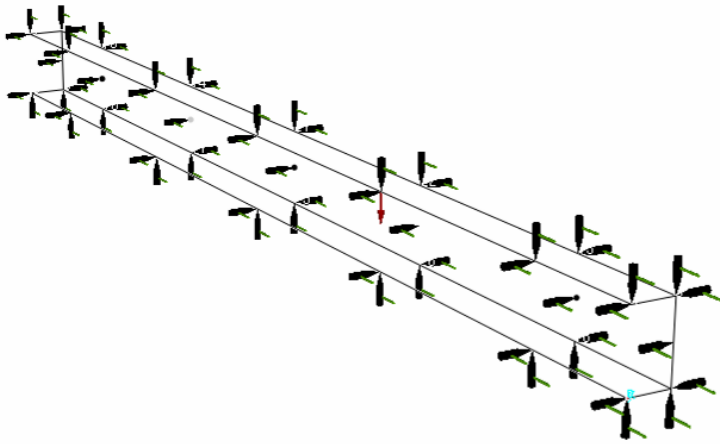

Figure 79. Establishing points and directions for hammer striking

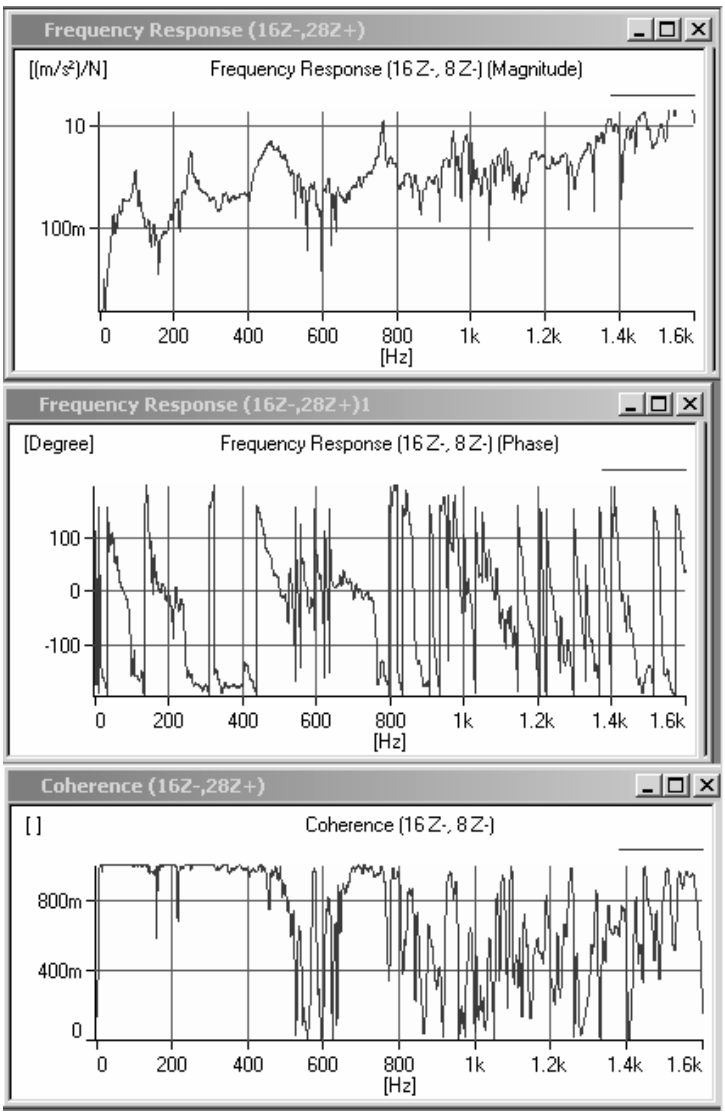

Figure 80. Frequency Response Functions for one strike

FRF measurement

The measurement for experimental modal analysis is to acquire FRF data from a test structure. Experimental modal analysis is a system identification endeavour. The structure is a "black box" that needs to be deciphered. The traditional approach is to provide the "black box" with a known input, measure the output and proceed with the identification.

For this measurement, the force input was used so that the FRF can be derived directly from the input force and member response information. The excitation force can be random, sinusoidal, and periodic or of impact nature. Theoretically, the type of force does not matter as the FRF is defined as the ratio between the response and force.
In practice, whenever practical one uses a force that has sufficient energy and frequency components to excite all vibration modes of interest and to allow minimum errors in signal processing, leading to the formation of accurate FRF data. The FRF was given by the acceleration divided by the input force.

Obtained results

The modal frequencies were estimated as the frequencies where maximum amplitudes were detected in the FRF plots. The results are in good compliance with those obtained from FEA but only after the FE model calibration which is soon discussed.

Table 21. Modal frequencies: FEA vs. experimental test

Eigen mode	FEA modal frequencies (Hz)	Experimental modal frequencies (Hz)
1	52.93	52
2	89.33	97
3	299.65	253
4	456.27	457
5	759.65	759

Frequency range of the two analyzes are similar, only in some cases (mode 2, mode 3) there is still a significant difference between FEA and experimental values, but these differences may be due to material imperfections of the bar. The mode shapes are similar in both cases.

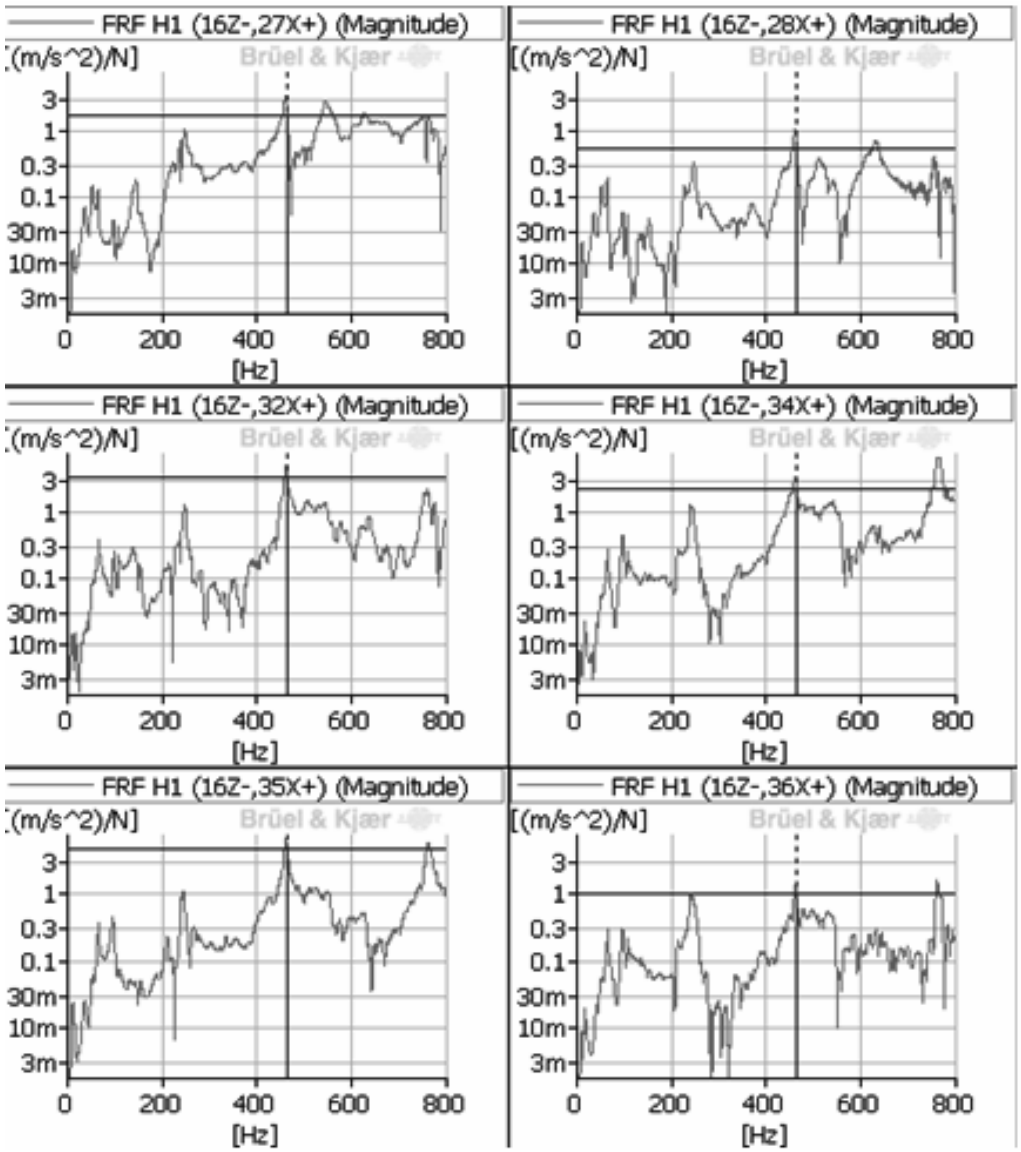

Figure 81. FRF plots

A vibration mode can be considered valid if the FRF plots can identify the correspondence between peaks in all points considered to determine the experimental analysis. Thus, in Figure 81 one can see the correspondence between peaks in FRFs, which are represented in different nodal points.

FE model calibration

The presented results were obtained only after the calibration of the model in the FE code. Because in reality the member ends are not perfectly fixed, adjustments were made in the FEA using elastic supports on the direction of vertical displacements and trying several stiffness values. Thus, the bar's ends were partially fixed on vertical direction with a stiffness value (elastic coefficient) K_z = 180kN/m.

Conclusions

This section presents an experimental test of a beam as an example of experimental modal analysis. The results were used to identify the beam dynamic characteristics and more important to calibrate the FE model. Same procedure can be made using similar equipment in order to perform structural dynamic testing of large civil engineering structures. The techniques that may be used under normal operation conditions can provide a solid basis for:

- development of FE correlation analyses
- FE updating and validation
- defining a set of dynamic properties of the initially undamaged structure that can later be used for the application of vibration-based damage detection techniques
- integrating classical or operational modal identification techniques in health monitoring systems
- implementing vibration-control devices

Civil engineering structures have peculiar characteristics (large size and relatively low natural frequencies) that make the current application of classical input-output modal identification techniques difficult. Therefore, there is presently a clear tendency worldwide to explore and improve the potential of output-only (operational) modal identification techniques.
The modal identification of bridges and other civil structures is required for validation of finite-element models used to predict static and dynamic structural behaviour either at the design stage or at rehabilitation. After appropriate experimental validation, FE models can provide essential baseline information that can subsequently be compared with information captured by long-term monitoring systems to detect structural damage.

4.2.2 Experimental modal testing of a concrete bridge

Introduction

This section reports on the experimental analysis of a concrete bridge. Vibration problems generated by the resonance phenomenon are often encountered in bridges. Even though the serviceability and resistance demands are being met, due to the use of higher resistance materials and larger spans, such structures tend to fail the vibrations criterion. Cases such as Tacoma Narrows, Washington, USA and Millennium Bridge, London, UK, are just two examples of structures that showed problems with resonance due to the exterior, dynamic actions. The concrete bridge whose dynamic response has been measured tends to vibrate excessively under car traffic.
The present study was made on a concrete bridge over the Someş River, Cluj County, Romania. Built in 1967, the bridge has severe vibration problems; therefore measurements have been necessary in order to acquire more information about its dynamic behaviour. After assessing the natural frequencies, several comparisons have to be made with the frequencies of the exterior, dynamic actions in order to establish the danger of resonance. If there is a match, methods of changing the natural frequencies need to be considered.

Structure description

The total length of the bridge is 180.5 meters. The 6 spans, 27.45 m each, are made of 3 continuous reinforced concrete beams of π section, as shown in Figure 82. The 2 longitudinal beams, 40 cm width, with an approximate height of 170 cm (Figure 83), are coupled transversally at every 9.15 meters by floor beams. The static scheme of the bridge consists of 3 π-beams, each continuous over 2 spans. The beams are pinned at both ends with mobile joints. On each intermediate support, the beams are coupled at the lower part with a 6m long plate, in order to handle the compression stress better. The deck of the bridge has 1.33 m long cantilevers on each side. According to the tests performed with a concrete test hammer, the class of the concrete that can be used in calculations is C16/20.

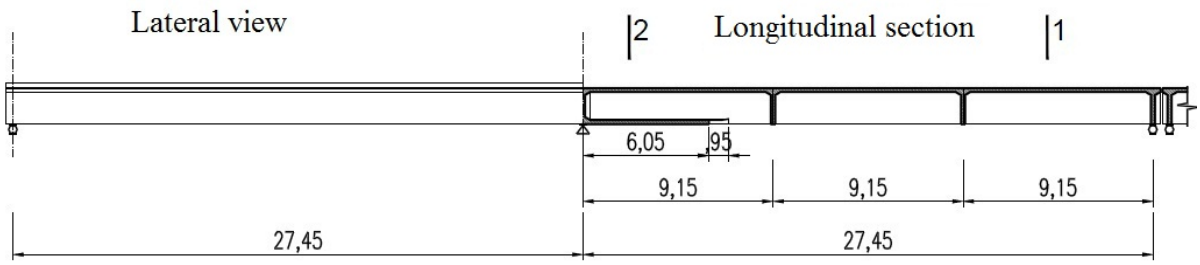

Figure 82. Lateral view and longitudinal section of the bridge

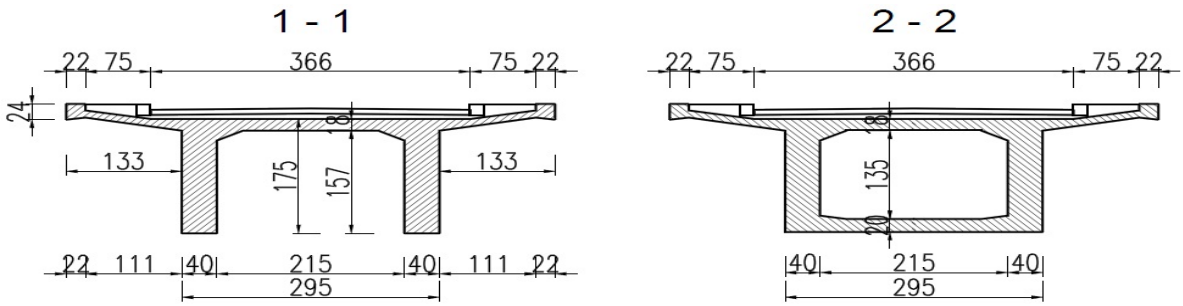

Figure 83. Cross section of the bridge

Equipment

The equipment used consisted in a Bruel&Kjaer Pulse Type 3560-C Portable Data Acquisition unit connected to a portable computer, an 8210 heavy duty modal impact hammer, a 8340 seismic accelerometer (see Figure 84a) and 4 piezoelectric accelerometers type 4507B002.

Measurement methods

The measurements have been performed in two different methods: classical modal analysis [76] using the impact hammer, and operational modal analysis [77] measuring the bridge response under traffic loading. In order to perform the measurement task for classical modal analysis, a grid of measurement points on the length of the bridge, has been marked at equal distances. In each of these points, the bridge has been excited with the impact hammer 3 times, in order to have an average of the registered impact force (see Figure 84).

Figure 84. a)Bridge excitation with the impact hammer; b) 8340 seismic accelerometer

The response of the structure has been recorded in terms of accelerations with the 8340 seismic accelerometer in a fixed point. In order to compare the dynamic response of different bridge spans, measurements have been performed on the first, third and fifth span, taking in

consideration the existing joints at every two spans. The interpretation of the results made with the program Pulse Labshop provided by Bruel&Kjaer, has shown differences up to 6% between the spans, which were considered to be negligible. The first five eigenmodes have been identified, and the eigenfrequencies for each of the modes (with variation depending on the bridge span) are listed in Table 22.

Table 22. Natural frequencies for the first 5 modes

Mode no	Frequency (Hz)
1	3,15 - 3,25
2	5,75 – 6,00
3	12,25 – 14,00
4	15,25 – 16,33
5	25,5 – 27,10

The fundamental mode is represented in Figure 85, for a single span, and the points defining it, can be identified in Figure 86, that represents the mode shapes for two spans.

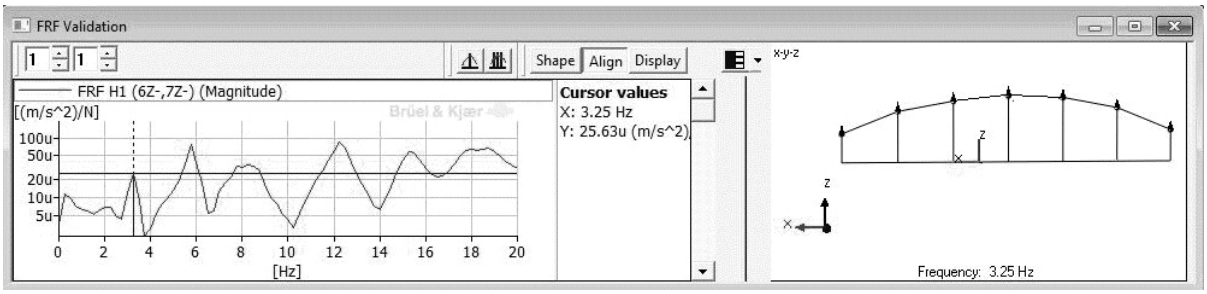

Figure 85. Fundamental mode: frequency and mode shape for a span (7 interior points) obtained from the experiment.

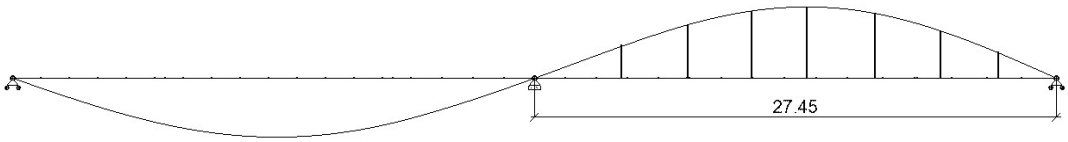

Figure 86. Fundamental mode: the mode shape for two spans from a FEM software

For operational modal analysis, 4 piezoelectric accelerometers type 4507B002 (see Figure 87) and the 8340 accelerometer have been used.

Figure 87. Piezoelectric accelerometer type 4507B002

The analysis has been performed by crossing the bridge with a standard vehicle (including a small artificial bump made from a wooden board presented in Figure 88) in three different steps of constant speed ranging from 10 to 30 km/h. The 5 accelerometers have recorded the

response accelerations of the structure on a grid of points along the spans, from the moment of the vehicle entrance on the bridge, until the vibrations were completely damped.

Figure 88. Dynamic excitation with a standard vehicle

Results interpretation

In the case of the output-only experimental modal analysis, the interpretation of the results has been performed using the program Operational Modal Analysis Pro (OMA) provided by Structural Vibration Solutions A/S [79].
The dynamic characteristics obtained (frequency and mode shapes) are the same with the ones obtained using classical modal analysis for the first 5 mode shapes, an analysis performed directly by the acquisition software Pulse Labshop. Due to the high intensity loading, other eigenmodes were identified, all having superior frequency values to those already presented.
Starting with the recorded accelerations, the displacements of the points along the spans have been determined using OMA and also a Matlab code based on the so called Spectra-Omega Arithmetic algorithm [80]. The maximum/minimum displacements have been registered during the vehicle crossing with a speed of 10km/h and have the values $D_{max/min}$ = +5.4/-3.1mm.

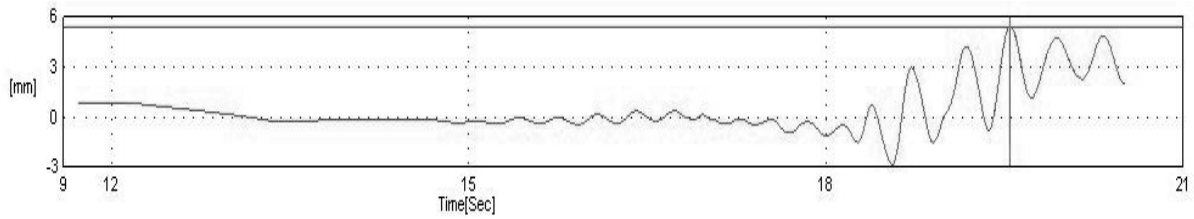

Figure 89. Displacement/time graphic

On all the displacement/time graphics, oscillations with an approximate period $T = 0.3$s can be observed, oscillations corresponding to the fundamental mode with a frequency F =3.15-3.25 Hz.

Conclusions

The measured oscillations had maximum amplitudes for low speeds of the convoy. It is well known that car traffic induces dynamic loads in the 1.5 – 4.5 Hz range [81]. Due to the fact that the fundamental frequency is in the same frequency range as the one of the exterior loads, the resonance phenomenon appears. Nowadays, the oscillations have low amplitudes, and have not led to a major decrease of the bearing capacity or stability of the bridge. However, the vibrations are perceived by the pedestrians and also by car drivers. Not only that these vibrations are discomfortable for the ones previously mentioned, but the danger that resonance can affect in time the structural integrity of the bridge due to uncontrolled increase of the amplitudes under dynamic loads, requires immediate measures to consolidate the structure, in order to change the fundamental frequency and the bridge stiffness.

4.2.3 Tension estimation of cables by vibration analysis

Article 10 and the following paper fully describe the latest developments in this recent research direction of the candidate:

- **Nedelcu M**, Chira N (2013) „Analiza şi reabilitarea unei estacade metalice suspendate peste râul Someş", Simpozionul "Cercetări actuale în domeniul construcțiilor metalice: sisteme structurale şi soluții inovative", a-XIII-a ediție a *"ZILELOR ACADEMICE TIMIŞENE"*, 24 mai 2013

Introduction

Structural steel cables have been widely applied in cable-supported bridge systems, in which they are arguably the most crucial elements of the entire structure. The axial force in cables must be measured accurately in order to properly assess the state of stress in the entire structure. Currently, available techniques for estimating cable tension include the direct measurement, magneto-elastic and vibration methods. The direct method measures the tension force by a calibrated load cell or a hydraulic system. The second method is based on the measurement of the magneto-elastic permeability in cables [86]. However, the vibration methods represent the first choice in practical applications owing to their simplicity, speed and economy.

The typical procedures of the vibration methods are as follows: first, the free vibration response of cables in time domain is collected by a data logger after the excitation with an impact hammer or other ambient sources. Next, the natural frequencies and mode numbers are extracted by various experimental modal analysis techniques for the collected data sets. Finally, the tension forces are determined by using an appropriate analytical closed-form or numerical algorithm-form relationship between natural frequencies and cable tension. From a theoretical point of view, the cable can be considered as an intermediate case between the beam and the string, and therefore its equation of motion includes not only the flexural stiffness but also the tension. Moreover, the cable response is affected by the sag-extensibility, the stiffness of the end-supports and other secondary effects that can influence the modal parameters, especially when analyzing complex structures.

One of the most peculiar aspects of the cables is that it is not possible to obtain an analytical formula linking the natural frequencies, the tension and the flexural stiffness, except for the hinge supports. This limitation prevents us to directly estimate the tension because, in real applications, the cables do not have hinge end-supports. For this reason, many scientists tried to develop specialized methods to overcome this problem. One of the first important researches in the field was conducted by Zui et al. [87]: they proposed practical formulas for the estimation of the tension from the identified natural frequencies, taking into account the sag extensibility. Triantafyllou and Grinfogel [88] presented a formulation that considers the

sag extensibility without bending stiffness. Ren et al. [89] presented a new version of the practical formulas, after having explained the relative influence of the sag-extensibility and of the flexural stiffness. Kim et al. [90], [91] developed a method for the simultaneous estimation of the tension, flexural rigidity and axial rigidity of a cable system. Firstly, a finite element model that can consider both sag-extensibility and flexural rigidity is constructed for a target cable system. Next, a frequency-based sensitivity-updating algorithm is applied to identify the model. Moreover the same authors made an overview of all the available methods, based on their applications on two real bridges. Ceballos and Prato [92] introduced rotational springs at the cable ends to represent all the possible boundary conditions and then proposed a technique to determine the stiffness of the springs based on experimental information. Consequently, the axial force of the cable can be calculated. A different approach [93] introduces the concept of cable equivalent length which is a length that corresponds to the extracted natural frequencies and to the known properties of the cable based on the formula for simply supported cables. The cable tension is successively estimated by comparing the natural frequencies of the standard configuration with those of a new configuration considering a mass mounted on the cable.
The objective of this study was to estimate the axial forces in two types of cables (vertical and inclined) of a pipeline suspension bridge using vibration analysis. The effect of sag extensibility was neglected for both types of cables, for obvious reasons in the case of the vertical ones. For the inclined cables, the vibrations were measured in the cable plane perpendicular to the vertical one knowing that the effect of the sag in the ”out-of-plane” frequencies is negligible in both short and long cables typical for the sag/diameter ratios found in cable-stayed bridges [92]. Also in this study, the effect of the rotational stiffness of the cable supports was neglected.

Available Vibration-based Methods

The simplest formula used by vibration methods is based on the Taut String Theory, the flexural stiffness is neglected and the axial force is computed as follows:

$$T = 4ml^2\left(\frac{f_n}{n}\right)^2 \tag{112}$$

where T is the axial force, n is the natural mode number, f_n is the n^{th} natural frequency in Hz and m, l refer to the distributed mass and cable length, respectively. The tension force can be determined from measuring the system variables in the right hand side of Eq. (112). However, this simple formula is only valid for flat slender doubly-hinged cables. Although Eq. (112) is unreliable for cables with high flexural stiffness, sag and rotational stiffness of the supports, it is helpful for the first approximation of tension. In the presented study this approach was successfully used for vertical thin cables.
The following formulation is based on Beam Theory (the vibration equation of the axially loaded beam), it takes into account the cable flexural stiffness and it is described below [94]:

$$T = 4ml^2\left(\frac{f_n}{n}\right)^2 - \frac{EI}{l^2}(n\pi)^2 \tag{113}$$

where EI is the cable flexural stiffness and the other variables were previously explained. With respect to the unknown tension force and flexural rigidity, the linear regression procedure is applied to the next equation derived from Eq.(113).

$$\left(\frac{1}{4ml^2}\right)T + \left(\frac{n^2\pi^2}{4ml^4}\right)EI = \left(\frac{f_n}{n}\right)^2 \tag{114}$$

All the terms in brackets are known, consequently by linear regression, the tension and the flexural rigidity can be simultaneously estimated. Although the estimated results are very reliable for thick hinged cables, the estimated flexural rigidity is unreliable for high sagged cables. Furthermore, the use of higher modes provides better accuracy while the higher modes of a long cable are hardly excited by the ambient sources. Despite these limitations, this formulation is often used in the field due to its simplicity and speediness and based on the characteristics of the investigated inclined cables, it was successfully applied in the presented study.

Field Study

The objective of this study was to estimate the cable tension of a pipeline suspension bridge (Figure 90), built in 1981 in Dej, Cluj, Romania, using vibration analysis.

Figure 90. Pipeline suspension bridge

Pipeline suspension bridge characteristics

The suspension bridge is a type of bridge in which the deck (the load-bearing portion) is hung below the main suspension cables on vertical suspenders. The suspension cables are supported by metallic pillars and they are anchored at each end of the bridge, so any load applied to the pipeline bridge is transformed into a tension in these main cables. The main cables continue beyond the pillars to deck-level supports and they are held in position by massive concrete anchor blocks. The deck is supported by vertical suspended cables or rods, called hangers. The span of the pipeline suspension bridge is 130m across Someş River. The cable types are: for suspension cables - Φ 63 – 6x61 (STAS 1353-71) and for the vertical suspenders: Φ10 - 6x19+FC (STAS 1513, DIN 3052, SR EN 12385-4+A1).

The measurement equipment

The vibrations of the investigated cables have been measured with Bruel&Kjaer equipment (Laboratory „Actions in Buildings and Structures", Faculty of Constructions, TUCN), namely the DAQ system PULSE 3560C and piezoelectric accelerometers 4507B002 (Figure 91). The data manipulation was done using the licensed softwares: Pulse Bruel&Kjaer, Matlab ver. R2011b, ABAQUS v. 6.11 and Sap2000v14.

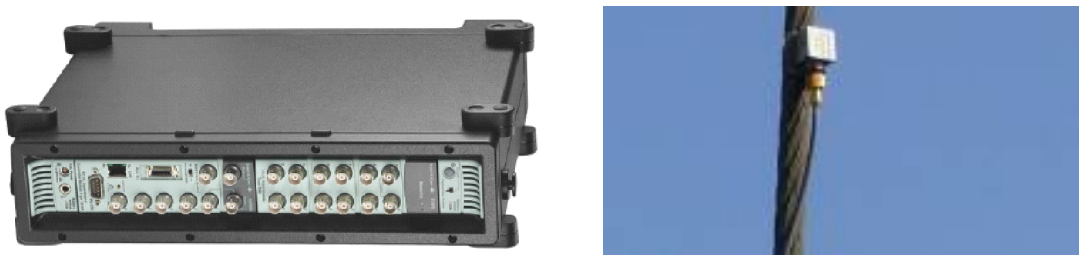

Figure 91. a) DAQ front-end hardware; b) accelerometer placed on cable

Vertical suspenders

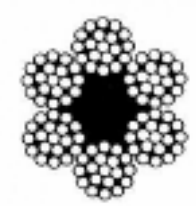

Figure 92. Vertical suspender's cross-section

The characteristics of the vertical suspenders type Φ10 - 6x19+FC are presented as follows:

Table 23. Characteristics of the vertical suspender

Diameter [mm]	Mass [kg/m]	Minimum breaking force [kN]
10	0.346	54.34

The type of boundary conditions can have significant effect on the cable natural frequencies, especially for the first modes. In this case, cables are hinged, as it can be seen in Figure 93. For hinged cables, the formulas presented at the beginning of this section can be used, depending on cables characteristics. In Figure 93b, it can also be observed the tensioning device. Because the tensioning is done manually, there is no way to control the cable tension, except by continuous measuring of the deck displacements which is a tedious and very rough way to predict the axial forces, therefore, the need of the presented study.

Figure 93. a) Top and b) bottom supports of the vertical suspenders

The testing direction of vertical suspenders was from the left to the right bank of river Someş. At the same time, 4 cables were measured, 2 on each side of the deck. The acceleration time-history was recorded by an accelerometer installed on the surface of the cable (Figure 91b). The vibration tests were done for all vertical suspenders, 84 in total, 42 on each side. Exciting the stressed cable (Figure 94), the acceleration time histories are collected through the DAQ system, then by the Fast Fourier Transform (FFT) they are converted into the frequency domain. Using a computer code written in Matlab, the frequencies of vertical suspenders are found by detecting the peaks in the amplitude/frequency graph (Figure 95).

Figure 94. Exciting the cables

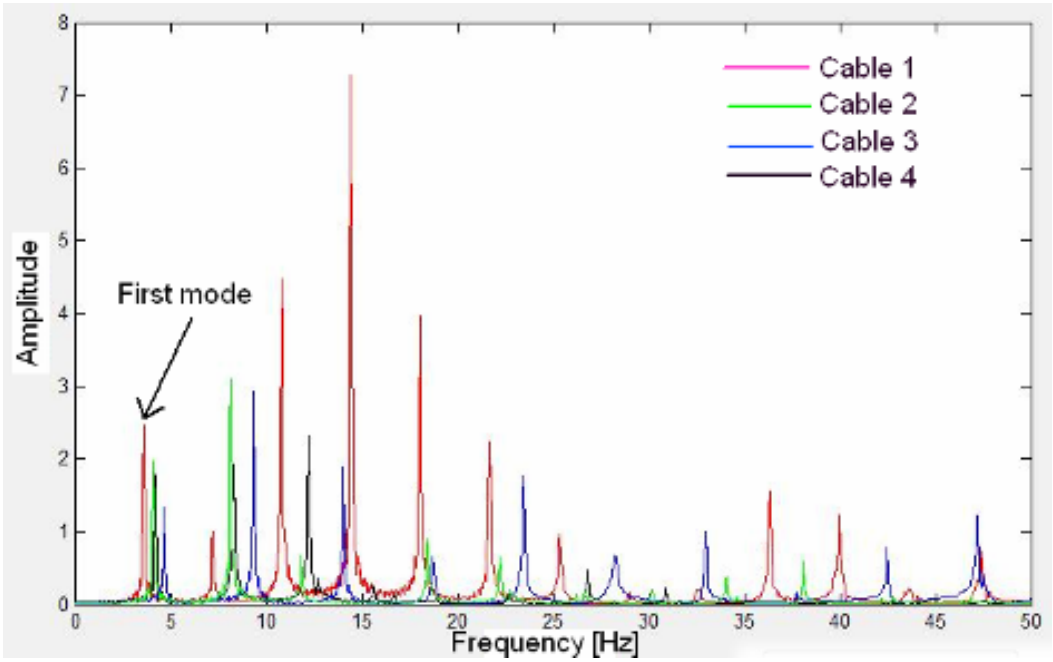

Figure 95. Acceleration amplitude vs. frequency for 4 vertical suspenders

Next the axial forces were found using Eq. (112) and Figure 97 shows the obtained values for all vertical suspenders which are situated on the left and right side of the pipe. This figure should be analysed together with Figure 96 which presents the lateral view of pipeline suspension bridge together with the location of cables.

Discussion. The cables near the bridge ends are less stressed than the others, because the bridge is there simply supported on concrete blocks. It can be seen that peaks of axial forces are followed by low values, which is only natural to happen if some cables were not properly tensioned. In the right side, cables the axial forces are generally bigger than in the left side, because of the influence of an additional pipeline which was still in situ at the time of measurements (Figure 98). Being in contact with the vertical suspenders near their bottom end, the additional pipeline acted as an intermediary support, decreasing the length and increasing the natural frequencies and, following Eq. (112), the resulting axial force. However, the actual values of the axial forces are not so important as the relative differences between cables. The aim of this study is to assess these differences and to correct them by obtaining in the end a homogeneous state of stress in all cables.

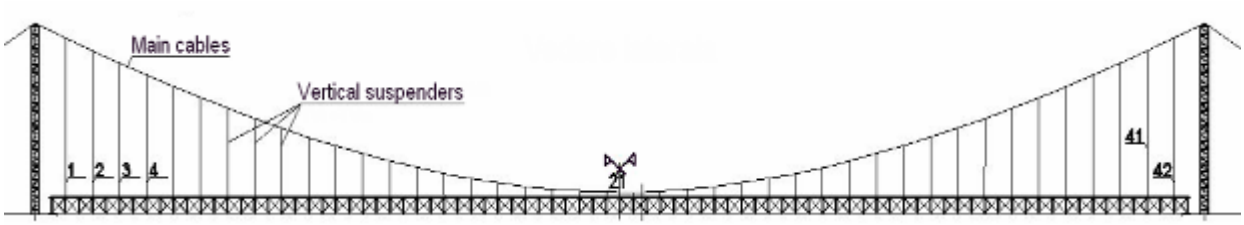

Figure 96. Lateral view of the pipeline suspension bridge

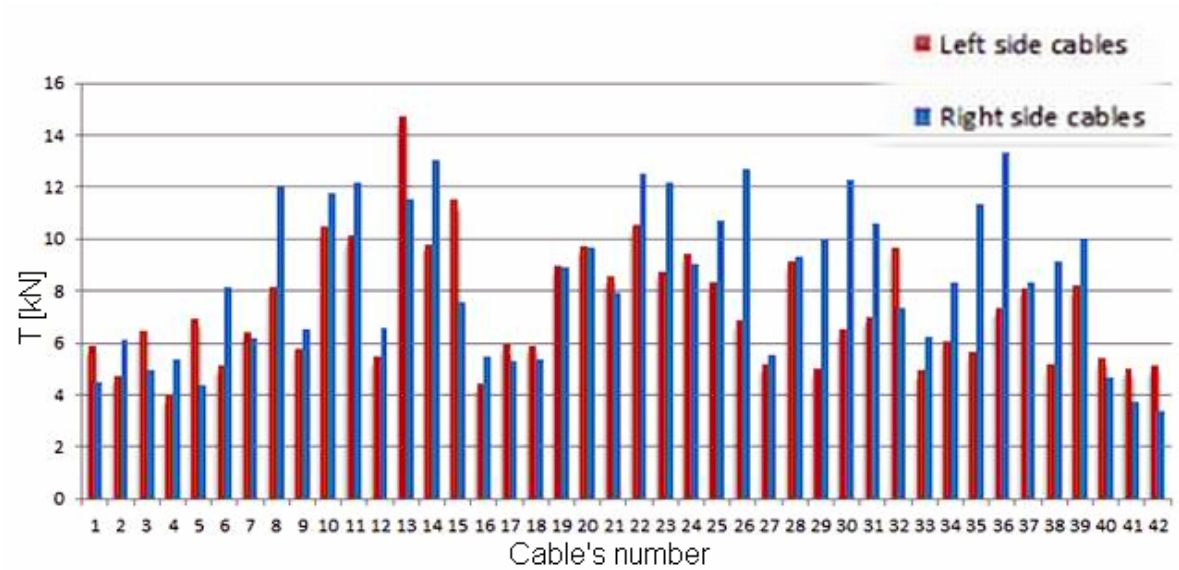

Figure 97. The axial forces in the left and right side cables

Figure 98. The additional pipe

Main suspension cables

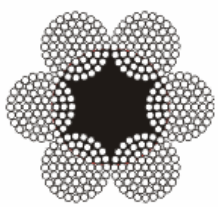

Figure 99. Suspension cable's cross-section

It is also important to find the axial forces of the suspension cables, in order to understand the behaviour of the pipeline suspension bridge. Eq.(113) was used because the influence of the flexural stiffness can no longer be neglected (thick cables). The characteristics of the suspension cables type Φ 63 – 6x61 are presented as follows (*L* - length , *D* - diameter, *I* - moment of inertia, *A* – area):

Table 24. Characteristics of the suspension cables

L [m]	D [mm]	I [cm^4]	A [cm^2]	Density [daN/ m^3]	Angle of cable inclination
26.77	63	57.41	18	9300	37^0

Figure 100 presents the investigated inclined segment of the four suspension cables. In order to overcome the sag effect, the measurements of suspension cables were done by vibrating the cables perpendicular to their plane.

Figure 100. Suspension cables: a) inclined segment; b) numbering and cable excitation

After the measurement process, the natural frequencies were found based on the acceleration amplitude vs. frequency graph given in Figure 101.

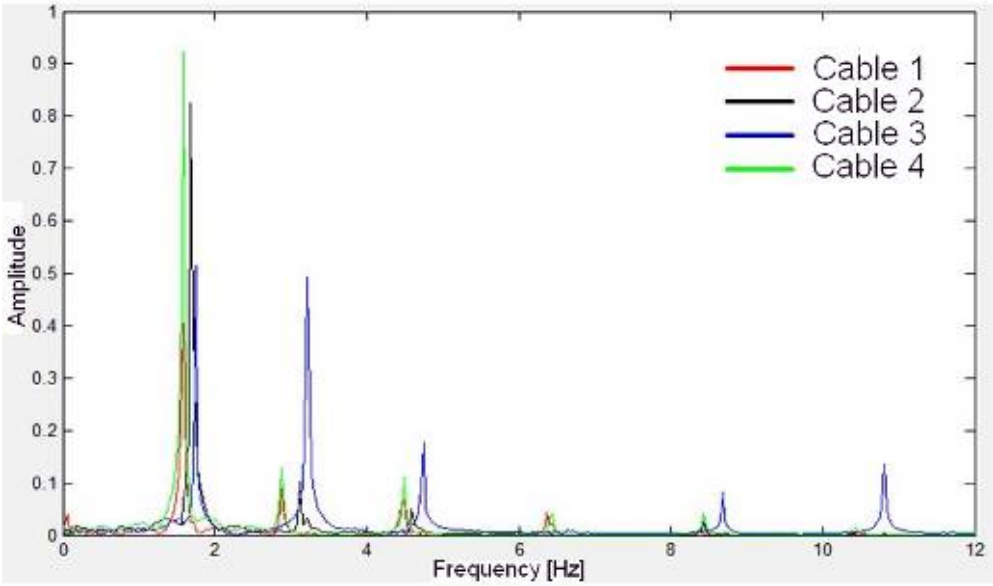

Figure 101. Acceleration amplitude vs. frequency for the suspension cables

With respect to the unknown tension force and flexural rigidity, the linear regression procedure was applied to the terms in brackets of Eq.(114). Hence, the flexural rigidity and tension can be simultaneously estimated. Results are presented in Table 25 and it can be seen that the obtained values are close with those obtained from the structural analysis of pipeline suspension bridge. The numerical simulation was made in SAP2000 [95] introducing the Young's modulus $E = 160GPa$ and the cable's axial force was found $T = 100–120kN$ (depending on the pipe filling).

Table 25. Tension force and flexural rigidity of suspension cables

Cable no.	Measured frequencies [Hz]						L = 26.77m	
	f_1	f_2	f_3	f_4	f_5	f_6	EI [kNm^2]	T [kN]
Cable 1	1.625	2.906	4.500	6.406	8.406	10.375	101.12	99.30
Cable 2	1.719	3.156	4.625	6.500	8.469	10.500	88.49	107.36
Cable 3	1.781	3.250	4.781	6.688	8.719	10.844	94.27	114.11
Cable 4	1.625	2.906	4.531	6.469	8.469	10.469	105.95	99.84
E_{med} [GPa]	169.76			Average values			97.46	105.16

The suspension cables were also modelled in ABAQUS, and the first 6 natural frequencies are presented in Table 26 and they can be compared with those obtained using vibration analysis (presented in Table 25). The small differences between the measured frequencies and those obtained from FEA may be caused by the additional mass introduced by the tensioning devices (Figure 100b). Also, it can be noticed that the biggest difference appear for the first natural frequency. This is because in reality the cable is not hinged at its ends and the rotational stiffness of the supports has the biggest influence on the first natural modes. The higher modes are clearly less affected by the boundary conditions.

Table 26. Cable natural frequencies [Hz] obtained from FEA

f_1	f_2	f_3	f_4	f_5	f_6
1.5	3.050	4.697	6.48	8.447	10.618

Conclusions

This section briefly presented the most commonly used vibration-based tension estimation methods and their application limits were re-examined. The taut string method and the axially tensioned beam method were applied to estimate the axial forces of the cables supporting a pipeline suspension bridge. Finally, the results were compared with those from FEA and the good agreement between them proved the validity of this procedure.
Based on the numerical results and their interpretation, the following conclusions can be made: first, the cable tension forces estimated by the taut string theory are reliable for the vertical hinged cables with low flexural stiffness as was the case of the bridge vertical suspenders. Second, the reliable estimation of cable tension force and flexural stiffness by the linear regression of the beam vibration equation requires for different boundary conditions, the experimental determination of higher natural frequencies.
Tension estimation of cables using vibration analysis is an important and fast tool which provides reliable results if the correct method is applied.

Personal Contribution

The candidate conducted many vibrations measurements and analyses in time/frequency domain for bridges and other civil engineering structures At present time, under the candidate supervision, successful experimental modal analyses were performed on real-world structures (beam and suspension bridges, metallic structures, tall concrete buildings, hollow-core slabs

etc.) and also on small elements inside laboratory. The presented experimental studies were included in the Master Theses supervised by the candidate (2013).

(b-ii) Scientific, professional and academic future development plans

As presented in (b-i), the candidate's scientific activities are developed in two main thematic directions.
The first one is related to "Buckling analysis of thin-walled members", which continues and diversifies the work done during the candidate's PhD programme. In this area, the candidate's theoretical formulations thoroughly presented in this thesis are related to the Generalised Beam Theory (GBT), a specialised theory for the analysis of thin-walled members. The candidate published several ISI papers in the field of GBT and the personal contributions of theoretical nature can be summarised as follows: (i) a new GBT formulation to analyse the behaviour of tapered thin-walled members, (ii) a GBT formulation to analyse the buckling behaviour of isotropic circular conical shells, (iii) an original method for buckling mode decomposition from FEA of thin-walled members which is able to identify the participation of pure deformation modes of Global, Distorsional and Local nature in a general, eigenvalue buckling mode provided by FEA.
The second one is related to "Vibration analysis of civil engineering structures", it is a relatively new scientific area for the candidate and it contains both theoretical and experimental developments. The theoretical formulations concentrated on the vibration analysis of thin-walled members and they are greatly influenced by the candidate's theoretic developments concerning the buckling analysis of thin-walled members. The modal decomposition method was successfully applied to vibration modes provided by FEA.
The experimental work mainly focused on "Experimental modal analysis". At present time the candidate is the coordinator of laboratory „Actions in Buildings and Structures", Department of Structural Mechanics, Faculty of Civil Engineering, Technical University of Cluj-Napoca, which contains Bruel&Kjaer and PCB Piezotronics equipment and dedicated software suited to perform experimental vibration analyses. Under the candidate's supervision, successful experimental modal analyses were performed on real-world structures (concrete buildings and bridges, suspension bridge, metallic structures, hollow-core slabs etc.) and also on small elements inside laboratory. Also, the candidate conducted many vibrations measurements and analyses in time/frequency domain for bridges and civil engineering structures (acceleration, velocity, displacement, level of vibrations) estimating the risk of having the resonance phenomenon. The tension estimation of cables by means of vibration response is another research area in which the candidate obtained promising results.

a) Concerning the future research and development plans of the candidate, related to the field of research "Analysis of thin-walled members" the following research topics will be continued and developed:

1. *Buckling/vibration analysis of tapered thin-walled members with arbitrary cross-sectional variation*

The candidate is the first researcher who extended the Generalised Beam Theory (GBT) for tapered thin-walled members (see article 1) which are extensively used in the construction of steel buildings (see Figure 102).

Figure 102. Example of steel buildings with tapered elements

Until present time, linear cross-sectional variation along the member's axis was adopted but the theoretical formulations can be easily extended to parabolic (and even higher polynomial degree) variation along the entire longitudinal axis. The variation law may also be changed along the member's axis, having different expressions on different intervals, thus providing the possibility to analyse a wide range of complex structures. The application and validation of these theoretical formulations will contribute to a superior understanding of the buckling/vibration behaviour of tapered thin-walled members of various types such as: cold formed steel beams and columns having C, I, Z or Σ-sections and variable web height or flange width, steel beams and columns constructed by joining a member with constant cross-section with a tapered member, hyperbolic thin-walled members such as concrete cooling towers etc.

Until now, the extension of GBT for tapered elements was derived by the candidate using the approximation that the warping displacements are still perpendicular to the cross-sectional plane. This approximation gave good results for tapered members with small tapering slope, but in future the candidate wishes to improve the theoretical formulations in order to handle large values of this parameter.

A software application dedicated to buckling/vibration analysis of tapered thin-walled members with arbitrary cross-sectional variation will be developed together with a friendly graphical interface and made publicly available, similar with GBTUL [17] or CUFSM [6] (nowadays these codes can handle only prismatic thin-walled members).

2. Buckling/vibration analysis of conical shells based on GBT

The candidate is the first researcher who extended GBT for conical shells and validated the new theoretical formulations (see articles 2, 5 and 6). The GBT extension covered the buckling behaviour of columns (axially compressed members), beams (flexural members), beam-columns and shafts (torsion members) having classical bar boundary conditions and simple loading. The development plan contains the diversification of these last parameters, namely to be able to introduce arbitrary boundary conditions and loading and also to connect on the same longitudinal axis, conical shells with various longitudinal slopes and also with cylindrical shells. As GBT was already developed for elliptical cylindrical shells [31], a new research direction is to extend the theoretical formulation for the special case of elliptical conical shells, following a similar procedure with the one already created for the GBT extension from the circular cylindrical shells to circular conical shells.

It is only natural to create in the near future a publicly available software application which will analyse circular/elliptical conical and cylindrical shells with much greater speed than the presently available codes based on FEM. GBT is also superior to FEM on the account of the

modal identification capabilities, being created precisely for this reason as a specialised method for the analysis of thin-walled members.

3. Improving the modal decomposition method

The first objective in this area consists in the elimination of certain simplifying hypotheses (for instance the Vlasov's hypothesis) by taking into account the influence of deformation modes containing membrane transverse extensions and shear strains, deformations neglected by classical GBT and by the present modal decomposition method. Also, the assumption that the warping displacements are linear along the bar's cross-section, will be eliminated. Nowadays, GBT was developed in these directions by several researchers ([15], [66], [83]), and the integration of their solutions into the candidate's method is possible and highly advantageous.
A second objective consists in the assessment of the modal participation based on the strain energy accumulated by each pure deformation mode in a general eigenvalue buckling/vibration mode. Until now the formula used for the modal participation is based only on the amplitude functions of the pure deformation modes [13]. Although it is an easy and intuitive approach, it has its drawbacks due to the arbitrary normalization of the cross-sectional pure deformation modes.

4. Buckling/vibration mode decomposition for tapered thin-walled members, cylindrical and conical shells

The candidate developed an original modal decomposition method for prismatic thin-walled members, able to identify the Global, Distorsional and Local (GDL) deformation modes (also called the *pure* modes) inside a general buckling or vibration mode (see article 3). The method is a union between GBT and FEM, benefiting of the best features of these two methods. In future, this method will be developed in order to assess the GDL deformation modes participation for tapered thin-walled members, circular/elliptical cylindrical and conical shells. Having a significant experience in the study of these types of elements, a fact proved by the ISI and conference proceedings publications, the candidate is confident that the theoretical extensions are possible, highly advantageous in comparison with the existing analysis methods and very useful from the research and structural design point of view.
Recently, the modal decomposition method was also extended for members with regular rectangular holes and this application was discussed in section 3.3 for prismatic sections. In the near future the method will also be extended for circular/elliptical cylindrical and conical shells with holes.
A software application able to identify the pure modes and quantify their participation in a coupled instability or vibration shape will be developed together with a friendly graphical interface and made publicly available.

5. Buckling/vibration mode decomposition for thin-walled members with arbitrary holes

Perforations (holes) are a common need in cold-formed and hot-rolled steel systems; whether for services in buildings, for convenient connection of other members, or other uses. Perforations in thin-walled steel members come in a variety of different forms, as shown in Figure 103. The two most common types of perforations are isolated holes and patterned holes. Isolated holes include load bearing studs with holes for services and/or bridging (Figure 103a), and isolated holes in joists, purlins, and girts (Figure 103a). Patterned holes include those in pallet rack post uprights for tabbed beam connections (Figure 103b). Other more unique situations exist for cold-formed steel members with perforations; including isolated holes that include formed-in flanges for increased stiffness around the hole (Figure 103c) and new ideas for better thermal behavior using small patterned perforations (Figure 103d).

Until present time due to technical difficulties, the modal decomposition method created by the candidate was applied for prismatic members with rectangular holes placed in a regular pattern along the member's length. However the theoretical formulations introduced by the candidate can handle arbitrary shape, size and distribution of the holes inside the member's walls. The aim is to improve the used methodology and computer code in order to analyse prismatic, tapered thin-walled members, circular/elliptical cylindrical and conical shells with arbitrary holes.

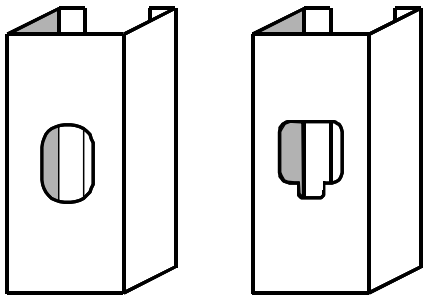

(a) *Isolated holes in studs*, may also be found in joists, purlins, and girts, several holes may exist along the length, though spacing is generally far apart

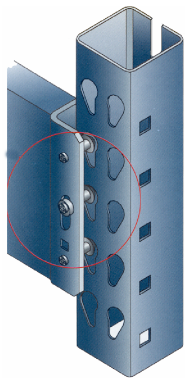

(b) *Patterned perforations in rack posts*, and in some rack beams, in addition other specialty industries include such perforations (*picture from UNARCO product catalog*)

(c) *Isolated flanged holes in joists*, purlins; holes stiffened through transverse and possibly longitudinal external stiffeners also relevant (*picture from Dietrich web site*)

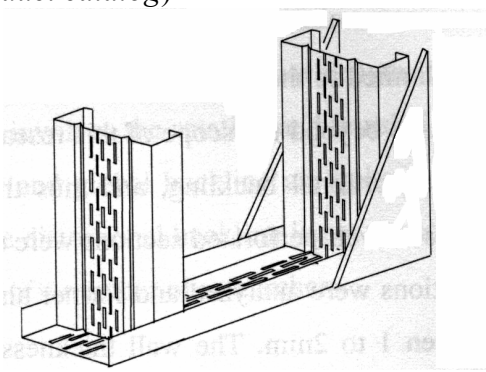

(d) *Specialty perforations* as found in slitted cross-sections used in Europe for improved thermal performance (Sections tested and analyzed in Kesti 2000, *picture from Kesti 2000*)

Figure 103. Examples of perforation patterns found in cold-formed steel systems

6. The effect of imperfections in non-linear analysis of thin-walled members

The goal of this research is to find the most unfavourable imperfection shape in a geometric nonlinear analysis. One starting point is the method proposed by Sadovsky et al. [84] that begins with a classical buckling analysis of the thin-walled member using FEM and finds as many buckling modes as possible. The geometric imperfections are represented by the member eigenmode shapes. Along with the classical measure — the amplitude of imperfections, an energy measure defined by the square root of the elastic strain energy hypothetically required to distort the originally perfect structural element into the considered imperfect shape is used. Based on the measures, two approaches for the choice of the most unfavourable imperfections were suggested. Normalising imperfections by the amplitude, the energy measure is calculated as indicative parameter of imperfection significance. Vice versa,

when adopting normalisation by the energy measure, the amplitude is used as a supporting parameter.
After the most unfavourable shapes are obtained a modal identification will be carried out using the modal decomposition method developed by the candidate. From this modal identification, the value of the magnitude of the geometrical imperfection is determined as a combination of the magnitudes shown Table 27, inspired from EC 3 part 1–5 and from literature [85].

Table 27. Imperfection magnitudes for the pure deformation modes

Failure mode typology	Imperfection magnitude
Local	web/200 (EC 3 part 1-5)
Distorsional	flange/50 (EC 3 part 1-5)
Global	length/1000 (literature)

The expressions given in Table 27 are highly empirical, so based on large number of numerical simulations, their accuracy will be checked and if it the case, they will be improved. Of course, the imperfection values will be limited by the manufacturing tolerances. The candidate expects to be the first to write with the help of his future PhD students, a publicly available computer program, capable to implement the above described procedure. The program will be written in the Matlab programming language and for the start it will use the ABAQUS code for all the FE analyses. Next step is to write a computer code based on FEM, dedicated for the buckling, vibration and non-linear analysis of thin-walled structures.

b) Concerning the future research and development plans of the candidate, related to the field of research on "Vibration analysis of civil engineering structures" the following research topics will be continued or developed:

1. New experimental vibration analyses

The candidate will continue to perform experimental modal analyses on real structures such as civil and industrial constructions with the purpose of optimisation of structure's dynamic characteristics (mass, stiffness, damping), risk assessment of having the resonance phenomenon, prediction of dynamic behaviour, evaluating the damping for inclusion in FE models, correlation of FE models with real structures, damage detection and assessment, long term building monitoring. Classical (input-output) experimental modal analyses using an impact hammer or shaker will be performed on flexible structures small enough to be excited in this manner. For the other range of structures, the operational (output-only) experimental modal analysis will be used. Beside the research purposes, these analyses will be part of the future technical studies and valuations for the civil engineering industry, covering the following demands: analysis of dynamic properties of new or damaged structural systems, experimental support for structural consolidation projects, experimental assessment of traffic or other human activities induced vibrations, long term monitoring of dynamic structural behaviour.
The candidate will also perform and supervise experimental vibration analyses on small elements and scale models of existing buildings inside the laboratory „Actions in Buildings and Structures", Department of Structural Mechanics, Faculty of Civil Engineering, Technical University of Cluj-Napoca. The goal of these analyses is to verify and improve the experimental procedures used on real structures, and to calibrate the computer numerical simulations. The Matlab code created by the candidate with the purpose of finding the

displacements and velocities from the measured accelerations will be further improved by advanced filtering and tested in comparison with existing similar computer programs and also with available examples in scientific literature.

2. Tension estimation of cables

Until present time, the tension estimation in cables was made under the following assumptions: the boundary conditions of the cable were considered hinged and the "sag" effect was neglected. In reality a perfectly hinged support doesn't exist, and for cables with significant bending stiffness the effect of the partially fixed support must be considered. Also the "sag" effect always exists. Consequently a series of numerical simulations were recently performed and a couple of methods available in literature were tested [87]-[93].
The next step is to apply these methods which take into account all the influencing parameters (natural frequencies, bending stiffness, "sag" effect and the rotational stiffness of the cable's ends) on real world structures when such opportunities will arise.

Finally, it have to be underlined that the active role of the candidate will continuously increase by participation with new research topics to international conferences and papers published in specialised journals.

(b-iii) References

[1] EUROCODE 3, EN 1993-1.3. Design of steel structures. Part 1-3: General – Cold formed thin gauge members and sheeting, European Committee for Standardisation, Final Draft, 2001.

[2] AISI – American Iron and Steel Institute: Cold-formed steel design manual, Washington, DC, 1996.

[3] AISI – American Iron and Steel Institute: North American Specification for the Design of Cold-Formed Steel Structural Members with Commentary, Washington, DC, 2001.

[4] AS/NZS 4600 – Australian Standards / New Zealand Standards. Cold-formed Steel Structures, Sydney, 1996.

[5] AISI – American Iron and Steel Institute: Supplement 2004 to the North American Specification for the Design of Cold-Formed Steel Structural Members 2001 Edition: Appendix 1, Design of Cold-Formed Steel Structural Members Using Direct Strength Method, Washington, D.C., 2004.

[6] CUFSM: Elastic Buckling Analysis of Thin-Walled Members by Finite Strip Analysis, CUFSM v2.6, http://www.ce.jhu.edu/bschafer/cufsm/

[7] Schardt R. Verallgemeinerte Technische Biegetheorie. Berlin Springer Verlag; 1989 (in German).

[8] Schardt R. Generalized beam theory – An adequate method for coupled stability problems. Journal of Thin-Walled Structures 1994; 19:161-80.

[9] Eisenberger M. Nonuniform torsional analysis of variable and open cross-section bars. Journal of Thin-Walled Structures 1995; 21:93-105.

[10] Sapountzakis EJ, Mokos VG. Nonuniform torsion of bars of variable cross-section. Journal of Computers and Structures 2004; 82:703-15.

[11] Gonçalves R, Dinis PB, Camotim D. GBT formulation to analyse the first-order and buckling behaviour of thin-walled members with arbitrary cross-sections. Journal of Thin-Walled Structures 2009; 47(5):583-600.

[12] Silvestre N, Camotim D. First-order generalised beam theory for arbitrary orthotropic materials. Journal of Thin-Walled Structures 2002; 40:755-89.

[13] Silvestre N, Camotim D. Second-order generalised beam theory for arbitrary orthotropic materials. Journal of Thin-Walled Structures 2002; 40: 791-820.

[14] Silvestre N, Camotim D. GBT-based local and global vibration analysis of loaded composite thin-Walled members. Journal of Structural Stability and Dynamics 2006; 6:1-29.

[15] Silvestre N, Camotim D. Local-plate and distortional post-buckling behaviour of cold-formed steel lipped channel columns with intermediate stiffeners. Journal of Structural Engineering, ASCE 2006;132: 529-40.

[16] Basaglia C, Camotim D, Silvestre N. Non-linear GBT formulation for open-section thin-walled members with arbitrary support conditions. Journal of Computers and Structures 2011; 89: 1906-19.

[17] GBTUL 1.0b Buckling and Vibration Analysis of Thin-Walled Members, http://www.civil.ist.utl.pt/gbt/

[18] Ádány S, Schafer BW. A full modal decomposition of thin-walled, single-branched open cross-section members via the constrained finite strip method. Journal of Constructional Steel Research 2008; 64:12-29.

[19] Dinis PB, Camotim D, Silvestre N. GBT formulation to analyse the buckling behaviour of thin-walled with arbitrarily 'branched' open cross-sections. Journal of Thin-Walled Structures 2006; 44:20–38.

[20] Matlab Version 7.1.0246 Documentation, The Mathwork Inc., 2005. MathWorks - MATLAB and Simulink for Technical Computing.

[21] Sapountzakis EJ, Panagos DG. Nonlinear analysis of beams of variable cross section, including shear deformation effect. Archive of Applied Mechanics 2007; 78(9):687-710.

[22] Ronagh HR, Bradford MA, Attard MM. Nonlinear analysis of thin-walled members of variable cross-section. Part I: Theory. Journal of Computers and Structures 2000; 77:285-99.

[23] Ronagh HR, Bradford MA, Attard MM. Nonlinear analysis of thin-walled members of variable cross-section. Part II: Application. Journal of Computers and Structures 2000; 77:301-13.

[24] Hibbit, Karlsson and Sorensen Inc. ABAQUS Standard (Version 6.3) 2002.

[25] Bebiano R, Silvestre N, Camotim D. GBT formulation to analyze the buckling behaviour of thin-walled members subjected to non-uniform bending. International Journal of Structural Stability and Dynamics 2007; 7(1):23-54.

[26] Andrade A, Camotim D, Dinis PB. Lateral-torsional buckling of singly symmetric web-tapered thin-walled I-beams: 1D model vs. shell FEA. Journal of Computers and Structures 2007; 85(17-18):1343-59.

[27] Cole PP, Abel JF, Billington DP. Buckling of cooling tower shells: Bifurcation results. Journal of the Structural Division, ASCE 1975; 101(ST6):1205-22.

[28] Cole PP, Abel JF, Billington DP. Closure of "Buckling of cooling tower shells: Bifurcation results". Journal of the Structural Division, ASCE 1977; 103(4): 917-19.

[29] Abel JF, Billington DP, Nagy DA, Wiita-Dworkin C. Buckling of cooling towers. Journal of the Structural Division, ASCE June 1982; 108: ST10, 2162-74.

[30] Silvestre N. Generalised beam theory to analyse the buckling behaviour of circular cylindrical shells and tubes. Journal of Thin-Walled Structures 2007; 45(2):185-98.

[31] Silvestre N. Buckling behaviour of elliptical cylindrical shells and tubes under compression. Journal of Solids and Structures 2008; 45(16):4427-47.

[32] Lorenz R. Achsensymmetrische Verzerrungen in dünnwandingen Hohlzzylindern. Z Vereines Deutscher Ing. 1908; 52(43):1706-13.

[33] Love AEH. A Treatise on the Mathematical Theory of Elasticity. 1944; fourth ed. Dover, New York.

[34] Donnell LH. A new theory for the buckling of thin cylinders under axial compression and bending. Trans ASME 1934; 56:795-806.

[35] Von Karman T, Tsien HS. The buckling of thin cylindrical shells under axial compression. Journal of Aeronautical Sciences 1941; 8(6):303-12.

[36] Seide P. Axisymmetric buckling of circular cones under axial compression. Journal of Applied Mechanics 1956; 23:625-8.

[37] Seide P. Buckling of circular cones under axial compression. Journal of Applied Mechanics 1961; 28:315-26.

[38] Singer J. Buckling of circular conical shells under axisymmetrical external pressure. Journal of Mechanical Engineering Science 1961; 3:330-9.

[39] Baruch M, Singer J. General instability of stiffened conical shells under hydrostatic pressure. The Aeronautical Quarterly 1965; 26:187-204.

[40] Baruch M, Harari O, Singer J. Influence of in-plane boundary conditions on the stability of conical shells under hydrostatic pressure. Israel Journal of Technology 1967; 5(1–2):12–24.

[41] Baruch M, Harari O, Singer J. Low buckling loads of axially compressed conical shells. Journal of Applied Mechanics 1970; 37: 384-92.

[42] Singer J. Buckling of orthotropic and stiffened conical shells 1962; NASA TN D-1510:463–79.

[43] Singer J. Donnell-type equations for bending and buckling of orthotropic conical shells. Journal of Applied Mechanics 1963; 30:303-5.

[44] Weigarten VI, Seide P. Elastic stability of thin walled cylindrical and conical shells under combined external pressure and axial compression. Journal of the American Institute of Aeronautics and Astronautics 1965; 3:913-20.

[45] Weigarten VI, Seide P. Elastic stability of thin walled cylindrical and conical shells under combined internal pressure and axial compression. Journal of the American Institute of Aeronautics and Astronautics 1965; 3:1118-25.

[46] Pariatmono N, Chryssanthopoulos MK. Asymmetric elastic buckling of axially compressed conical shells with various end conditions. Journal of the American Institute of Aeronautics and Astronautics 1995; 33 (11): 2218-27.

[47] Spagnoli, A. Koiter circles in the buckling of axially compressed conical shells. Journal of Solid Structures 2003; 40: 6095-109.

[48] Tong L. Buckling load of composite conical shells under axial compression. Journal of Applied Mechanics 1994; 61(3): 718-9.

[49] Naj R, Sabzikar Boroujerdy M, Eslami MR. Thermal and mechanical instability of functionally graded truncated conical shells. Journal of Thin-Walled Structures 2008; 46: 65–78.

[50] Donnell LH. Stability of thin-walled tubes under torsion. National Advisory Committee for Aeronautics 1933; TR-479.

[51] Sanders JL. Nonlinear theories for thin shells. Quarterly Journal of Applied Mathematics 1963; 21 (1): 21-36.

[52] Timoshenko S, Woinowsky-Krieger S. Theory of Plates and Shells, McGraw-Hill, New York 1959.

[53] Timoshenko S, Gere JM. Theory of Elastic Stability. McGraw-Hill Book Company, New York 1961.

[54] Goldfeld Y, Sheinman I, Baruch M. Imperfection sensitivity of conical shell. Journal of the American Institute of Aeronautics and Astronautics 2003; 4(3): 517-24.

[55] Goldfeld Y. Imperfection sensitivity of laminated conical shells. International Journal of Solids and Structures 2007; 44:1221-41.

[56] Silvestre N, Camotim D. GBT buckling analysis of pultruded FRP lipped channel members. Journal of Computers and Structures 2003; 81(18–19):1889-904.

[57] Ascher U, Mattheij R, Russell R. Numerical Solution of Boundary Value Problems for Ordinary Differential Equations. Society for Industrial and Applied Mathematics, Philadelphia, PA 1995.

[58] Ventsel E, Krauthammer T. Thin plates and shells: theory, analysis, and applications. CRC Press; 1 edition (Aug 24 2001)

[59] Li Z, Schafer BW. Buckling analysis of cold-formed steel members with general boundary conditions using CUFSM: Conventional and constrained finite strip methods. Twentieth International Specialty Conference on Cold-Formed Steel Structures, Saint Louis, Missouri, USA, November 3 & 4, 2010.

[60] Casafont M, Marimon M, Pastor MM, Ferrer M. Linear buckling analysis of thin-walled members combining the Generalised Beam Theory and the Finite Element Method. Journal of Computers and Structures 2011; 89(21-22):1982-2000.

[61] Ádány S, Joó AL, Schafer BW. Buckling modes identification of thin-walled members using cFSM base functions. Journal of Thin-Walled Structures 2010; 48:806-17.

[62] Crisan A, Ungureanu V, Dubina D. Behaviour of cold-formed steel perforated sections in compression. Part 1 - Experimental investigations. Journal Thin-Walled Structures 2012; 61:86-96.

[63] Lau SCW, Hancock, GJ. Buckling of thin flat-walled structures by a spline finite strip method. Journal of Thin-Walled Structures 1986; 4(4): 269-94.

[64] Davies JM, Leach P, Taylor A. The design of perforated cold-formed steel sections subject to axial load and bending. Journal of Thin-Walled Structures 1997; 29:141-57.

[65] Moen CD, Schafer BW. Direct strength method for design of cold-formed steel columns with holes. Journal of Structural Engineering 2011; 137(5):559-70.

[66] Silvestre N, Camotim D. Nonlinear generalized beam theory for cold-formed steel members. Journal of Structural Stability and Dynamics 2003; 3(4):461-90.

[67] Camotim D, Silvestre N, Bebiano R. GBT local and global vibration analysis of thin-walled members, in: N.E. Shanmugam, C.M. Wang (Eds.). Dynamics of Plated Structures: Analysis and Design 2007, Woodhead Publishing Ltd., Cambridge, 36–76.

[68] Bebiano R, Silvestre N, Camotim D. Local and global vibration of thin-walled members subjected to compression and non-uniform bending, Journal of Sound and Vibration 2008; 315: 509–35.

[69] Silvestre N, Camotim D. Vibration behaviour of axially compressed cold-formed steel members, Journal of Steel and Composite Structures 2006; 6(3): 221-36.

[70] Bruel&Kjaer, www.bksv.com

[71] PCB Piezotronics, www.pcb.com

[72] Bracewell RN. The Fourier Transform. Scientific American June 1989; 86-95.

[73] Avitabile P. Experimental Modal Analysis.University of Massachusetts Lowell, Massachusetts, USA, 2001.

[74] Avitabile P. Modal Space Back To Basics, Experimental Techniques. Society for Experimental Mechanics and Blackwell Publishing, July/August 2002.

[75] Autodesk Robot Structural Analysis Professional, usa.autodesk.com

[76] Cunha A, Caetano E. Experimental Modal Analysis of Civil Engineering Structures, Sound and Vibration 2006; 6(40): 12-20.

[77] Wei-Xin Ren, Zhou-Hong Zong. Output-only identification of civil engineering structures. Journal of Structural Engineering and Mechanics 2004; 17: 3-4.

[78] Maia M, Silva JMM. Modal analysis identification techniques. The Royal Society 2001; 359(1778): 29–40.

[79] Operational Modal Analysis – Artemis, Structural Vibration Solutions A/S www.svibs.com

[80] Mercer C. Acceleration, Velocity and Displacement Spectra-Omega Arithmetic. Prosig Signal Processing Tutorials (2006), signalprocessing.prosig.com/OmegaArithmetic.pdf.

[81] Kwon SD, Kim CY, Chang SP. Change of Modal Parameters of Bridge Due to Vehicle Pass. IMAC-XXIII, Conference & Exposition on Structural Dynamics, Orlando, Florida, USA, 2005.

[82] Naik S, Mallik W. Experimental modal testing for estimating the dynamic properties of a cantilever beam. Jadavpur University, Kalkota, http://fosetonline.org/Thought/CA-77.pdf.

[83] Miranda S, Gutiérrez A, Miletta R, Ubertini F. A generalized beam theory with shear deformation. Journal of Thin-Walled Structures 2013; 67: 88-100.

[84] Sadovský Z, Kriváček J, Ivančo V, Ďuricová A. Computational modelling of geometric imperfections and buckling strength of cold-formed steel. Journal of Constructional Steel Research 2012; 78:1–7.

[85] Bonada J, Casafont M, Roure F, Pastor MM. Selection of the initial geometrical imperfection in nonlinear FE analysis of cold-formed steel rack columns. Journal of Thin-Walled Structures 2012; 51: 99–111.

[86] Wang ML, Chen ZL, Koontz, Steve S, Lloyd, GM. Magnetoelastic permeability measurement for stress monitoring în steel tendons and cables. Proc. SPIE. Int. Soc. Opt. Eng. 2000; 3995: 492–500.

[87] Zui H., Shinke T, Namita YH. Practical formulas for estimation of cable tension by vibration method. Journal of Structural Engineering, ASCE 1996; 122(6): 651-6.

[88] Triantafyllou MS, Grinfogel L. Natural frequencies and modes of inclined cables. Journal of Structural Engineering, ASCE 1986; 112(1): 139-48,.

[89] Ren WX. Chen G, Hu WH, Empirical formulas to estimate cable tension by cable fundamental frequency, Journal of Structural Engineering and Mechanics 2005; 20(3): 363-80.

[90] Kim BH, Park T. Estimation of cable tension force using the frequency-based system identification method. Journal of Sound and Vibration 2007; 304(3–5): 660–676.

[91] Kim BH, Park T, Shin H, Yoon TY. A comparative study of the tension estimation methods for cable supported bridges. Journal of Steel Structures 2007; 7: 77-84.

[92] Ceballos MA, Prato CA. Determination of the axial force on stay cables accounting for their bending stiffness and rotational end restraints by free vibration tests, Journal of Sound and Vibration 2008; 317: 127-41.

[93] Bellino A, Garibaldi L, Fasana A, Marchesiello S. Tension estimation of cables with different boundary conditions by means of the added mass technique, Journal Mecanique et Industries 2010.

[94] Buzdugan G, Fetcu L, Rades M. Vibratiile sistemelor mecanice. Ed. Academiei RSR, 1975.

[95] SAP2000, Integrated Finite Element Analysis and Design of Structures - Analysis Reference, Computers & Structures Inc., ver. 7.0, 1998.